

## Abstract

Title of Document: Photoresponsive Systems Based on Self-Assembly  
Hyuntaek Oh, Doctor of Philosophy, 2014

Directed By: Professor Srinivasa R. Raghavan,  
Department of Chemical and Biomolecular Engineering

Photoresponsive systems based on self-assembled nanostructures have received considerable attention recently. There is a wide range of applications for these fluids such as in drug delivery, coatings, sensors, or microfluidic valves and dampers. Current photoresponsive systems have typically required the use of specialized molecules with various chemical modifications. However, the requirement of complicated chemical synthesis prevents these systems from being used widely for practical applications. In this study, we focus on creating photoresponsive systems using only commercially available photoresponsive molecules and structure-forming components.

In our first study, we describe simple reversible photorheological (PR) fluids, *i.e.*, fluids whose rheological properties can be tuned by light. Our PR fluids are created by combining an azobenzene derivative, 4-azobenzene carboxylic acid (ACA), into micelles of the cationic surfactant erucyl bis(2-hydroxyethyl)methyl ammonium chloride (EHAC). We show that certain aqueous mixtures of EHAC and ACA, which are low-viscosity solutions at the outset, undergo nearly a million-fold increase in viscosity when irradiated with UV light. The same solutions revert to their initial viscosity when subsequently

exposed to visible light. The above changes in viscosity are repeatable, and the sample can be reversibly cycled back and forth between low and high viscosity states.

In our second study, we report a class of photoresponsive vesicles composed of inexpensive and commercially available cationic and anionic surfactants. The mixture of these amphiphiles forms vesicles due to ionic interactions between the cationic and anionic headgroups. When irradiated by UV light, the cationic surfactant loses its charge and, in turn, the vesicles are converted into micelles due to the loss of ionic interactions. In addition, a mixture of these photoresponsive vesicles and a hydrophobically modified biopolymer gives a photoresponsive vesicle-gel that can undergo a gel-to-sol transition with UV light.

In our final study, we demonstrate practical applications of PR fluids as a light-activated fluidic valve in microchannels. Current PR fluid formulations are not suitable for this application. Here, we report a PR fluid composed of alginate, a photoacid generator (PAG) as a photo-trigger, and a chelated complex of divalent strontium ( $\text{Sr}^{2+}$ ) (Sr-EGTA). Upon exposure to UV, free  $\text{Sr}^{2+}$  ions are released, which self-assemble with the alginate chains to give a nanostructured gel with a high gel modulus ( $\sim 2000$  Pa). We flow our PR fluid in a microchannel and expose a specific point to UV light. At this point, alginate is converted into a gel, which blocks the flow. When the UV light is removed, the gel is gradually dissolved by the flow and the channel reopens. The above concept relies entirely on physical (non-covalent) bonds, *i.e.*, on self-assembly, rather than on covalent crosslinking of dissolved monomers or polymers.

# **Photoresponsive Systems Based on Self-Assembly**

By

Hyuntaek Oh

Dissertation submitted to the Faculty of the Graduate School of the  
University of Maryland, College Park, in partial fulfillment of  
the requirements for the degree of

Doctor of Philosophy

2014

## **Advisory Committee:**

---

Prof. Srinivasa Raghavan, Dept. of Chemical & Biomolecular Engineering, Advisor

Prof. Kyu Yong Choi, Dept. of Chemical & Biomolecular Engineering

Prof. Panagiotis Dimitrakopoulos, Dept. of Chemical & Biomolecular Engineering

Prof. Robert M. Briber, Dept. of Materials Science & Engineering

Prof. Daniel Falvey, Dept. of Chemistry & Biochemistry

Dr. Boualem Hammouda, National Institute of Standards & Technology

© Copyright by  
Hyuntaek Oh  
2014

## Acknowledgements

First, I would like to thank my advisors Prof. Srinivasa Raghavan for providing me the opportunity to be a member of his wonderful group. He always encouraged me to explore new research areas. In particular, his philosophy of the research greatly moved me and affected my research directions, adopting a physical principle of biology and developing a new technology using a simple method. I was also infected by his positive thinking.

Next, I owe a lot of thanks to my family for their unconditional love and support. Particularly, I am extremely grateful to my wife, Mieun. She's been a silent supporter in my life and always encourages me to seek a greatness rather than a comfort zone. Also, I would like to thank my parents, Oklan and Munkwan. They taught me the importance of education and constant effort. Also, I thank my daughters, Subin and Jeonghyo. Their laugh has been the most valuable energy source to my life. I also appreciate parents-in-law for their sacrificial support.

I would like to thank my committee members: Prof. Kyu Yong Choi, Prof. Panagiotis Dimitrakopoulos, Prof. Robert Briber, Prof. Daniel Falvey, Dr. Boualem Hammouda for their invaluable guidance, suggestions and input for my projects.

I also appreciate many collaborators who contributed a lot to my researches. I thank to Prof. Dganit Danino, Ellina Kesselman, Ludmila Abezgauz at Technion for

cryo-TEM studies, and Prof. Daniel Falvey, Romina Heymann for NMR studies, and Dr. Boualem Hammouda, Dr. Paul Butler at NIST for SANS studies.

I owe a lot of thanks my present and past colleagues from Dr. Raghavan's lab: Hee-Young Lee, Jae-Ho Lee, Stephen Banik, Anand Bagal, Veidhes Basrur, Vishal Javvaji, Kunqiang Jiang, Bani Cipriano, Charles Kuo, Kunal Pandit, Chanda Arya, Kevin Diehn, Annie Lu, Jasmin Athas, Ankit Gargava, Ankit Goyal, Veena Rao, Brady Zarket, Ian MacIntire, Matthew Dowling, Salimeh Gharazi, Joe White. It has been a great pleasure to work with them. I was fortunate to be a part of such an enthusiastic, intellectual and productive groups.

# Table of Contents

<b>Acknowledgements</b> .....	<b>ii</b>
<b>Table of Contents</b> .....	<b>iv</b>
<b>List of Figures</b> .....	<b>vi</b>
<b>Chapter 1. Introduction and Overview</b> .....	<b>1</b>
1.1. Problem Description and Motivation.....	1
1.2. Proposed Approach.....	2
1.2.1. Photoreversible Photorheological Fluids .....	2
1.2.2. Photoresponsive Vesicles and Vesicle-gels .....	4
1.2.3. Light-activated fluidic valve .....	5
1.3. Significance of This Work.....	6
<b>Chapter 2. Background</b> .....	<b>8</b>
2.1. Self-Assembly of Surfactants .....	8
2.2. Wormlike Micelles.....	10
2.3. Photochemistry of Azobenzene .....	14
2.4. Characterization Technique – I: Rheology .....	18
2.5. Characterization Technique – II: SANS .....	20
2.6. Characterization Technique – III: UV-Vis Spectroscopy.....	22
<b>Chapter 3. Reversible Photorheological Fluids</b> .....	<b>24</b>
3.1. Introduction.....	24
3.2. Experimental Section .....	27
3.3. Results and Discussion .....	30

3.4. Conclusions.....	48
<b>Chapter 4. Photoresponsive Vesicles and Vesicle Gels.....</b>	<b>49</b>
4.1. Introduction.....	49
4.2. Experimental Section.....	53
4.3. Results and Discussion .....	57
4.4. Conclusions.....	72
<b>Chapter 5. Light-Activated Fluidic Valve .....</b>	<b>73</b>
5.1. Introduction.....	73
5.2. Experimental Section.....	78
5.3. Results and Discussion .....	81
4.4. Conclusions.....	97
<b>Chapter 6. Conclusions and Recommendations.....</b>	<b>99</b>
6.1. Project Summary and Principal Contributions .....	99
6.2. Recommendations for Future Work.....	101
6.2.1. Photoresponsive Capsules.....	101
6.2.2. Reversible gel-to-sol transition.....	105
<b>Chapter 7. References.....</b>	<b>108</b>



## List of Figures

- Figure 1.1.** Reversible PR fluid described in Chapter 3 based on the structure transition between vesicles and wormlike micelles. ....3
- Figure 1.2.** Photoresponsive vesicles described in Chapter 3, showing transition from vesicles to spherical micelles upon UV exposure. ....4
- Figure 1.3.** A light-activated fluidic valve in Chapter 5. ....6
- Figure 2.1.** Schematics depicting the connection between the geometry of amphiphilic molecules and the structures they form in water. The hydrophilic heads of the amphiphiles are shown in blue and the hydrophobic tails in red. ....9
- Figure 2.2.** Schematic showing the structure of an individual wormlike micelle as well as the entanglement of micellar chains into a transient network. ....11
- Figure 2.3.** Binding of salicylate (o-hydroxy benzoate) counterions to cationic micelles. The aromatic ring is embedded into the hydrophobic interior of the micelle shown in red. The hydrophilic groups (OH and COO<sup>-</sup>) protrude out of the micelle, shown in blue.<sup>39</sup>...13
- Figure 2.4.** Photoisomerization of azobenzene upon irradiation by light. The *cis* to *trans* isomerisation can also be induced by heat. ....14
- Figure 2.5.** Schematic of a SANS experiment (adapted from [www.gkss.de](http://www.gkss.de)). ....21
- Figure 3.1.** Composition and mechanism of reversible PR fluids. The fluids are composed of the cationic surfactant EHAC and the azobenzene derivative ACA. When ACA is in its *trans* form, its mixture with EHAC forms discrete unilamellar vesicles that yield a low viscosity. Upon UV irradiation, *trans* ACA is photoisomerized to *cis* ACA, and in turn, entangled wormlike micelles are formed, which have a much higher viscosity. Upon subsequent irradiation with visible light, *cis* ACA is isomerized back to *trans* ACA, and the structure and rheology revert to their initial state. ....26
- Figure 3.2.** Phase behavior and rheology at 25°C of EHAC/ACA mixtures at a fixed [EHAC] of 40 mM and varying [ACA]. The molar ratio of NaOH to ACA is fixed at 1.1. The plot (a) shows the optical density at a wavelength of 700 nm, which quantifies the amount of light scattered from the sample. The plot (b) shows the zero-shear viscosity  $\eta_0$  obtained from steady-shear rheology. Samples at ACA concentrations between 10 and 16 mM are transparent and highly viscous (top left) and show flow-birefringence (bottom left). In contrast, samples with greater than 18 mM ACA have a low viscosity close to water and appear cloudy (top right) due to light scattering and do not show any flow-birefringence (bottom right). ....32
- Figure 3.3.** (a) SANS data at 25°C from EHAC/ACA mixtures in D<sub>2</sub>O at a fixed [EHAC] of 10 mM with various ACA concentrations. The molar ratio of NaOH to ACA is fixed to 1.1. For ACA concentrations of 6 and 6.5 mM,  $I$  follows a slope of -2 at low  $q$ , which is indicative of scattering from vesicles. (b), (c) Cryo-TEM images of a sample containing 40 mM EHAC, 20 mM ACA, and 22 mM NaOH show mostly vesicle structures (see

Figure 3.10 (a) also). In some parts of the sample, stretched and interwoven wormlike micelles were also observed in rare cases, as seen in the above images. ....34

**Figure 3.4.** UV-Vis spectra of 40 mM EHAC, 20 mM ACA, and 22 mM NaOH before irradiation (cyan line), after UV irradiation for 1 hr (blue line), and after subsequent visible light irradiation for 1.5 hr (dotted red line). The sample was diluted 20 times with water. The changes at the visible wavelengths are enlarged and shown in the inset. ....35

**Figure 3.5.** A sample containing 40 mM EHAC, 20 mM ACA, and 22 mM NaOH was used for reversible photorheological response. Visual observations illustrate the dramatic light-induced changes in fluid properties: initially, the sample is a cloudy, water-like fluid (Photo 1 and 2) whereas UV light transforms it into a transparent viscoelastic and gel-like fluid that shows the tubeless siphon (Photo 3) and rod climbing (Photo 4) effects. This is reversed by irradiation with visible light. ....36

**Figure 3.6.** Steady-shear rheology of a sample of 40 mM EHAC, 20 mM ACA, and 22 mM NaOH. Data for the apparent viscosity vs. shear rate are shown for the initial sample (cyan circles), after UV irradiation for 30 min (purple circles), and after subsequent visible light irradiation for 30 min (red circles). ....37

**Figure 3.7.** Dynamic rheology of a sample of 40 mM EHAC, 20 mM ACA, and 22 mM NaOH. Data for the elastic modulus  $G'$  and the viscous modulus  $G''$  as functions of frequency  $\omega$  are shown for the initial sample (a), after UV irradiation for 30 min (b), and after subsequent visible light irradiation for 30 min (c). ....38

**Figure 3.8.** Rheological cycling of a 40 mM EHAC / 20 mM ACA / 22 mM NaOH under repeated UV and visible light irradiation. The rheology is quantified in terms of the zero-shear viscosity  $\eta_0$ . The data show that the sample can be cycled between low and high viscosity states ( $10^5$ -fold difference) by repeated UV and visible light irradiation. ....39

**Figure 3.9.** SANS spectra on a diluted sample in D<sub>2</sub>O (10 mM EHAC, 6.5 mM ACA, and 7.2 mM NaOH) reveal a reversible light-induced transition between two types of self-assembled structures: initially, the intensity  $I$  follows a slope of -2 at low  $q$  (cyan circles), which is characteristic of vesicles at low  $q$ . Upon UV irradiation, the slope is decreased and approaches -1 (violet circles), which is indicative of cylindrical (wormlike) micelles. Upon subsequent visible light irradiation, the original spectrum is recovered (red circles). ....40

**Figure 3.10.** The structural transition is confirmed by cryo-TEM. A typical image of the initial sample containing 40 mM EHAC, 20 mM ACA, 22 mM NaOH (a) reveals discrete unilamellar vesicles, whereas after UV irradiation (b) the sample is found to contain long, entangled wormlike micelles, and finally, after subsequent visible light irradiation (c) the sample reverts to the vesicle state. ....41

**Figure 3.11.** Influence of sample composition on the PR effect. The zero-shear viscosity  $\eta_0$  is plotted for samples at constant [EHAC] of 40 mM and varying [ACA] for three cases: initial, *i.e.*, before any irradiation (cyan circles); after 1 h of UV irradiation (violet circles); and after subsequent 1.5 h of visible-light irradiation (red circles). ....42

**Figure 3.12.** Molecular arrangement of *trans* and *cis* ACA in the EHAC-ACA aggregates. <sup>1</sup>H NMR spectra of 2 – 6.5 mM ACA in 10 mM EHAC and 1 mM ACA in D<sub>2</sub>O (control) are plotted: (a) before UV irradiation and (b) after 1 h of UV irradiation.

The signals a - d correspond to the protons of *trans* ACA shown in the schematic structure (c). The signals a', b', c', and d' correspond to the protons of *cis* ACA shown in (d). (c) and (d) represent the most reasonable molecular arrangement of EHAC–ACA, which is inferred from the chemical shift differences ( $\Delta\delta$ ) for *trans* ACA and *cis* ACA respectively. ....45

**Figure 3.13.** Photoresponsive character of the EHAC–ACA system at the molecular, nanostructural, and macroscopic scales. At the molecular scale, initially *trans* ACA binds strongly to EHAC and the net molecular arrangement is in a cylindrical geometry, which results in self-assembly into unilamellar vesicles at the nanoscale, and thereby results in a freely flowing low-viscosity fluid at the macroscopic scale. When UV-irradiated, at the molecular scale, *trans* ACA is photoisomerized to *cis* ACA. The arrangement of *cis* ACA with EHAC is altered to a truncated-cone geometry, thus dictating self-assembly into long wormlike micelles at the nanoscale, and thereby producing a highly viscoelastic fluid at the macroscopic scale. Finally, exposure to visible light reverts the ACA back from *cis* to its *trans* isomer, and thereby reverts the nanostructure and rheology to their initial states. ....47

**Figure 4.1.** Components of our photoresponsive vesicles: (a) the cationic amphiphile ODPI and (b) the anionic surfactant SDBS. Vesicles formed by combining ODPI and SDBS are transformed by UV light into spherical micelles. This is shown schematically in (c). ....52

**Figure 4.2.** (a) Reaction scheme for synthesis of hm-alginate. This involves amidation of sodium alginate with n-octylamine using the coupling agent EDC. <sup>1</sup>H NMR spectra of alginate (b) and hm-alginate (c). From the peaks of anomeric protons, the G content of alginate was calculated to be 51.2%.<sup>120</sup> The <sup>1</sup>H NMR spectrum of hm-alginate shows additional peaks (0.8 ~ 3.3 ppm, 4.9 ppm) which indicate the successful modification of alginate with octyl groups. From the ratio of methyl protons to anomeric protons, the degree of modification was obtained to be 23%.<sup>118</sup> .....55

**Figure 4.3.** Surface tension values are plotted over the range of concentrations of ODPI in 50 mM phosphate buffer. The plot shows the typical behavior expected for surfactants, *i.e.*, a drop in surface tension followed by a plateau. The CMC value obtained from the intersection point of the two regressed lines is 1.3mM. ....58

**Figure 4.4.** Phase behavior of ODPI–SDBS mixtures at a fixed total concentration of 1 wt% in aqueous buffer. Samples at ODPI : SDBS weight ratios between 2 : 8 and 4 : 6 show the presence of vesicles. The bluish tinge of these samples reflects light scattering from vesicles. At higher ODPI content (5 : 5 and 6 : 4), samples reveal a whitish precipitate. At even higher ODPI content (7 : 3 to 9 : 1) the samples separate into two liquid phases. ....59

**Figure 4.5.** Vesicle to micelle transition induced by UV light, as shown by visual observations and cryo-TEM images. The sample is a 1 wt% mixture of ODPI : SDBS = 3 : 7. (a) Initially (before UV exposure), the sample shows a bluish tinge and high turbidity (Photo 1). Under cryo-TEM, numerous unilamellar vesicles with diameters between 30 and 120 nm are seen. (b) After 1 h of UV irradiation, the sample is transformed into a transparent, yellowish solution that weakly scatters light (Photo2). Under cryo-TEM, spherical micelles with a size around 3–5 nm are seen. ....60

**Figure 4.6.** Mechanism for the UV-induced conversion of ODPI–SDBS vesicles to micelles. Initially, ODPI is cationic and it pairs with the anionic SDBS, giving a cylindrical geometry ( $p \sim 1$ ) that leads to vesicles. UV irradiation transforms ODPI into uncharged byproducts (pink tails). In this case, the lack of cationic species to pair with the anionic heads of SDBS implies a net cone shape ( $p \sim 1/3$ ), in turn leading to spherical micelles. The pink tails are embedded in the hydrophobic cores of these micelles. ....62

**Figure 4.7.** Vesicle gel formation by combining hm-alginate and ODPI–SDBS vesicles. (a) Molecular structure of hm-alginate. (b) Photographs and rheological data demonstrating the formation of a vesicle gel. A sample of 3 wt% ODPI : SDBS = 3 : 7 vesicles is initially a low-viscosity fluid (Photo 1) and shows Newtonian behavior in steady-shear rheology (Plot 1). This is combined with a 1 wt% solution of hm-alginate (Photo 2), which is moderately viscous, as shown by data from dynamic rheology (Plot 2). The mixture results in a vesicle gel that holds its weight in the inverted vial (Photo 3) and shows an elastic response in dynamic rheology (Plot 3). In plots 2 and 3, the elastic modulus  $G'$  (filled circles) and the viscous modulus  $G''$  (unfilled circles) are depicted as functions of the angular frequency  $\omega$ . ....65

**Figure 4.8.** Gel-to-sol transition of the photoresponsive vesicle gel upon UV irradiation. Data from steady-shear rheology (a) and dynamic rheology (b) are shown for a vesicle-gel obtained by mixing a 3 wt% ODPI : SDBS = 3 : 7 vesicles and a 1 wt% hm-alginate solution. In (a) the apparent viscosity is shown as a function of shear stress. In (b), the elastic modulus  $G'$  (filled circles) and the viscous modulus  $G''$  (unfilled circles) are plotted against the angular frequency  $\omega$ . Before UV irradiation (blue symbols), both sets of data indicate gel-like behavior of the sample. After UV irradiation, the sample is reduced to a thin fluid that exhibits purely viscous, Newtonian behavior. This is corroborated by the photos shown in the inset of (a). ....67

**Figure 4.9.** Mechanism for the UV-induced gel-to-sol transition. Initially, when ODPI–SDBS vesicles and hm-alginate are combined, a vesicle-gel is obtained, as shown in (a). Here, the hm-alginate chains are depicted with a blue backbone and red hydrophobic pendant groups. The hydrophobes embed in the bilayers of vesicles, also shown in red, *via* hydrophobic interactions. The result is that the vesicles becomes connected by the polymer chains into a network, which explains the gellike behavior. Upon UV irradiation, the vesicles are transformed into spherical micelles (b). These micelles enclose and sequester the hydrophobes on the polymer chains. As a result, the crosslinks in the network are eliminated and the sample is converted to a sol. ....68

**Figure 4.10.** Rheology of vesicle gels before and after UV irradiation: Effect of altering the hm-alginate concentration at a constant ODPI/SDBS vesicle concentration of 2 wt%. (a) Representative steady-shear rheology data for samples before (closed circles) and after 45 min of UV irradiation (open circles): 2 wt% hm-alginate (green symbols); 0.5 wt% hm-alginate (blue symbols). (b) From the steady rheology data, the zero-shear viscosity  $\eta_0$  is plotted against the hm-alginate concentration: before UV irradiation (closed red circles); after 45 min of UV irradiation (open red circles). ....70

**Figure 4.11.** Rheology of vesicle-gels before and after UV irradiation: Effect of altering the ODPI/SDBS vesicle concentration at a fixed hm-alginate concentration of 1 wt%. (a) Steady-shear rheology data for samples before (closed circles) and after 45 min of UV

irradiation (open circles) for vesicle concentrations of 1 wt% (blue symbols), 2 wt% (red), 3 wt% (green) and 4 wt% (cyan). (b) From the steady-shear data, the zero-shear viscosity  $\eta_0$  and the apparent yield stress (point of sharp drop in viscosity) are plotted against the vesicle concentration:  $\eta_0$  before UV irradiation (closed blue circles); yield stress before UV irradiation (closed green circles);  $\eta_0$  after 45 min of UV irradiation (open blue circles). .....71

**Figure 5.1.** Visual description and schematic of UV-induced photogelation of alginate. Sodium alginate (2.5 wt%) is combined with Sr-EGTA ( $\text{Sr}^{2+}$  source) and PAG-CD complex ( $\text{H}^+$  source). The resulting sample is a clear solution that flows freely in the petri dish, photo (a). (c) Upon exposure to UV light, the PAG is photolyzed and thereby releases  $\text{H}^+$  ions, which decrease the chelating efficiency of EGTA. Consequently,  $\text{Sr}^{2+}$  ions are released from the Sr-EGTA chelates and gel the alginate. As shown in the schematic,  $\text{Sr}^{2+}$  ions bind with adjacent alginate chains and form “egg-box” junctions, which act as physical crosslinks. As shown in photo (b), the final gel is transparent and strong enough to hold by one’s fingers. ....77

**Figure 5.2.** pH-dependent release of free  $\text{Sr}^{2+}$  ions is presented as a plot of mol% of released  $\text{Sr}^{2+}$  ions vs. pH. As pH decreases, mol% of released  $\text{Sr}^{2+}$  ions is increasing in a reverse sigmoidal pattern which has an onset pH of around 7.5. (data points obtained from MaxChelator)<sup>146</sup> .....82

**Figure 5.3.** pH sensitive gelation of alginate (2.5 wt%) and Sr-EGTA (40 mM) solution. 0.05 mM of phenol red was added to indicate the pH with different concentration of GDL (D-(+)-gluconic acid  $\delta$ -lactone). When GDL is added to aqueous alginate solution, GDL gradually undergoes hydrolysis and decreases pH. The final pH values of the solutions depend on the amount of GDL added. As a reference, the color of phenol red with different pH is presented on the bottom. ....83

**Figure 5.4.** Transparent photoacid generating system. Upon exposure to UV, transparent 30 mM PAG solution (photo 1) become opaque (photo 3) due to the hydrophobic byproducts of photodissociation. Meanwhile, the sample containing 30 mM PAG and 90 mM m- $\beta$ -CD remains transparent before (photo 2) and after (photo 4) UV irradiation. ..85

**Figure 5.5.** Dynamic rheology of the sample containing alginate 2.5 wt%, Sr-EGTA 40mM, and PAG-CD complex 30mM before (a) and after 20 min UV irradiation (b). (a) Before UV irradiation, the sample is freely flowing transparent solution as seen on photo 1. Dynamic rheology data confirms this visual observation and shows a viscous response with strong dependency of viscous modulus  $G''$  on frequency while elastic modulus  $G'$  is almost negligible. (b) After 20 min UV irradiation, the sample becomes a transparent gel which can be hold with fingers as seen on the photo 2. The dynamic rheology data also shows an elastic response (*i.e.*,  $G' > G''$ ) with both moduli being nearly independent on frequencies. ....87

**Figure 5.6.** Ungelling of an alginate photogel upon addition of chelating agent EGTA or base solution. Due to the physical nature of crosslinks rather than a covalent bond, the gel formed through photogelation can be ungelled by adding 100 ml of EGTA 0.3M ((a)-(c)) or NaOH 0.3M solution ((d)-(f)). When EGTA or NaOH solution was added, a gel turn into a non-viscous solution in 10 min with gentle shaking by chelating  $\text{Sr}^{2+}$  ions involving formation of egg-box junctions with alginate. ....88

**Figure 5.7.** The effect of Sr-EGTA concentration on the steady shear rheology of samples before UV irradiation (open circle) and after 20 min UV irradiation (closed circle). The concentration of alginate and PAG-CD complex was fixed at 2.5 wt% and 30 mM each. All samples showed clear transitions from a low-viscous solutions to gels with different yield stresses upon UV irradiation. As Sr-EGTA concentration increases from 5 mM to 60 mM, the yield stress of the gel increased from around 10 Pa to 60 Pa. ....89

**Figure 5.8.** The effect of PAG-CD complex concentration on the steady shear rheology of samples before UV irradiation (open circle) and after 20 min UV irradiation (closed circle). The concentration of Sr-EGTA, and alginate was fixed at 40 mM and 2.5 wt% each. Upon UV irradiation, samples with PAG-CD complex with concentrations of 15 – 60 mM shows clear transitions from a low-viscous Newtonian fluids to gels. However, the yield stress depends on the PAG-CD complex concentration, and increases from 10 Pa to 300 Pa as increasing its concentration. ....90

**Figure 5.9.** Fast growth of gel with UV exposure. (a) A sample with alginate 2.5 wt%, Sr-EGTA 40 mM, phenol red 0.05 mM, and PAG-CD complex 60 mM was placed in rectangular cuvette and exposed to UV. Upon UV exposure, the gel grew rapidly from the top, and the thickness became around 1.5 cm after 10 min UV irradiation. After 30 min the thickness reaches 2.3 cm and the gel was extruded from the container (b). The color boundary clearly represents the interphase of gel and solution layers. ....91

**Figure 5.10.** Slow photogelation of the alginate 2.5 wt% solution containing Sr-EGTA 40 mM and PAG 30 mM. With opaque photoacid generation system, *i.e.*, a sample without cyclodextrin, upon UV exposure, opaque gel layer was formed on the surface and prevent UV light penetrating deep into the solution. Before UV irradiation, the sample was non-viscous and transparent (a), while the sample after 20 min UV became a non-viscous opaque solution with fragments of an opaque gel layer (after UV, the sample was scraped with a spatula). ....92

**Figure 5.11.** Self-dissolution of a gel with time. In order to demonstrate photogelation and subsequent self-ungelling of our PR fluid, part of solution (circular with 1cm diameter) was gelled with UV irradiation (b). After 30 min of gentle shaking in dark, the circular gel was dissolved completely (c). ....93

**Figure 5.12.** Demonstration of flow control with photogelation of alginate. Initially, all three microchannels are open and solution is flowing freely (a). The flow is stopped and the photomask is placed (b), and then, a specific part (~ 3 mm length) of microchannel is exposed to UV (c) for 2 min. The irradiated part turns to a gel (yellow gel indicated by arrow) and block the channel A (d). Once the channel is blocked, it takes around 2 hours to reopen the channel through self-ungelling. This valving action can be done selectively; channel A and B are blocked (e), all channels are blocked (f). ....94

**Figure 5.13.** Spatial selective deposition of model material (red and green fluorescent beads) in the microchannel. (a) First, flow our PR fluid containing red fluorescent beads through the microchannel with three wells. Then, stop the flow and shine UV on specific area (corresponding to well A and C of (e)). The channel is flushed with water. Red fluorescent beads in alginate photogel are deposited in Well A and C selectively (b). (c - d) These steps are repeated with another PR fluid containing green fluorescent beads. Finally, the deposited gels are reinforced by flowing 30 mM SrCl<sub>2</sub> solution. (e)

Fluorescent microscope image clearly shows site-selective deposition of red and green fluorescent beads in the microchannel. (f) Deposited beads are released by flowing EGTA solution by ungelting Sr-alginate gel. ....96

**Figure 6.1.** Photoresponsive capsules made by alginate and ODPI solution. (a) Three drops of 2 wt% alginate solution turned into capsules in 1 wt% ODPI solution. (b) Alginate-ODPI capsules on the benchtop. (c) An alginate-ODPI capsule held by tweezers. (d) The liquid core squeezed out when ruptured by tweezers. ....102

**Figure 6.2.** Time-dependent rupture of the alginate ODPI capsules under UV light. ..103

**Figure 6.3.** Photoresponsive micro capsules were ruptured by UV. ....104

**Figure 6.4.** Reversible transition of MGCB between non-ionized (left) and ionized (right) form.<sup>161</sup> When MGCB is ionized, it gives OH<sup>-</sup> ions and increases the pH of the solution.

.....106

# Chapter 1

## Introduction and Overview

---

### 1.1. Problem Description and Motivation

Self-assembly refers to a process whereby discrete components such as molecules and nanoparticles are spontaneously organized into ordered macroscopic structures.<sup>1</sup> This process is thermodynamically driven, *i.e.*, the organized structures at the equilibrium state have a minimum in the system's free energy.<sup>1</sup> The technical importance of self-assembly relies on the fact that the organized structures can be controlled by modulating the thermodynamic forces which arise from specific interactions or external stimuli such as magnetic fields, electric fields, and light. In this sense, directed self-assembly, the process whereby an intrinsically self-assembling system is aided or modulated using directing agents, external fields, or templates, has been the subject of much interest due to its practical applications.<sup>2</sup> Directed self-assembly has been frequently exploited to design stimuli responsive systems because the self-assembled structural change at the nanoscale or microscale can induce dramatic changes in macroscopic properties such as flow, surface, mechanical, and optical properties.

In particular, light-directed (photoresponsive) self-assembly systems have promising technological applications due to the advantages of using light as an external stimulus. Light is easy to control and can be directed at a precise point with a resolution on the order of microns. Thus, photoresponsive systems may be useful in fabrication of



microstructures,<sup>3,4</sup> site-selective controlled release,<sup>5</sup> and microscale or nanoscale devices.<sup>6,7</sup> However, most photoresponsive fluids that have been developed so far require complicated chemical modification with suitable chromophores.<sup>3,5,8-15</sup> For this reason, widespread applications of photoresponsive fluids have not been realized. In this study, we are working toward simple classes of photoresponsive systems that require no special synthesis and can thereby be easily replicated in any laboratory from inexpensive chemicals.

## **1.2. Proposed Approach**

In this dissertation, we will describe three different concepts for photoresponsive systems: reversible photorheological (PR) fluids, photoresponsive vesicles and vesicle-gels, and light-activated fluidic valve in microchannels.

### **1.2.1. Reversible Photorheological Fluids**

Our initial study, presented in Chapter 3, is on reversible photorheological (PR) fluids, as depicted in Figure 1.1. PR fluids are those whose rheological properties, such as viscosity, can be tuned by light irradiation.<sup>16</sup> This work is motivated by the need for simple, low-cost PR fluids that can be easily created using inexpensive, commercially available ingredients and that show substantial, reversible changes in rheology upon exposure to different wavelengths of light. Towards this end, we report a class of photoreversible PR fluids prepared by combining the azobenzene derivative 4-azobenzene carboxylic acid (ACA) (in its salt form) with the cationic surfactant erucyl bis(2-hydroxyethyl)methyl ammonium chloride (EHAC). We show that certain aqueous

mixtures of EHAC and ACA, which are low viscosity solutions at the outset, undergo nearly a million-fold increase in viscosity when irradiated with UV light. The same solutions revert to their initial viscosity when subsequently exposed to visible light. Using an array of techniques including UV-VIS and NMR spectroscopies, small-angle neutron scattering (SANS) and cryo-transmission electron microscopy (cryo-TEM), we have comprehensively characterized these PR fluids at the molecular, nanostructural, and macroscopic scales. Initially, EHAC–ACA are self-assembled into unilamellar vesicles, which are discrete container structures and give the sample a low viscosity. Upon exposure to UV light, ACA undergoes a *trans* to *cis* photoisomerization, which alters the geometry of the EHAC–ACA complex. In turn, the molecules self-assemble into a different structure, *viz.*, wormlike micelles, which are long, entangled chains and impart a high viscosity to the sample. The above changes in viscosity are repeatable, and the sample can be reversibly cycled back and forth between low and high viscosity states.

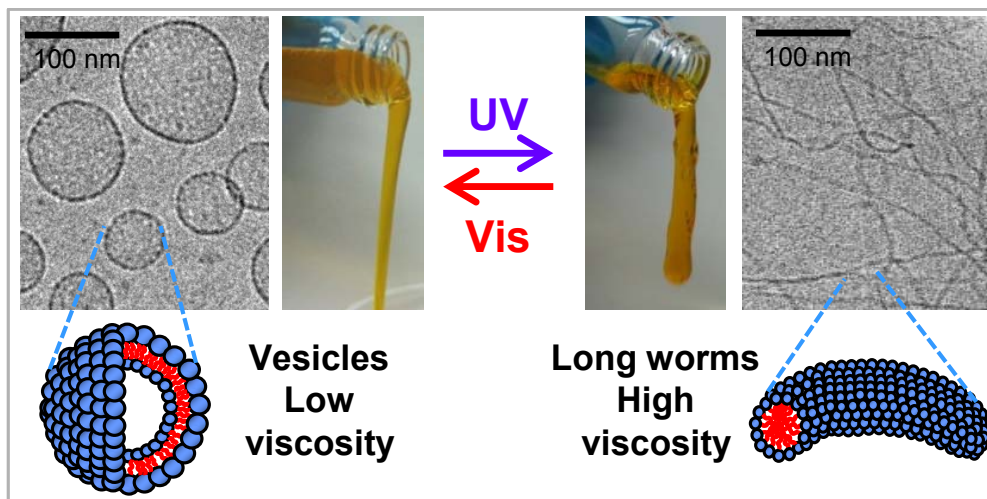


**Figure 1.1.** Reversible PR fluid described in Chapter 3 based on the structure transition between vesicles and wormlike micelles.

### 1.2.2. Photoresponsive Vesicles and Vesicle-gels

In Chapter 4, we present a new class of photoresponsive vesicles based on two inexpensive and commercially available amphiphiles. While several photoresponsive vesicle formulations have been reported, these systems are rather complex as they rely on special light-sensitive amphiphiles that require complicated chemical synthesis.<sup>5,8,17-21</sup> In this study, we report a new class of photoresponsive vesicles based on two inexpensive and commercially available amphiphiles. Specifically, we employ p-octyloxydiphenyliodonium hexafluoroantimonate (ODPI), a cationic amphiphile that finds use as a photoinitiator, and a common anionic surfactant, sodium dodecylbenzenesulfonate (SDBS). Mixtures of ODPI and SDBS form “catanionic” vesicles<sup>22,23</sup> at certain molar ratios due to ionic interactions between the cationic and anionic headgroups. As seen in Figure 1.2, when irradiated with UV light, ODPI loses its charge and, in turn, the vesicles are converted into micelles due to the loss of ionic interactions. In addition, a mixture of these photoresponsive vesicles and a hydrophobically modified biopolymer gives a photoresponsive vesicle-gel. The vesicle-gel is formed because hydrophobes on the polymer insert into vesicle bilayers and thus induce a three-dimensional network of

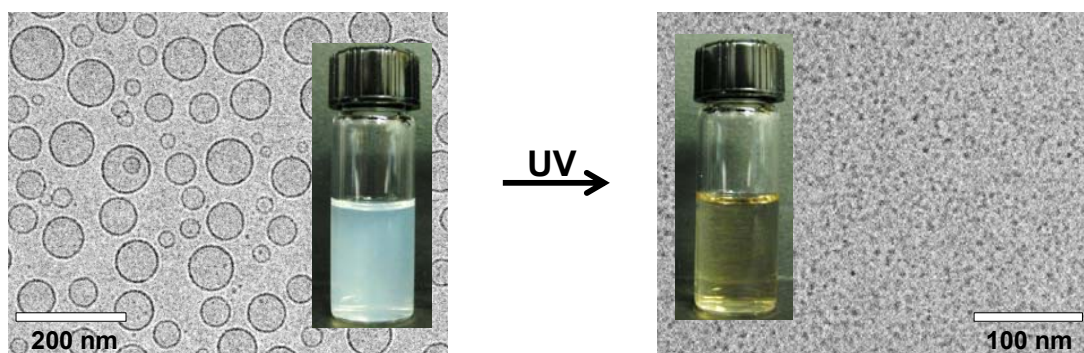


**Figure 1.2.** Photoresponsive vesicles described in Chapter 3, showing transition from vesicles to spherical micelles upon UV exposure.

vesicles connected by polymer chains.<sup>24</sup> Upon UV irradiation, the network is disrupted because of the conversion of vesicles to micelles, with the polymer hydrophobes getting sequestered within the micelles. As a result, the gel is converted to a sol, which manifests as a 40,000-fold light-induced drop in sample viscosity.

### 1.2.3. Light-Activated Fluidic Valve

In Chapter 5, we demonstrate a potential application of PR fluids that leverages the spatial selectivity of light. The objective is flow control within fluidic devices, *e.g.*, to stop the flow at a precise location within a network of fluidic channels (valving action). Despite a variety of existing PR fluid formulations, current fluids are not suitable for this application. Here, we report a PR fluid based on the biopolymer, alginate, that could be useful in this context. The fluid is composed entirely of commercially available components: alginate, a photoacid generator (PAG) as a photo-trigger, and a chelated complex of divalent strontium ( $\text{Sr}^{2+}$ ) ions (Sr-EGTA). Upon exposure to UV, the PAG dissociates to give  $\text{H}^+$  ions, which induce the release of free  $\text{Sr}^{2+}$  ions from the Sr-EGTA. The released  $\text{Sr}^{2+}$  ions then self-assemble with the alginate chains to give a nanostructured gel<sup>25</sup> with a high gel modulus ( $\sim 2000$  Pa). To test the possibility of fluidic valving, we flow the above fluid through a microchannel and expose a specific point in the channel to UV light. At that point, alginate is converted into a strong gel in a few minutes, and we find that the resulting gel blocks the flow as shown in Figure 1.3. When the UV light is removed, the gel is gradually diluted by the flow and the channel reopens. We have thus shown a new kind of light-activated fluidic valve; note that the

above concept relies entirely on physical (non-covalent) bonds, *i.e.*, on self-assembly, rather than on covalent crosslinking of dissolved monomers or polymers.

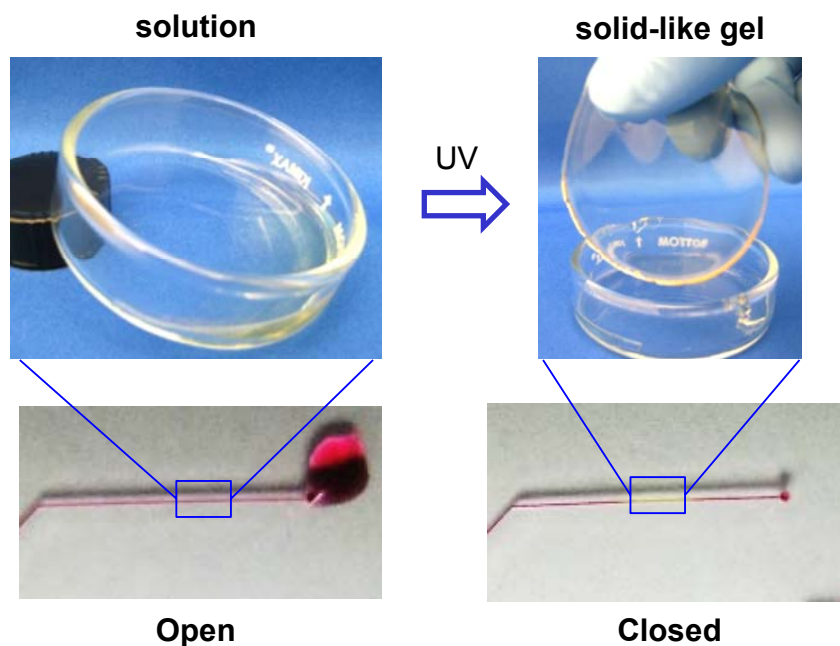


**Figure 1.3.** A light-activated fluidic valve in Chapter 5.

### 1.3. Significance of This Work

The significance of this work is that it seeks to overcome current limitations in the field of photoresponsive fluids. In our first study, we report a simple route to photoreversible PR fluids that exhibit significant viscosity changes upon exposure to light with different wavelengths. These PR fluids can be easily replicated in any industrial or academic lab. Recently, our collaborators at Ohio State University incorporated our PR fluids as smart drag-reducing fluids in recirculating systems for district heating and cooling.<sup>26</sup>

Next, photoresponsive vesicles presented in Chapter 4 are developed using a simple and low-cost route, and these represent a convenient alternative to previously reported systems that require multiple steps of chemical synthesis. In addition, we demonstrate vesicle-gels by combining photoresponsive vesicles with a hydrophobically modified biopolymer. The photoresponsive vesicle-gels undergo gel-to-sol transition upon UV exposure. Because the gel-to-sol transition is accompanied by the disruption of vesicles, the above gel could also be envisioned as an injectable material for light-controlled delivery of drugs or other payloads.

In Chapter 5, we widen the applicability of PR fluids by overcoming the limitation of currently available PR formulations, which is a weak strength in the gel state. Specifically, we have developed another simple class of PR fluids that undergo a transition from a non-viscous liquid to a very stiff gel (via non-covalent bonds) upon exposure to UV light. With these fluids, we successfully demonstrate their use in a light-activated fluidic valve. The same fluids can also serve as a platform for the site-specific deposition and release of materials in microfluidic channels.

We hope that the availability of new, simple photoresponsive fluids will help to popularize these fluids both in academia and industry. We anticipate that the new directions we set forth in this field will be further explored by other researchers, and this will ultimately lead to practical applications in both existing as well as emerging technologies.

## Chapter 2

### Background

---

This dissertation is focused on photoresponsive self-assembled fluids whose rheological properties or self-assembled structures can be tuned by light. In this chapter we will discuss the basics of amphiphile self-assembly in aqueous media and the photochemistry of some photoresponsive molecules such as the azobenzenes. Then, we will describe the characterization techniques used in this work such as rheology, small-angle neutron scattering (SANS), and UV-VIS spectroscopy.

#### 2.1. Self-Assembly of Surfactants

Surfactants (also referred to as detergents or lipids) are amphiphilic molecules with distinct hydrophilic (head) and hydrophobic (tail) portions. Typically, the hydrophobic tail is composed of aliphatic or aromatic hydrocarbons and the hydrophilic head group is made up of ionic molecules (anionic, cationic, or zwitterionic) or nonionic molecules (multiple units of ethylene oxide, glycerine, sucrose, *etc.*). Typical surfactant molecules are illustrated in Figure 2.1 and are denoted with blue hydrophilic heads and red hydrophobic tails. Because of the amphiphilic nature of surfactant molecules, they spontaneously organize into specific structures in a nonpolar solvent (like hydrocarbons) or a polar solvent (like water). This process of spontaneous organization is known as self-assembly. As we are interested in aqueous photoresponsive systems in this proposal, we will mainly describe the self-assembly of surfactants in water. Self-assembly is a

thermodynamically driven process *i.e.*, the self-assembled structure that is formed at equilibrium is dictated by the minimization of the Gibbs free energy of the system. The dominant driving force for this process is the hydrophobic effect, *i.e.*, the gain in entropy of water molecules when surfactant hydrophobes are separated from water and buried in a micelle. The most common self-assembled structure of surfactant molecules is the micelle. There exists a threshold concentration known as the critical micelle concentration (CMC) for the formation of micelles.

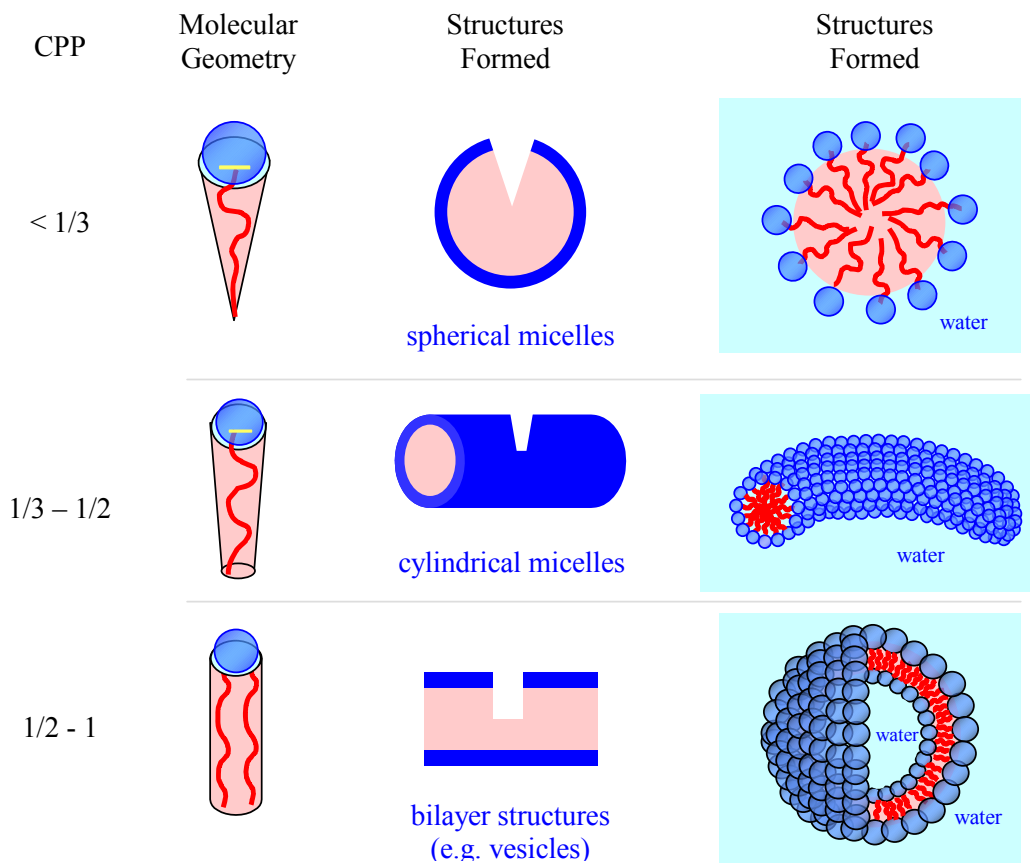


**Figure 2.1.** Schematics depicting the connection between the geometry of amphiphilic molecules and the structures they form in water. The hydrophilic heads of the amphiphiles are shown in blue and the hydrophobic tails in red.



As mentioned above, self-assembly of surfactants is governed by thermodynamic factors such as temperature, concentration, ionic strength, and the physical properties of the surfactant molecule itself. One of the critical parameters that can control the size and shape of self-assembled structures is the geometry of the surfactant molecule. This geometry depends on the structure and charge of the surfactant. Based on the geometry, the surfactant can assemble into spherical micelles, cylindrical micelles, or bilayers and vesicles. The size of these structures also covers a wide spectrum, ranging from a few nanometers to several microns. The correlation between the molecular geometry and self-assembled structures is generally quantified by a parameter known as the critical packing parameter (CPP),<sup>1</sup> which is defined as:

$$\text{CPP} = \frac{a_{\text{tail}}}{a_{\text{hg}}} \quad (2.1)$$

where  $a_{\text{tail}}$  is the average cross-sectional area of the hydrophobic tail and  $a_{\text{hg}}$  is the effective cross-sectional area of the hydrophilic headgroup.<sup>27-29</sup> The larger the CPP, the greater the curvature of the resulting self-assembled structure, as described in Figure 2.1. In particular, surfactants with a  $\text{CPP} = 1/3$  (corresponding to a cone shape) form spherical micelles, whereas those with a  $\text{CPP} = 1/2$  (corresponding to a truncated cone geometry) form cylindrical micelles. Finally, for surfactants with a cylindrical geometry, *i.e.*, areas of the head and tail are equal ( $a_{\text{tail}} \approx a_{\text{hg}}$ ) and a  $\text{CPP} = 1$ , vesicles and bilayers are the favored structures.

## 2.2. Wormlike Micelles

As mentioned above, surfactants self-assemble into cylindrical micelles when the  $\text{CPP} = 1/2$ . In some cases, these cylindrical micelles can grow and form very long, flexible

chains and they are referred to as wormlike or threadlike micelles (Figure 2.2).<sup>30,31</sup> In general, the diameters of these wormlike micelles are similar to spherical micelles (5-10 nm) while the end-to-end (contour) length of wormlike micelles can be as long as a few microns, *i.e.*,  $> 1,000$  nm.<sup>31-35</sup> Similar to a solution of flexible polymers, the wormlike micelles tend to become entangled in a transient network due to their long length (Figure 2.2). In turn, the solution becomes highly viscous and viscoelastic. The term viscoelastic implies that the solution has both viscous (or liquid-like) character and elastic (or solid-like) character at the same time. The viscoelasticity of the solution causes it to show the rod climbing phenomenon upon stirring and bubbles remain trapped in the sample.

Another characteristic property of wormlike micelles is their flow-birefringence *i.e.*, when a sample vial of a wormlike micelle solution is shaken, bright streaks of light are observed under crossed-polarizers. This phenomenon is called birefringence, also known as double refraction, and it refers to a difference in refractive indices along mutually perpendicular directions. It is a characteristic property of anisotropic materials

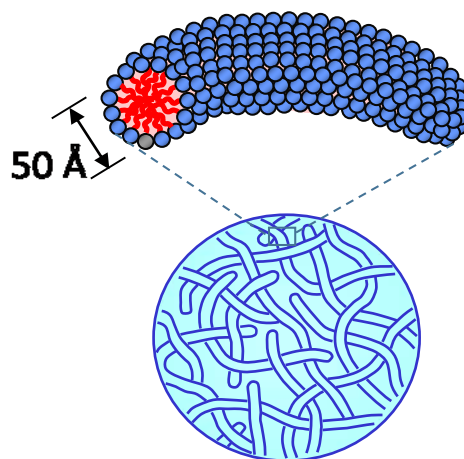


**Figure 2.2.** Schematic showing the structure of an individual wormlike micelle as well as the entanglement of micellar chains into a transient network.

such as liquid crystals.<sup>36</sup> In the case of wormlike micelles, flow or shear induces the alignment of the chains along the direction of shear, and thus the sample temporarily becomes anisotropic. Note that the birefringence disappears quickly after the shear is stopped, *i.e.*, the chains go back to a randomly oriented state at rest and the solution becomes completely isotropic.

Wormlike micelles can be formed from several different types of surfactants. Most academic studies have focused on cationic surfactants. In particular, long tailed cationic surfactants such as erucyl bis(2-hydroxyethyl)methyl ammonium chloride (EHAC) are interesting in that they can form exceptionally long wormlike micelles.<sup>37,38</sup> EHAC is an amphiphilic molecule with a 22-carbon length hydrophobic tail and a cationic head group. Generally, due to the strong electrostatic repulsions between head groups, the head groups of ionic surfactants like EHAC have a large effective area. Thus EHAC favors a cone-like shape ( $CPP = \frac{1}{3}$ ), and accordingly, it will self-assemble into spherical micelles. However, when salt is added to an EHAC solution, due to the screening of electrostatic repulsions induced by the added ions, the head group areas are reduced and the CPP is increased from  $\frac{1}{3}$  to  $\frac{1}{2}$ . In turn, the spherical micelles grow into wormlike micelles.

While the growth of ionic worms can be induced by any kind of salts, aromatic salts can induce a growth of worms at very low concentrations compared to inorganic salts like sodium chloride (NaCl). An example of an effective aromatic salt for cationic surfactants like EHAC is sodium salicylate (NaSal). As shown in Figure 2.3, the

salicylate counterions bind strongly to cationic micelles, with their hydrophobic phenyl ring inserted in the hydrophobic interior of the micelle. At the same time, the carboxylate anions from salicylate bind to the cationic headgroups of EHAC, resulting in neutralization of the surface charge. Thereby, the repulsions and effective areas of the headgroups are reduced. Consequently, NaSal promotes growth of EHAC worms at very low concentrations. Organic salts like NaSal are referred to as “binding salts” due to their ability to bind to micelles. In Chapter 3, we will show that salts of azobenzene carboxylic acid can also effectively bind to EHAC micelles.

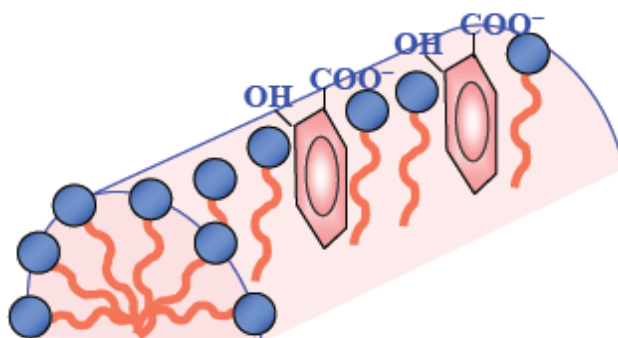


**Figure 2.3.** Binding of salicylate (o-hydroxy benzoate) counterions to cationic micelles. The aromatic ring is embedded into the hydrophobic interior of the micelle shown in red. The hydrophilic groups (OH and COO<sup>-</sup>) protrude out of the micelle, shown in blue.<sup>39</sup>

### 2.3. Photochemistry of Azobenzene

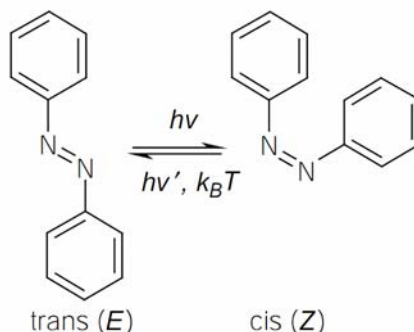


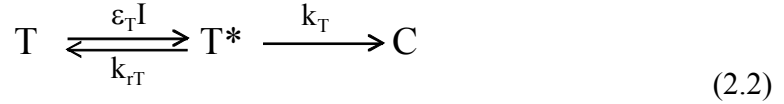
**Figure 2.4.** Photoisomerization of azobenzene upon irradiation by light. The *cis* to *trans* isomerization can also be induced by heat.

Azobenzene, one of the most common photoswitchable molecules, has been incorporated in our photoresponsive system (Chapter 3) because of the following reasons: it is thermally stable, provides a clean and efficient reversible photoisomerization without side reactions, shows a large dipole moment and geometry change, and it is easy to monitor using an UV-Vis spectrometer. As shown in Figure 2.4, azobenzene has an N-N double bond with a phenyl group on each nitrogen. Azobenzene compounds generally have two absorption peaks: a high-intensity peak at UV wavelengths and a low intensity peak in the visible range of the wavelength spectrum.<sup>40,41</sup> When *trans*-azobenzene is irradiated with UV light ( $330 < \lambda < 380$  nm), it isomerizes to its *cis* form with the photostationary state corresponding to approximately 80% *cis* and 20% *trans*. On the other hand, when *cis*-azobenzene is irradiated with visible light ( $\lambda > 420$  nm), it isomerizes back to a mostly *trans* form.<sup>40,41</sup>

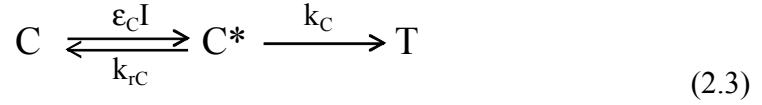
Because the *trans* isomer is more stable by ~50 kJ/mol, the *cis* to *trans* transition of azobenzene can also be carried out by heat instead of light.<sup>41</sup> In order to design a photoswitchable system, the stability of the *cis* isomer is a matter of concern. If the stability of the *cis* form is not sufficient, the thermal isomerization of *cis* to *trans* will occur rapidly (within milliseconds) and it becomes hard to maintain a *cis*-isomer-rich state. This thermal isomerization rate shows strong dependency on the substituents present in the molecule. Based on the nature of substituents, azobenzenes are classified into three classes; azobenzene-type (yellow), aminoazobenzene-type (orange), and pseudo-stilbene-type (red).<sup>40,41</sup> Usually, the *cis* isomers of aminoazobenzenes and pseudo-stilbenes are unstable compared to azobenzenes and have a lifetime of minutes or less.<sup>42</sup> Also, when bulky substituent groups are attached on the azobenzene moiety, the lifetime of the *cis* isomer tends to increase.<sup>42</sup>

When a solution of azobenzenes is exposed to light of a particular wavelength, the system will reach a photostationary state, where the compositions of *cis* and *trans* do not change with further irradiation of light. This state is an equilibrium state where the rate of the *trans* to *cis* photoisomerization becomes equal to the rate of the *cis* to *trans* isomerization (photo and thermal). The composition at the photostationary state depends on the quantum yields and the thermal isomerization rate constant. The quantum yields vary according to the wavelength and solvent properties and the thermal isomerization rate constant also depends on the temperature.<sup>42,43</sup>

The photoisomerization of azobenzene can be considered a two-step reaction. First, the *trans* isomer T absorbs a photon and becomes an excited species T\*, while the reverse reaction from T\* to T also takes place. Second, the excited molecule can turn into the *cis* isomer, C.<sup>44</sup> The reaction can be described as follows:



$\varepsilon_T$  is the molar absorption coefficient and  $I$  is the intensity of exposed light. The rate constant for  $T \rightarrow T^*$  corresponds to  $\varepsilon_T I$ . The rate constant of  $T^* \rightarrow T$  is  $k_{rT}$  and that of  $T^* \rightarrow C$  is  $k_T$ . Similarly, a reverse photoisomerization reaction takes place at the same time and can be expressed as follows:



In the above reaction schemes, thermal relaxation was ignored. When we compare the time scales for the photo and thermal isomerizations, this assumption is reasonable. The thermal isomerizations of azobenzenes used in our study are slow (about 4 days). For the photoisomerization, it takes less than 2 h to reach photostationary state. The time-dependent concentration of isomers can be expressed as follows:

$$\frac{\partial[T]}{\partial t} = -\varepsilon_T I[T] + k_{rT}[T^*] + k_C[C^*] \quad (2.4)$$

$$\frac{\partial[T^*]}{\partial t} = \varepsilon_T I[T] - k_{rT}[T^*] - k_T[T^*] \quad (2.5)$$

$$\frac{\partial[C]}{\partial t} = -\varepsilon_C I[C] + k_{rC}[C^*] + k_T[T^*] \quad (2.6)$$

$$\frac{\partial[C^*]}{\partial t} = \varepsilon_C I[C] - k_{rC}[C^*] - k_C[C^*] \quad (2.7)$$

We can assume quasi steady state, *i.e.*, the concentrations of excited species, T\*, C\*, are small and  $\frac{\partial[T^*]}{\partial t} = 0$ ,  $\frac{\partial[C^*]}{\partial t} = 0$ . Then the rate of formation of *trans* isomer T is:

$$\begin{aligned}\frac{\partial[T]}{\partial t} &= -\varepsilon_T \left( \frac{k_T}{k_{rT} + k_T} \right) I[T] + \varepsilon_C \left( \frac{k_C}{k_{rC} + k_C} \right) I[C] \\ &= -\varepsilon_T \varphi_T I[T] + \varepsilon_C \varphi_C I([T]_0 - [T])\end{aligned}\quad (2.8)$$

Here,  $\varphi_T$  and  $\varphi_C$  correspond to the quantum yields of the *trans* to *cis* and *cis* to *trans* reactions, respectively. The quantum yield is the ratio of the number of molecules isomerized to the number of photons absorbed. We assume single-photon excitation, and that one molecule can absorb only one photon. The apparent rate constant for the *trans* to *cis* photoisomerization can then be expressed as  $\varepsilon_T \varphi_T I$ , which means that to achieve fast photoisomerization, we need photoresponsive molecules with large absorption coefficients and high quantum yields, and also we require high intensity. As for the intensity, when irradiated light penetrates through the sample, the intensity of light will exponentially decrease due to absorption by the photoresponsive molecules. In the above equations,  $I$  is the local intensity of light. Thus, to achieve fast and homogeneous photoisomerization, we either need a sample of minimal thickness or we must use stirring.

At the photostationary state,  $\frac{\partial[T]}{\partial t} = 0$ , the conversion can be expressed as follows:

$$Conv. = \frac{[T]_0 - [T]}{[T]_0} = \left( 1 + \frac{\varepsilon_C \varphi_C}{\varepsilon_T \varphi_T} \right)^{-1}\quad (2.9)$$

Note that this conversion is independent of the intensity of light. The molar absorption coefficient and quantum yield depend on the wavelength of light. Therefore, by changing the wavelength, the direction of photoisomerization can be controlled.



## 2.4. Characterization Technique – I: Rheology

Rheology is defined as the study of the deformation and flow in materials.<sup>45,46</sup> Rheological measurements are useful in characterizing complex fluids and soft materials and they help to correlate the microstructure to the macroscopic flow properties of the material.<sup>36</sup> These measurements are usually performed under steady or dynamic shear. In the case of steady shear, the sample is subjected to a constant shear-rate  $\dot{\gamma}$ , and the response is measured as a shear-stress  $\sigma$ . The ratio of shear stress to shear rate gives the (apparent) viscosity  $\eta$ . A plot of  $\eta$  vs. shear rate is called the flow curve of the material. Several fluids show a Newtonian behavior in their flow curve at low shear rates *i.e.*, in this regime, the viscosity is *independent* of shear rate. The viscosity in this “Newtonian plateau region” is the zero-shear viscosity  $\eta_0$  and it corresponds to the viscosity of the sample in the limit of  $\dot{\gamma} \rightarrow 0$ .<sup>46</sup>

Rheological experiments can also be conducted in dynamic or oscillatory shear, where a sinusoidal strain  $\gamma = \gamma_0 \sin(\omega t)$  is applied to the sample. Here  $\gamma_0$  is the strain-amplitude (*i.e.*, the maximum applied deformation) and  $\omega$  is the frequency of the oscillations. The sample response will be in the form of a sinusoidal stress  $\sigma = \sigma_0 \sin(\omega t + \delta)$  which will be shifted by a phase angle  $\delta$  with respect to the strain waveform. Using trigonometric identities, the stress waveform can be decomposed into two components, one in-phase with the strain and the other out-of-phase by  $90^\circ$ :

$$\sigma = \gamma_0 \left[ G'(\omega) \sin(\omega t) + G''(\omega) \cos(\omega t) \right] \quad (2.10)$$

where  $G'$  is the **Elastic** or **Storage Modulus** and  $G''$  is the **Viscous** or **Loss Modulus**. The dynamic experiment ultimately yields plots of  $G'$  and  $G''$  as functions of  $\omega$  (usually plotted on a log-log scale), which are collectively called the frequency spectrum of the material. Such a plot provides the viscoelasticity of the material as it varies with timescale, which in turn is a signature of the microstructure.<sup>45</sup>

The physical interpretation of  $G'$  and  $G''$  are as follows. The elastic modulus  $G'$  is obtained from the in-phase component of the stress, and provides information about the elastic nature of the material.  $G'$  is also called the storage modulus since elastic behavior implies the storage of deformational energy. The viscous modulus  $G''$  is extracted from the out-of-phase component of the stress, and it characterizes the viscous nature of the material.  $G''$  is also known as the loss modulus since viscous deformation results in the dissipation of energy.  $G'$  and  $G''$  are meaningful only if these values are independent of strain amplitude. At certain range of strain amplitude, which is called the “linear viscoelastic” or LVE regime, the stress response is linearly proportional to the strain and constant  $G'$  and  $G''$  are obtained regardless of the strain amplitude. In other words, in that case,  $G'$  and  $G''$  will be independent of strain amplitude and will be functions only of the frequency  $\omega$  – the moduli will then be true material properties.

An important advantage of dynamic rheology is that characterization of the material’s microstructure is possible without disrupting it. Since only small-amplitude strains are used (within the LVE regime), the net deformation imposed on the sample is minimal. Therefore, the linear viscoelastic moduli reflect the microstructure present in

the sample at rest.<sup>45</sup> In contrast, steady-shear rheology measures material properties under continuous flow conditions, which correspond to relatively large deformations. Therefore, dynamic rheological parameters can be correlated with static microstructures and steady-shear rheological measurements correspond to flow-induced changes in the microstructure.

## **2.5. Characterization Technique – II: SANS**

Scattering techniques are very useful for probing the structures of materials on the micro- and nanometer scale.<sup>47</sup> The basic principle behind these techniques is that the intensity of scattered radiation from a structured fluid is a function of the size, shape, and interactions of the “particles” present. We will use small-angle neutron scattering (SANS) to study our samples as it is useful in probing structure over size scales on the order of a few nanometers. Since a neutron beam carries low energy compared to X-ray, it doesn’t affect the structure of the investigated sample. Thus, SANS in particular is useful for structural investigation of soft materials. In SANS, the contrast between the solvent and the “particles” is achieved by switching the hydrogen in the solvent molecules with deuterium (for example using D<sub>2</sub>O instead of H<sub>2</sub>O). SANS experiments require a nuclear reactor to generate neutrons and we are fortunate to have one of the premier facilities for SANS nearby at the National Institute of Standards and Technology (NIST) in Gaithersburg, MD.

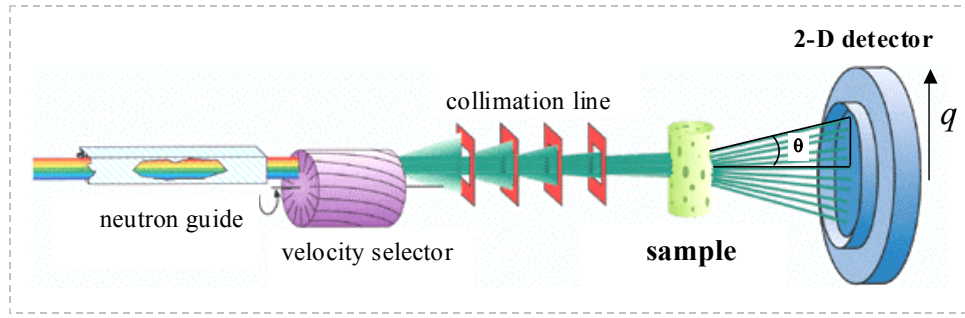


**Figure 2.5.** Schematic of a SANS experiment (adapted from [www.gkss.de](http://www.gkss.de)).

The basic geometry of a SANS experiment is illustrated in Figure 2.7. Neutrons from a nuclear reactor pass through a velocity selector set for a particular wavelength and wavelength spread. These neutrons then pass through several collimating sections and into the sample placed in the sample chamber. Finally, a 2-D detector collects the neutrons scattered by the sample. Using calibration standards, the collected 2-D data is corrected and placed on an absolute scale. This data is then spherically averaged to give a plot of the scattered intensity  $I$  vs. wave vector  $q$ . The wave vector is defined as:<sup>47</sup>

$$q = \frac{4\pi}{\lambda} \sin\left(\frac{\theta}{2}\right) \quad (2.11)$$

Here,  $\lambda$  is the wavelength of the incident radiation and  $\theta$  is the scattering angle.  $q$  can be considered an inverse length scale, with high  $q$  corresponding to small structures, and low  $q$  to large structures in the sample.

For a structured fluid containing  $n_p$  particles per unit volume, the intensity  $I(q)$  can be expressed as follows:<sup>47</sup>

$$I(q) = n_p \cdot P(q) \cdot S(q) \quad (2.12)$$

where  $P(q)$  is referred to as the form factor and  $S(q)$  as the structure factor.  $S(q)$  is the scattering that arises from *interparticle* interactions and thus reflects the interactions between particles in the sample.  $P(q)$  is the scattering that arises from *intraparticle* interferences, and thus is a function of the particle size and shape. When the particles are in dilute solution (*i.e.*,  $n_p$  is small), the interparticle interactions become negligible and therefore the structure factor  $S(q) \rightarrow 1$ . The SANS intensity  $I(q)$  can then be modeled purely in terms of the form factor  $P(q)$ , *i.e.*, the sizes and shapes of the particles. The form factors for several different particle geometries have been developed, which can be fit to the data to extract structural information about the particles.

## 2.6. Characterization Technique – III: UV-Vis Spectroscopy

UV-Vis absorption spectroscopy is an analytical technique used to study molecules that adsorb radiation in the ultraviolet (200 to 400 nm) and visible (400 to 800 nm) regions of the electromagnetic radiation spectrum.<sup>48</sup> Generally, when a molecule absorbs radiation, the energy gained is proportional to the energy of the incident photons. In the UV-Vis range, the absorbed energy typically acts to move electrons into higher energy levels *i.e.*, excited state.<sup>48</sup> A given molecule does not absorb energy continuously throughout a spectral range because the absorbed energy is quantized; therefore, the molecule will absorb at the wavelengths that provide the exact amount of energy necessary to promote it to the next higher energy level.<sup>48</sup> Therefore, each compound will have a unique UV-Vis absorption spectrum. UV-Vis can thus serve as a convenient analytical technique for a variety of compounds, especially those that have an aromatic group.

A typical UV-Vis experiment involves placing a solution containing a low concentration of solute ( $10^{-5}$  to  $10^{-2}$  M) in a cuvette, which is then placed in the sample cell of a UV-Vis spectrometer. Light is broken down into its component wavelengths in the spectrometer and passed through the sample. The absorption intensity is measured for each wavelength and a UV-Vis spectrum (plot of absorbance vs. wavelength) is produced for the sample. UV-Vis spectroscopy can be used as a quantitative analytical method to determine the concentration of a solute in solution. This can be done using the Beer-Lambert law:<sup>48</sup>

$$A = \varepsilon \cdot c \cdot \ell \quad (2.13)$$

where  $A$  is the measured absorbance at a particular wavelength,  $c$  is the concentration of the solute in mol/L,  $\ell$  is the path length of the sample, and  $\varepsilon$  is the molar extinction coefficient or molar absorptivity at that wavelength. Basically, Beer-Lambert law assumes that absorption of photons occurs linearly with path length. UV-Vis spectroscopy has an important role to play in the study of photoresponsive systems. For example, different photoisomers have different UV-Vis spectra, enabling their easy identification. Also, the peak absorption wavelength is generally the wavelength at which the compound is irradiated to induce a phototransition.

## Chapter 3

### Reversible Photorheological Fluids

---

The results presented in this chapter have been published in the following journal article: H. Oh, A. M. Ketner, R. Heymann, E. Kesselman, D. Danino, D. E. Falvey and S. R. Raghavan, “A simple route to fluids with photo-switchable viscosities based on a reversible transition between vesicles and wormlike micelles.” *Soft Matter*, 9, 5025-5033 (2013)

#### 3.1. Introduction

Scientists have recently exhibited a growing interest in “smart” fluids or materials, *i.e.*, those that undergo a macroscopic change in property in response to an external stimulus.<sup>49,50</sup> A stimulus of particular interest has been light. Compared to other stimuli such as temperature, pH, or electric fields, light has many advantages.<sup>42,51</sup> Light can be directed from a distance at a precise location (with micron-scale resolution), and light sources at distinct wavelengths are widely available. A range of light-responsive “smart” materials are being studied, and one set of material properties that researchers are looking to modulate are the rheological or flow properties, such as viscosity.<sup>9,49,52</sup> Fluids with light-tunable rheology can be termed photorheological (PR) fluids.<sup>16,52</sup> Due to the spatial selectivity of light, PR fluids may be particularly useful in microscale or nanoscale devices such as microrobots,<sup>53</sup> lab-on-a-chip devices,<sup>7</sup> or as micropatternable biomaterials.<sup>3</sup> For many applications, reversibility of the PR effect is key, *i.e.*, the fluid should be capable of being cycled between low and high viscosity states by exposure to

different wavelengths of light. For example, reversible PR fluids could be useful in recirculating systems<sup>26,54</sup> if they could be switched between a state enabling drag-reduction and one that permits rapid heat transfer.

A variety of PR fluids have been developed so far, but they have mostly relied on new, original classes of photoresponsive organic molecules that were synthesized in the laboratory. These molecules have typically consisted of a photoresponsive moiety attached to either a surfactant,<sup>9,10,55,56</sup> a polymer,<sup>12,44,57-59</sup> an organogelator<sup>3,13,60-64</sup> or other species.<sup>65,66</sup> While these past approaches have demonstrated impressive PR effects, it is not straightforward for other researchers to replicate these results. Synthesis of such organic molecules can be costly and time-consuming; moreover, it is not clear if the molecules can be generated in sufficiently large quantities for exploring applications. The lack of simple, low-cost PR systems has provided the motivation for our work. We have deliberately chosen to emphasize the design of PR fluids using only commercially available molecules or particles.<sup>67-72</sup> Our goal has been to make PR systems that can be easily recreated by scientists in both academia and industry without investing time and effort in organic synthesis. In turn, wider availability is likely to spur on the search for new applications for these fluids.

Over the last five years, we have reported several examples of such simple PR fluids, including both aqueous<sup>67,68,70</sup> and organic<sup>71,72</sup> systems. We have been able to show that dramatic (>1000-fold) rheological changes can be triggered by light in simple systems. However, most of these PR fluids only allowed for their rheological properties



to be changed in one direction (high to low, or low to high) by exposure to UV light; *i.e.*, the PR effect was not reversible.<sup>67-69,71</sup> There do exist a few simple systems that have demonstrated modest (10-fold) photoreversible viscosity change upon exposure to different wavelengths of light.<sup>72-74</sup> However, there is still very much a need for simple PR fluids that exhibit much larger (>1000-fold) photoreversible rheological changes.

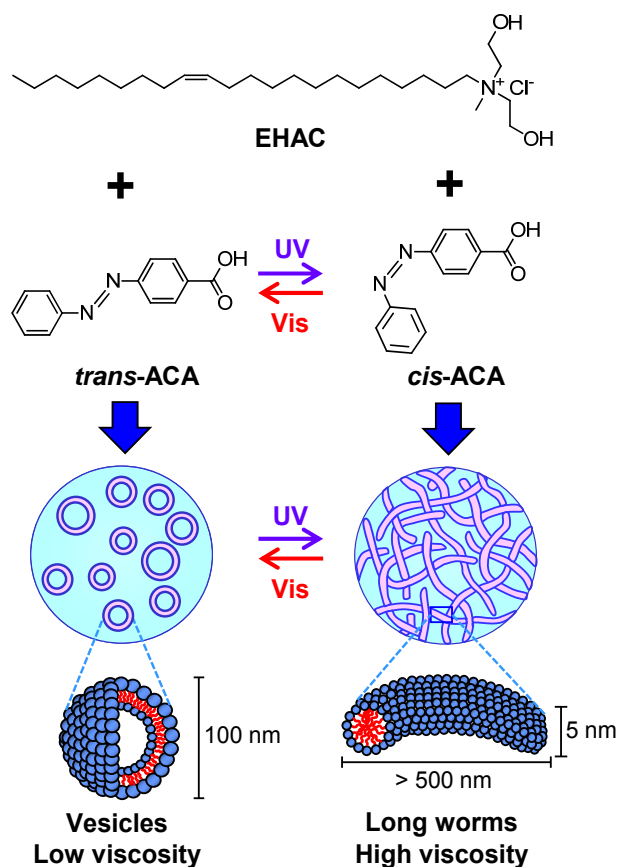


**Figure 3.1.** Composition and mechanism of reversible PR fluids. The fluids are composed of the cationic surfactant EHAC and the azobenzene derivative ACA. When ACA is in its *trans* form, its mixture with EHAC forms discrete unilamellar vesicles that yield a low viscosity. Upon UV irradiation, *trans* ACA is photoisomerized to *cis* ACA, and in turn, entangled wormlike micelles are formed, which have a much higher viscosity. Upon subsequent irradiation with visible light, *cis* ACA is isomerized back to *trans* ACA, and the structure and rheology revert to their initial state.

In this paper, we describe a class of aqueous PR fluids that exhibit dramatic (million-fold) photoreversible viscosity changes. The fluids are composed of two commercially available components: an azobenzene derivative, 4-azobenzene carboxylic acid (ACA) and the cationic surfactant, erucyl bis(2-hydroxyethyl)methyl ammonium chloride (EHAC).<sup>37</sup> Chemical structures of these molecules are shown in Figure 3.1. The PR effect occurs for certain molar ratios of EHAC and ACA, and for these samples exposure to UV light causes a *trans* to *cis* photoisomerization of ACA, which is accompanied by an increase in viscosity. Thereafter, when the sample is exposed to visible light, a *cis* to *trans* reverse photoisomerization of ACA occurs, and in turn the viscosity decreases to its initial value. We will show that the rheological changes correspond to a change in self-assembled structure, as indicated in Figure 3.1: *i.e.*, the low viscosity state corresponds to discrete unilamellar vesicles while the high-viscosity state corresponds to entangled wormlike micelles. The above changes in structure and hence rheology can be repeated, and the sample can be cycled between low and high viscosity states. We believe the above PR fluids can serve as a simple, workhorse system for use by academic and industrial researchers.

### 3.2. Experimental Section

**Materials.** EHAC (ETHOQUAD®E/12-75) was received as a gift from Akzo Nobel.<sup>37</sup> The product is supplied by the manufacturer as a solution of 75% surfactant in isopropyl alcohol (IPA). The IPA was removed in a vacuum oven at room temperature and the surfactant was dried to constant weight. ACA (greater than 98% in purity, mostly in *trans* form) was purchased from TCI. Ultrapure deionized water from a Millipore water

purification system was used in preparing samples. For the SANS and NMR studies, D<sub>2</sub>O (99.95% deuterated, from Cambridge Isotopes) was used.

**Sample Preparation.** Samples for rheological characterization and visual observation were prepared by dissolving weighed amounts of dried EHAC in ultrapure deionized water followed by the addition of desired amounts of ACA and 10% molar excess of sodium hydroxide (NaOH) to reach the final composition. Samples were stirred continuously around 40 °C for 5 hours to obtain homogeneous solutions. The solutions were stirred additionally for 1 day at room temperature and then left at rest to equilibrate for 3 days at room temperature before any experiments were conducted. The pH of the samples was between 6 and 7. For SANS studies, samples were prepared in D<sub>2</sub>O using EHAC, ACA and NaOH and with the same preparation procedure. For NMR studies, samples were similar to the above, but NaOH was replaced with sodium deuterioxide (NaOD).

**Sample Response Before and After UV Irradiation.** EHAC–ACA samples were irradiated with UV light from an Oriel 200 W mercury arc lamp. A dichroic beam turner with a mirror reflectance range of 350 to 450 nm was used to access the desired UV range of the emitted light. We used a filter for < 400 nm light to filter out the undesired visible wavelengths for the forward irradiation, and a filter for > 400 nm light to filter out the undesired UV wavelengths for the reverse irradiation. Samples (2.5 mL) were placed in a Petri dish with a quartz cover, and irradiation was done for a specific duration under stirring. After UV irradiation, 1 mL of sample was taken out for UV-vis spectra and

rheological measurements, and then consecutive visible light irradiation was done with the remaining 1.5 mL of the sample. Samples were covered with aluminum foil during storage to minimize undesired exposure to visible light. UV-vis spectroscopy before and after irradiation was carried out using a Varian Cary 50 spectrophotometer.

**Rheological Studies.** Rheological experiments were performed on an AR2000 stress controlled rheometer (TA Instruments, Newark, DE). 1 hour equilibration time was introduced before rheological measurement after light irradiation. Samples were run at 25 °C on a cone-and-plate geometry (40 mm diameter, 2° cone angle)

**SANS.** SANS measurements were made on the NG-7 (30 m) beamline at National Institute of Standards and Technology (NIST) in Gaithersburg, MD. Neutrons with a wavelength of 6 Å were selected. Three sample-detector distances were used to probe a wide range of wave vectors from 0.004 to 0.4 Å<sup>-1</sup>. Samples were studied in 2 mm quartz cells at 25 °C. The scattering spectra were corrected and placed on an absolute scale using calibration standards provided by NIST. The data are shown for the radially averaged intensity  $I$  as a function of the wave vector  $q=(4\pi/\lambda)\sin(\theta/2)$ , where  $\lambda$  is the neutron wavelength and  $\theta$  is the scattering angle.

**Cryo-TEM.** Specimens were prepared in a controlled environment vitrification system (CEVS) at 25 °C and 100% relative humidity.<sup>75</sup> A drop of solution was placed on a TEM grid covered with a perforated carbon film and blotted with a filter paper to form a thin solution film on the grid. The exact amount of blotting and its mode of application were

adjusted so as to obtain films ranging between 100 and 250 nm in thickness. The blotted samples were allowed to stand in the CEVS for 10-30 s to relax from shearing effects caused by the blotting. The relaxed samples were then plunged into liquid ethane at its freezing temperature ( $-183\text{ }^{\circ}\text{C}$ ) to form vitrified specimens and stored at  $-196\text{ }^{\circ}\text{C}$  in liquid nitrogen until examination. Specimens were examined in a Philips CM120 TEM optimized for cryo-TEM work. The microscope was operated at an accelerating voltage of 120 kV using an Oxford CT3500 cryo-specimen holder that maintained the vitrified specimens below  $-175\text{ }^{\circ}\text{C}$ . Specimens were examined in the low-dose imaging mode to minimize electron-beam radiation damage. Images were recorded digitally at nominal magnifications up to  $175000\times$  on a cooled Gatan MultiScan 791 CCD camera, using the Digital Micrograph software.

**$^1\text{H}$  NMR.**  $^1\text{H}$  NMR spectra were taken on a Bruker AVANCE 400MHZ spectrometer, BBI probe. The  $30^{\circ}$  pulse sequence was the standard “zg30” from Bruker. Particulars of the program include relaxation delay of 2 s, spectral width of 8012.82 Hz, and time domain 32768, giving a FID resolution of 0.244532 Hz. Spectra were processed on Topspin version 2.1 and referenced to the  $\text{H}_2\text{O}$  chemical shift signal of 4.8 ppm

### **3.3. Results and Discussion**

The reversible PR fluids described here are aqueous mixtures of the cationic surfactant EHAC and the azobenzene-containing acid ACA, with base (NaOH) added to convert the ACA to its salt form (the NaOH is at a 10% molar excess relative to the ACA). We use the abbreviation ACA to refer to its *trans* dominant form, which is the

commercially available one. Only certain EHAC-ACA mixtures show substantial PR effects and these correspond to a distinct nanostructure. To illustrate this point, we first describe the phase behavior, rheology, and nanostructure of EHAC-ACA mixtures at a fixed [EHAC] of 40 mM. A 40 mM solution of EHAC alone has a viscosity close to water. When ACA salt is added, the carboxylate anions bind to the cationic headgroups of EHAC, and this leads to the growth of long wormlike micelles, which entangle and thereby viscosify the solution. Accordingly, the zero-shear viscosity  $\eta_0$  of EHAC-ACA solutions increases by 5 orders of magnitude with increasing [ACA] and reaches a maximum around 14 mM ACA as seen in Figure 3.2. Samples at [ACA] between 10 and 16 mM are transparent and highly viscous, as shown by the photograph of a sample resisting flow in an inverted vial (top left on Figure 3.2). These samples are also flow-birefringent, as shown by the photograph of a sample viewed under crossed polarizers while being shaken (bottom left on Figure 3.2). Together, the high viscosity and flow-birefringence point to the presence of wormlike micelles.

Beyond 14 mM, further increase in [ACA] causes the viscosity to plummet (Figure 3.2 (b)). For [ACA] > 18 mM,  $\eta_0$  plateaus at a value  $\sim 3$  mPa s, which is 3 times the viscosity of water. A peak in  $\eta_0$  as a function of salt concentration is frequently seen in wormlike micellar systems and is thought to signify a transition from linear to branched wormlike micelles.<sup>30,37,76</sup> But the viscosity plateau for [ACA] > 18 mM is unusual, and samples in this region have features that are distinct from micelles. These low-viscosity samples also have a high optical density (turbidity), as shown by Figure 3.2 (a), indicating the presence of larger objects that scatter light.<sup>77</sup> Note that the onset of

turbidity and the viscosity plateau both occur around 20 mM ACA (Figure 3.2). Photographs of a typical sample in this region are shown in Figure 3.2 (top right) and we note that the sample is turbid but homogeneous; also there is no flow-birefringence

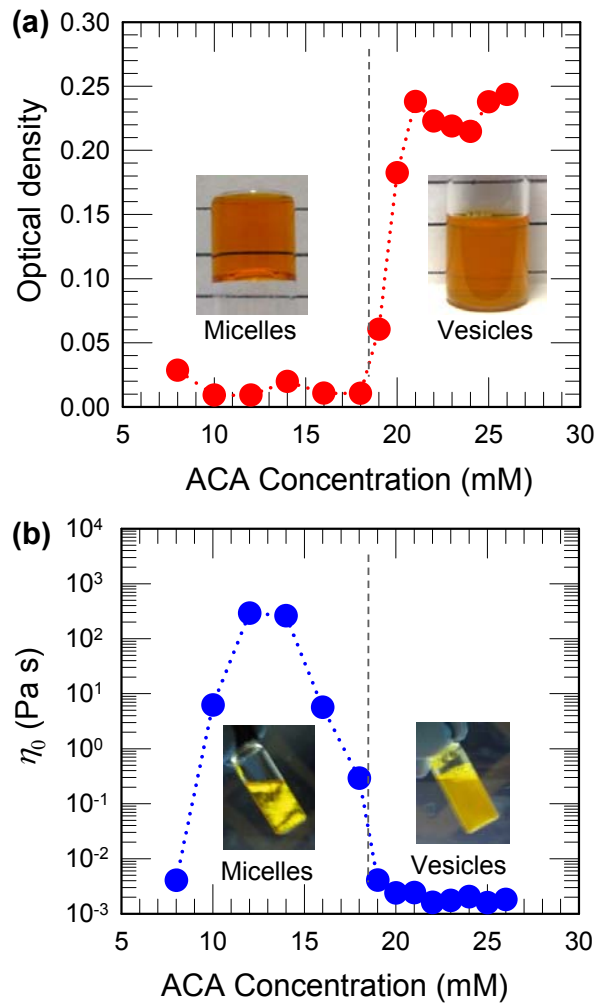


**Figure 3.2.** Phase behavior and rheology at 25°C of EHAC/ACA mixtures at a fixed [EHAC] of 40 mM and varying [ACA]. The molar ratio of NaOH to ACA is fixed at 1.1. The plot (a) shows the optical density at a wavelength of 700 nm, which quantifies the amount of light scattered from the sample. The plot (b) shows the zero-shear viscosity  $\eta_0$  obtained from steady-shear rheology. Samples at ACA concentrations between 10 and 16 mM are transparent and highly viscous (top left) and show flow-birefringence (bottom left). In contrast, samples with greater than 18 mM ACA have a low viscosity close to water and appear cloudy (top right) due to light scattering and do not show any flow-birefringence (bottom right).

(photograph of a shaken sample under crossed-polarizers in bottom right on Figure 3.2). These data are indicative of a phase transition from micelles to vesicles in EHAC–ACA mixtures with increasing ACA concentration.<sup>77,78</sup>

Support for the presence of wormlike micelles at moderate [ACA] and vesicles at higher [ACA] are provided by data from small-angle neutron scattering (SANS) and cryo-transmission electron microscopy (cryo-TEM). For SANS studies, EHAC-ACA samples were prepared in D<sub>2</sub>O to achieve enough contrast between scatterers and the solvent. The appearance and rheological properties of samples prepared in D<sub>2</sub>O were identical to those of samples prepared in H<sub>2</sub>O. Figure 3.3 (a) shows SANS spectra for EHAC/ACA mixtures at a fixed concentration of 10 mM EHAC with various ACA concentrations. With increasing ACA concentration, the low- $q$  intensity increases, which indicates the formation of large scatterers in the samples. The spectrum of the 2 mM ACA sample was similar to that of spherical or ellipsoidal micelles, which have a peak that comes from inter-micellar interactions and a decay at high  $q$  that comes from the form factor of a single particle. The spectra of samples with ACA concentrations of 4 mM and 5 mM resembled that of cylindrical or long ellipsoidal micelles. The spectra of samples with ACA concentrations of 6 and 6.5 mM showed a  $q^{-2}$  decay of the intensity at low  $q$ , which is a characteristic of scattering from vesicle bilayers.<sup>79</sup> Further evidence of vesicle structures in these samples is also provided by cryo-TEM images (Figure 3.10 (a)) and this is discussed below. Similar micelle-to-vesicle transitions in mixtures of a cationic surfactant and an organic salt are rare, but have been noted in a couple of previous studies.<sup>77,78</sup>



The samples that show large, reversible PR effects are those corresponding to the vesicle region in Figure 3.2. We will discuss typical photorheological results for a sample containing 40 mM EHAC, 20 mM ACA, and 22 mM NaOH. First, we confirmed by UV-vis spectroscopy that the ACA in this sample does undergo a reversible

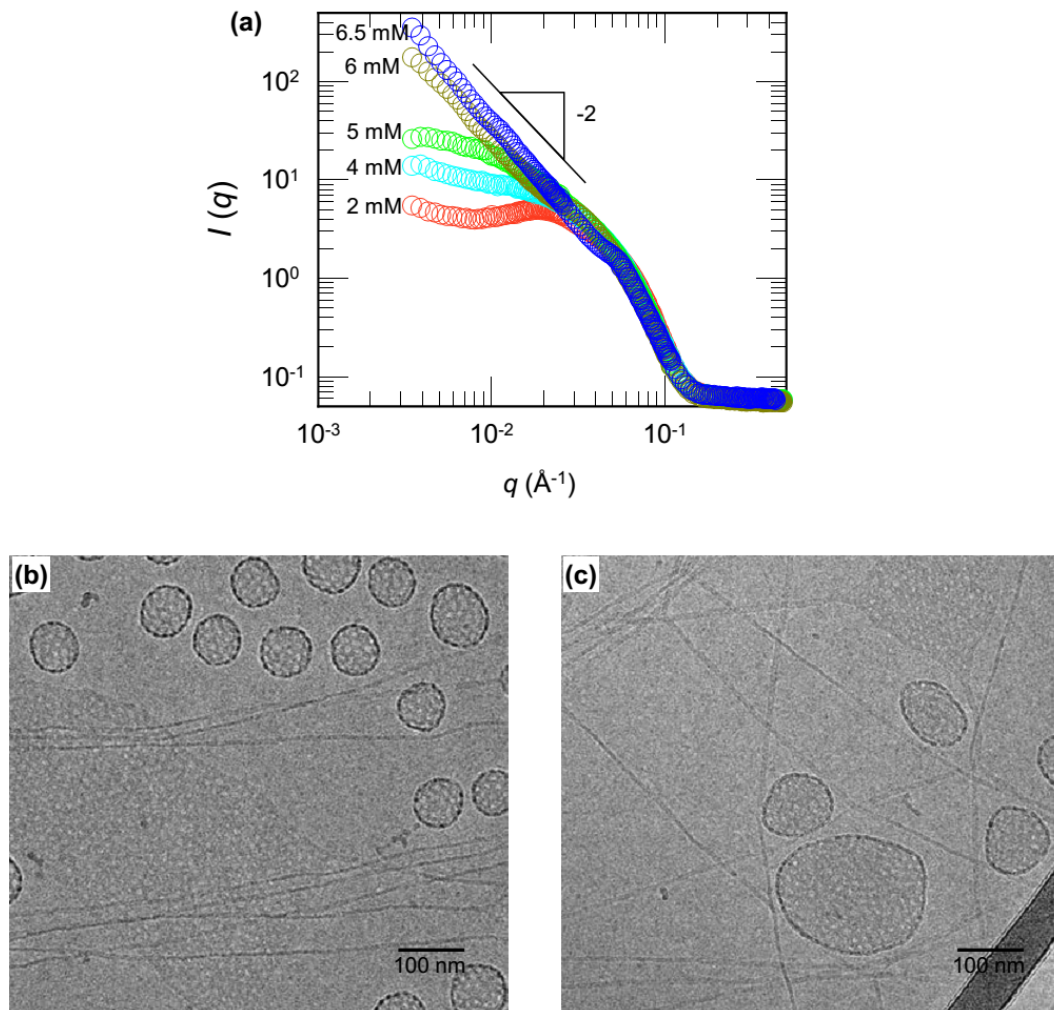


**Figure 3.3.** (a) SANS data at 25°C from EHAC/ACA mixtures in D<sub>2</sub>O at a fixed [EHAC] of 10 mM with various ACA concentrations. The molar ratio of NaOH to ACA is fixed to 1.1. For ACA concentrations of 6 and 6.5 mM,  $I$  follows a slope of -2 at low  $q$ , which is indicative of scattering from vesicles. (b), (c) Cryo-TEM images of a sample containing 40 mM EHAC, 20 mM ACA, and 22 mM NaOH show mostly vesicle structures (see Figure 3.10 (a) also). In some parts of the sample, stretched and interwoven wormlike micelles were also observed in rare cases, as seen in the above images.

photoisomerization in the presence of EHAC. As shown by Figure 3.4, the initial sample has two absorption bands: a main peak at 323 nm, corresponding to a  $\pi$ - $\pi^*$  excitation, and a secondary peak at 444 nm, corresponding to an  $n$ - $\pi^*$  excitation.<sup>40</sup> Upon 1 hr irradiation with broadband (300–350 nm) UV light, the peak at 323 nm drops by 25.3% and concomitantly the peak at 444 nm increases by 68.6% (Figure 3.4, inset), which together indicate a *trans* to *cis* photoisomerization of ACA. (The photostationary state was reached after 2 hr of UV irradiation, and corresponded to a 28.3% drop of the peak at 323 nm.) Subsequent irradiation with visible light (400–450 nm) for 1.5 hr causes a complete reversion of the spectrum to its original values *i.e.*, the peak at 323 nm grows back while the peak at 444 nm drops. Together, these data confirm that visible light induces the reverse *cis* to *trans* photoisomerization.<sup>40</sup>

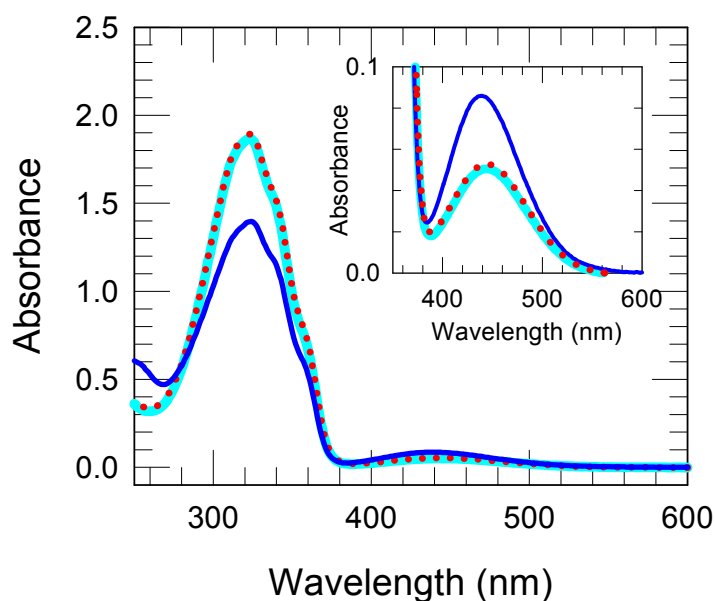


**Figure 3.4.** UV-Vis spectra of 40 mM EHAC, 20 mM ACA, and 22 mM NaOH before irradiation (cyan line), after UV irradiation for 1 hr (blue line), and after subsequent visible light irradiation for 1.5 hr (dotted red line). The sample was diluted 20 times with water. The changes at the visible wavelengths are enlarged and shown in the inset.

We now discuss the effect of UV- and visible-light irradiation on the rheology of the 40 mM EHAC, 20 mM ACA, and 22 mM NaOH sample. As shown by Photo 1 in Figure 3.5, this sample is initially turbid with an orange color and it is water-like in its viscosity - it thus flows readily out of the tilted vial. When the sample is stirred, the magnetic stir bar rotates smoothly and the fluid does not stick to the bar (Photo 2). Upon UV irradiation, the sample gradually becomes more transparent and viscous. The irradiated sample resists flow out of the tilted vial, and when it does flow, it moves as one mass (Photo 3) - this is a phenomenon associated with viscoelastic fluids called the “tubeless siphon” effect.<sup>36,45</sup> This sample is also flow-birefringent, and when bubbles are introduced in it, they remain trapped for long times. Also, during UV irradiation under stirring, the sample gradually gathers and sticks to the stir bar (Photo 4) - this is a manifestation of the “rod climbing” effect.<sup>45</sup> Taken together, it is clear that the UV irradiated sample is highly viscoelastic, as is typical of wormlike micellar systems.<sup>30</sup>

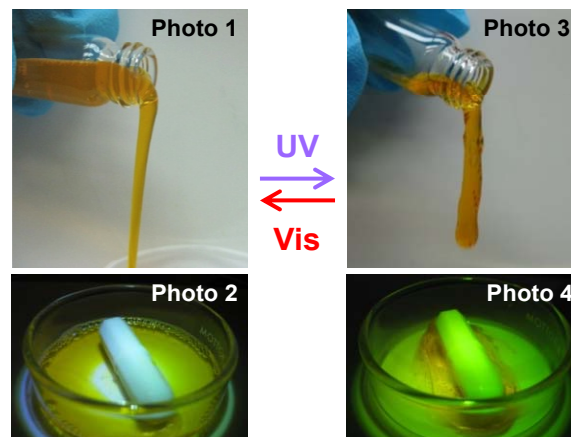


**Figure 3.5.** A sample containing 40 mM EHAC, 20 mM ACA, and 22 mM NaOH was used for reversible photorheological response. Visual observations illustrate the dramatic light-induced changes in fluid properties: initially, the sample is a cloudy, water-like fluid (Photo 1 and 2) whereas UV light transforms it into a transparent viscoelastic and gel-like fluid that shows the tubeless siphon (Photo 3) and rod climbing (Photo 4) effects. This is reversed by irradiation with visible light.

Subsequent irradiation with visible light reverts the sample to its original properties. The sample is converted back to a thin, runny fluid that can be poured easily out of the vial.

The above visual observations are quantified through steady shear (Figure 3.6) and dynamic (Figure 3.7) rheological measurements. From steady-shear rheology, the initial sample is seen to have a low viscosity (3 mPa s) that is nearly independent of shear rate, indicating Newtonian behavior (Figure 3.6). Correspondingly, the sample shows a purely viscous response in dynamic rheology: *i.e.*, the viscous modulus  $G''$  is strongly dependent on frequency  $\omega$  whereas the elastic modulus  $G'$  is too low to be detected (Figure 3.7 (a)). Upon UV irradiation, the sample becomes non-Newtonian and shear-thinning - the viscosity shows a plateau value  $\eta_0 \sim 500$  Pa s at low shear rates and decreases at higher shear rates (Figure 3.6). In turn, the dynamic rheological response is

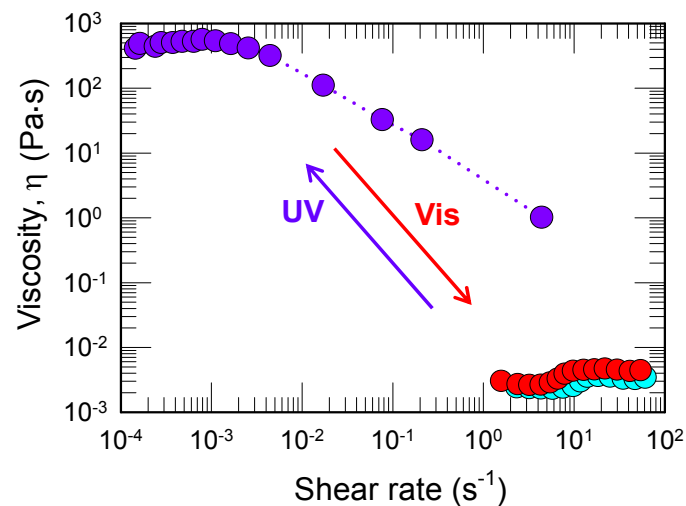


**Figure 3.6.** Steady-shear rheology of a sample of 40 mM EHAC, 20 mM ACA, and 22 mM NaOH. Data for the apparent viscosity vs. shear rate are shown for the initial sample (cyan circles), after UV irradiation for 30 min (purple circles), and after subsequent visible light irradiation for 30 min (red circles).

strongly viscoelastic (Figure 3.7 (b)): *i.e.*, the response is elastic at high frequencies or short timescales ( $G' > G''$ ) and viscous at low frequencies or long timescales ( $G'' > G'$ ).<sup>45</sup> Finally, upon subsequent visible-light irradiation, both the steady and dynamic rheological responses revert to their initial cases (Figure 3.6 and 3.7 (c)).

To measure the cyclability of the photorheological response, we characterize the sample by its zero-shear viscosity  $\eta_0$ . Figure 3.8 plots the values of  $\eta_0$  under repeated UV and visible light irradiation for 30 min each. The data show that  $\eta_0$  can be repeatedly cycled between a low value of 3 mPa s and a high value around 500 Pa s, *i.e.*, a  $>10^5$ -fold change. The magnitude of the response remains identical even after 3 full cycles, *i.e.*, there is no fatigue or deterioration in the response. During these cycling tests, repeated photoisomerization between *trans* and *cis* ACA was confirmed by UV-vis: we found a 21% drop of the absorbance at 323 nm after 30 min of UV and complete recovery to the initial absorbance after visible light irradiation for each of the 3 cycles.

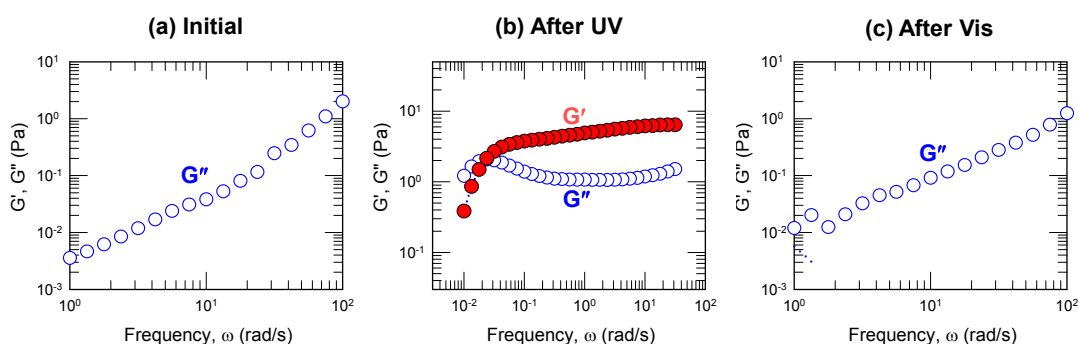


**Figure 3.7.** Dynamic rheology of a sample of 40 mM EHAC, 20 mM ACA, and 22 mM NaOH. Data for the elastic modulus  $G'$  and the viscous modulus  $G''$  as functions of frequency  $\omega$  are shown for the initial sample (a), after UV irradiation for 30 min (b), and after subsequent visible light irradiation for 30 min (c).

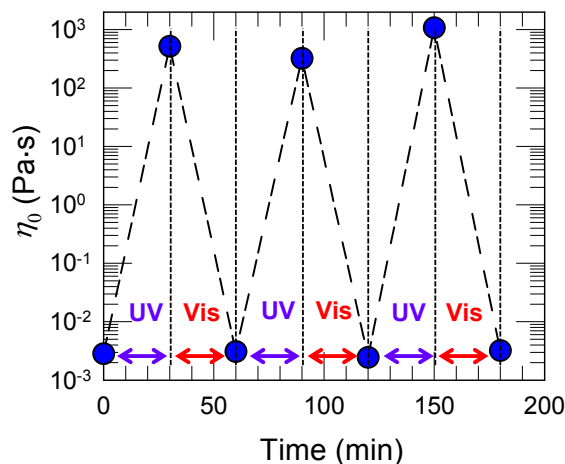


**Figure 3.8.** Rheological cycling of a 40 mM EHAC / 20 mM ACA / 22 mM NaOH under repeated UV and visible light irradiation. The rheology is quantified in terms of the zero-shear viscosity  $\eta_0$ . The data show that the sample can be cycled between low and high viscosity states ( $10^5$ -fold difference) by repeated UV and visible light irradiation.

Figure 3.9 and 3.10 present results from SANS and cryo-TEM confirming that the PR effects are due to a reversible vesicle-micelle transition. First, we show data from SANS for the intensity  $I$  vs. scattering vector  $q$  in Figure 3.9. These data were obtained on a diluted sample (10 mM EHAC/6.5 mM ACA/7.2 mM NaOH) to minimize structure factor effects. Initially, this sample shows a  $q^{-2}$  decay of the intensity at low  $q$ , which is characteristic of vesicles.<sup>79</sup> After 1 h of UV irradiation, a significant drop occurs in the intensity at low  $q$  and the intensity asymptotes to a slope close to -1 at low  $q$ , which is indicative of long, cylindrical micelles.<sup>79</sup> Next, after 1.5 h of visible-light irradiation, the SANS data perfectly overlap with that of the sample before UV irradiation.

Figure 3.10 presents cryo-TEM images of the 40 mM EHAC, 20 mM ACA, and 22 mM NaOH sample. As expected, the sample initially contains mostly unilamellar vesicles (Figure 3.10 (a)). The vesicles have diameters between  $\sim 80$  and 200 nm, and

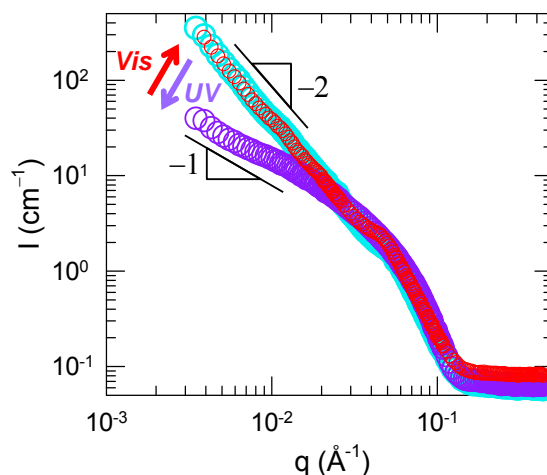


**Figure 3.9.** SANS spectra on a diluted sample in D<sub>2</sub>O (10 mM EHAC, 6.5 mM ACA, and 7.2 mM NaOH) reveal a reversible light-induced transition between two types of self-assembled structures: initially, the intensity  $I$  follows a slope of -2 at low  $q$  (cyan circles), which is characteristic of vesicles at low  $q$ . Upon UV irradiation, the slope is decreased and approaches -1 (violet circles), which is indicative of cylindrical (wormlike) micelles. Upon subsequent visible light irradiation, the original spectrum is recovered (red circles).

their surfaces appear to be perforated rather than smooth. In some images, we also observed coexistence of such vesicles with a few wormlike micelles (Figure 3.3 (b) and (c)). The perforated vesicles are evidently transitional structures between micelles and vesicles, and they have been observed in the transition regions between micelle and vesicle phases in other surfactant systems.<sup>80,81</sup> Next, we consider the sample after UV irradiation, and its cryo-TEM images clearly show the presence of long, entangled wormlike micelles,<sup>30</sup> as can be noted from the typical image in Figure 3.10 (b). The worms are seen to have a diameter  $<5$  nm whereas their contour (end-to-end) lengths extend up to a micron or more. These worms are responsible for the UV-induced increase in viscoelasticity (also the much smaller diameter of the worms relative to the vesicles explains why the latter solutions are much more turbid than the former). Finally, visible-light irradiation brings the structure back to perforated vesicles, as seen in Figure 3.10

(c). Overall, cryo-TEM, SANS, visual observations, and rheology are all in agreement in attributing the PR effect to a transition between unilamellar vesicles and wormlike micelles.

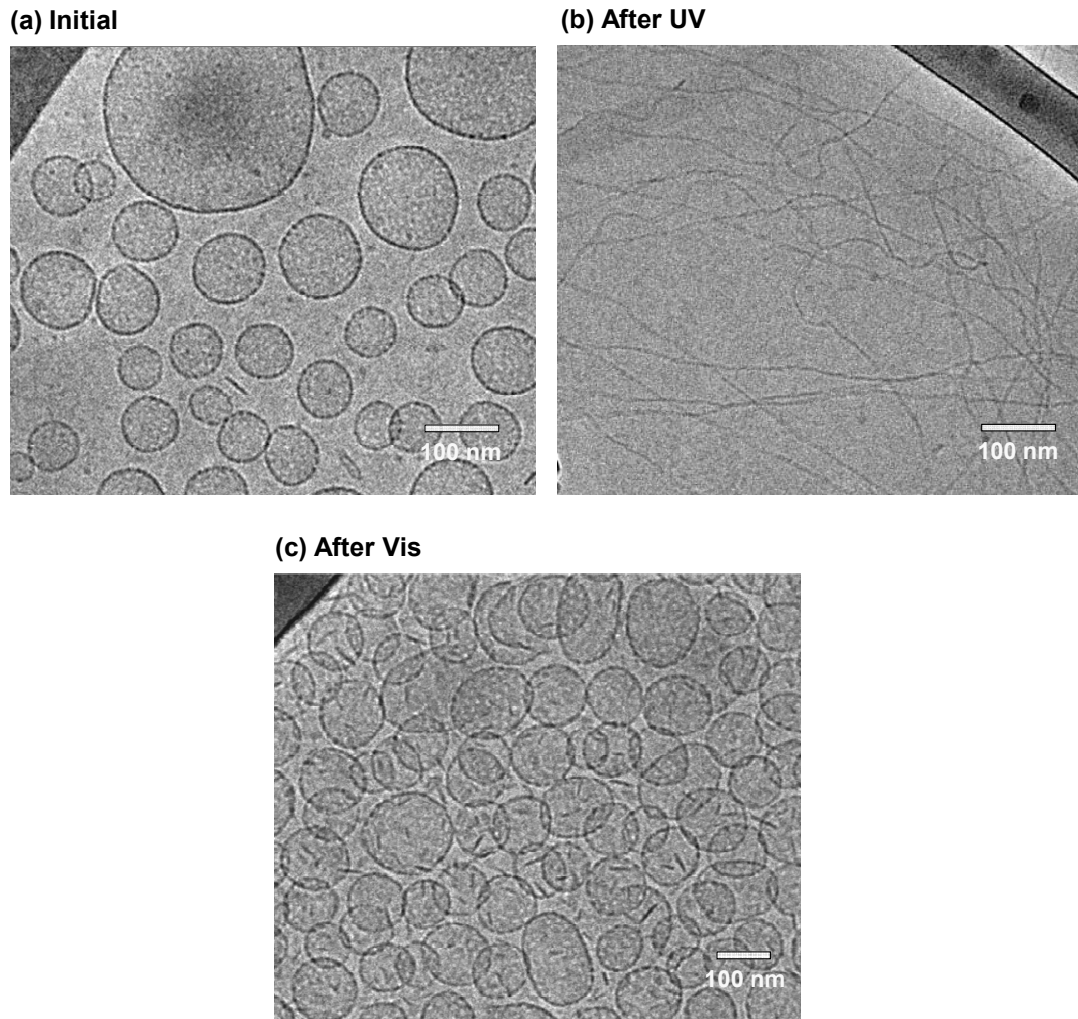


**Figure 3.10.** The structural transition is confirmed by cryo-TEM. A typical image of the initial sample containing 40 mM EHAC, 20 mM ACA, 22 mM NaOH (a) reveals discrete unilamellar vesicles, whereas after UV irradiation (b) the sample is found to contain long, entangled wormlike micelles, and finally, after subsequent visible light irradiation (c) the sample reverts to the vesicle state.



Figure 3.11 plots the influence of sample composition on the PR effect. This was studied at a constant [EHAC] of 40 mM and varying [ACA]. Data are shown for the zero-shear viscosity  $\eta_0$  of the samples before irradiation, following UV irradiation, and following subsequent visible-light irradiation. This plot shows that the PR effect is significant only for samples in the “vesicle” region, *i.e.*, [ACA] > 18 mM, which fall to the right of the viscosity peak. For these samples, 1 h of UV irradiation increased  $\eta_0$  by up to 6 orders of magnitude (million-fold). Specifically, the sample at an [ACA] of 20 mM shows a 1.4 million-fold increase in  $\eta_0$ . Subsequent visible-light irradiation for 1.5 h brought  $\eta_0$  back to nearly its original value. Note that samples to the left of the viscosity peak do not show any significant PR effects.

A final piece of this puzzle is to explain how *trans* and *cis* ACA lead to different

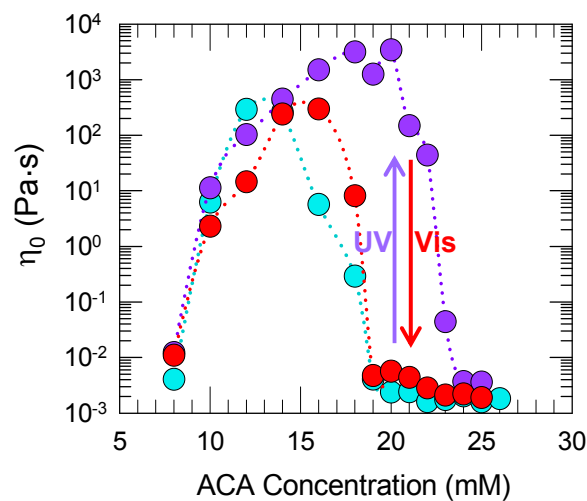


**Figure 3.11.** Influence of sample composition on the PR effect. The zero-shear viscosity  $\eta_0$  is plotted for samples at constant [EHAC] of 40 mM and varying [ACA] for three cases: initial, *i.e.*, before any irradiation (cyan circles); after 1 h of UV irradiation (violet circles); and after subsequent 1.5 h of visible-light irradiation (red circles).

self-assembled structures, *i.e.*, vesicles and worms, respectively. To address this issue, we collected  $^1\text{H}$  NMR spectra on EHAC - ACA mixtures in  $\text{D}_2\text{O}$  at a fixed EHAC concentration of 10 mM. Figure 3.12 (a) and (b) represent the chemical shifts of the ring protons of ACA before and after UV irradiation, respectively. The protons corresponding to each peak are shown in Figure 3.12 (c) and (d). The chemical shift difference  $\Delta\delta$  of the protons is indicative of the environment surrounding the molecules.<sup>82-85</sup> An upfield shift indicates a higher electron density of the environment; this occurs when aromatic protons are in the hydrophobic interior of micelles or vesicles and the magnitude of  $\Delta\delta$  reflects the insertion depth of these protons.<sup>82-85</sup> On the contrary, a down field shift indicates a lower electron density of the environment; this occurs when the protons are near the surface of the micelles or vesicles and thereby close to the charged headgroups of the surfactant.<sup>82-85</sup>

The  $^1\text{H}$  NMR spectra of ACA before UV irradiation show three groups of peaks for each *trans* and *cis* form, as seen in Figure 3.12 (a). The ratio of *cis* to *trans* ACA is 0.24 (80.6% *trans* and 19.4% *cis*), obtained by integrating the corresponding peaks of a control sample. Each group of peaks shows different shifts in the presence of 10 mM EHAC. At an ACA concentration of 6.5 mM, the peaks d and e experience the largest upfield shift  $\Delta\delta$  (- 0.46 ppm), which suggests that these protons are the farthest from the headgroup of EHAC. Peaks b and c show a  $\Delta\delta \sim - 0.19$  ppm while the peaks of a show a negligible  $\Delta\delta \sim - 0.02$  ppm. Although the  $\Delta\delta$  for these three groups keep changing with [ACA], their order is very consistent, *i.e.*, in magnitude,  $a < b, c < d, e$ . This suggests that the *trans* ACA is inserted vertically into the micelles or vesicles.<sup>82-86</sup> Note that the

broadening of signals at higher [ACA] is due to the binding of ACA to the micelles or vesicles rather than an increased viscosity of solution.

After UV irradiation, the intensity of peaks corresponding to the *cis* form increases whereas that of the *trans* form decreases, as seen in Figure 3.12 (b). The *cis* to *trans* ratio of ACA without EHAC after 30 min UV irradiation is 2.26 (30.7% *trans* and 69.3% *cis*). However, the *cis* to *trans* ratio of ACA after 1 h UV irradiation in the presence of 10 mM EHAC is 0.60 (62.6% *trans* and 37.4% *cis*) obtained by integrating peaks corresponding to d, e and d', e'. Although there is some inaccuracy due to peak broadening, this result is consistent with our UV-vis data in showing that ACA photoisomerization is somewhat restricted when ACA is bound to EHAC. Now, consider the  $\Delta\delta$  values for 6.5 mM ACA after UV irradiation. Notably, the  $\Delta\delta$  of a' (-0.01 ppm), b' and c' (-0.3 ppm) are all close to the corresponding protons of the *trans* form; however,  $\Delta\delta$  of d' and e' is -0.3 ppm, which is quite different from that of protons d and e (-0.46 ppm) of *trans* ACA. The smaller magnitude of  $\Delta\delta$  for d' and e' implies that these protons are shifted toward the interface of the EHAC aggregates. That is, when *trans* ACA is converted to *cis* ACA, the phenyl group far from the carboxylate is induced to move upward,<sup>82-85</sup> as shown in Figure 3.12 (c) and (d).

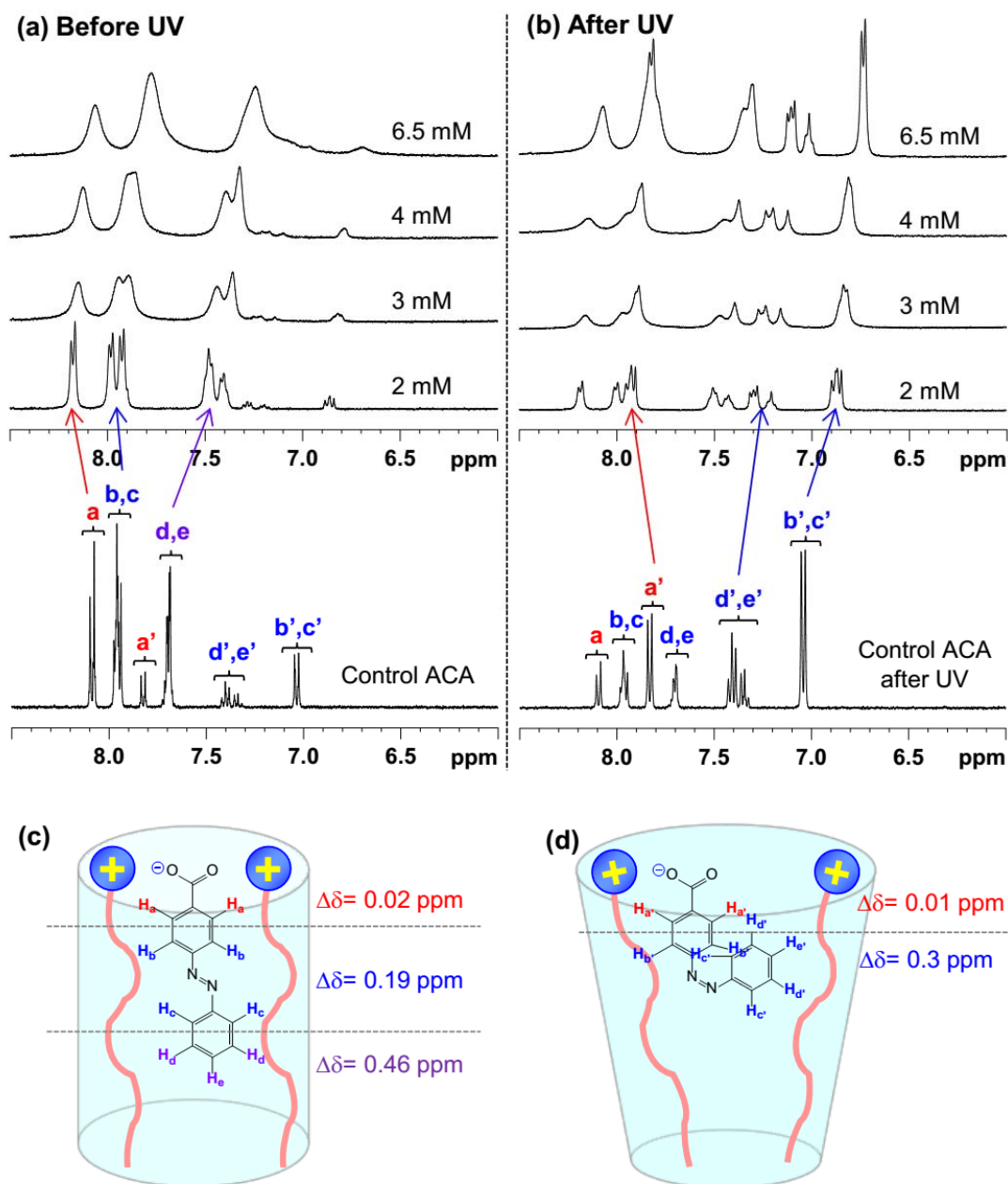


**Figure 3.12.** Molecular arrangement of *trans* and *cis* ACA in the EHAC–ACA aggregates. <sup>1</sup>H NMR spectra of 2 – 6.5 mM ACA in 10 mM EHAC and 1 mM ACA in D<sub>2</sub>O (control) are plotted: (a) before UV irradiation and (b) after 1 h of UV irradiation. The signals a - d correspond to the protons of *trans* ACA shown in the schematic structure (c). The signals a', b', c', and d' correspond to the protons of *cis* ACA shown in (d). (c) and (d) represent the most reasonable molecular arrangement of EHAC–ACA, which is inferred from the chemical shift differences ( $\Delta\delta$ ) for *trans* ACA and *cis* ACA respectively.

Figure 3.12 (c) and (d) present the most reasonable arrangement of *trans* and *cis* ACA in the EHAC-ACA aggregates, as per the NMR data. The impact of these geometric differences on self-assembly can be rationalized using the concept of the critical packing parameter  $p = a_{\text{tail}}/a_{\text{head}}$ , *i.e.*,  $p$  is the ratio of the average area of the tail portion ( $a_{\text{tail}}$ ) to the average area of the head portion ( $a_{\text{head}}$ ).<sup>1,87</sup> In the case of EHAC and *trans* ACA (Figure 3.12 (c)), the azobenzene group of ACA is embedded vertically and adjacent to the tail of EHAC while the carboxylate anion of ACA is next to the cationic headgroups of EHAC at the interface. The binding of anionic and cationic moieties reduces the electrostatic repulsions of the headgroup and  $a_{\text{head}}$  is thus maintained low. In effect,  $a_{\text{head}}$  and  $a_{\text{tail}}$  are comparable, *i.e.*,  $p = 1$ , so that the net molecular geometry is that of a cylinder (Figure (c)). Such a  $p$  value implies the formation of vesicles.<sup>1,87</sup> When *trans* ACA is photoisomerized to *cis* ACA, the lower phenyl ring of *cis* ACA is displaced toward the interface, which widens the gap between headgroups of EHAC, *i.e.*,  $a_{\text{head}}$  increases, while  $a_{\text{tail}}$  may not be altered as much.<sup>88</sup> In effect, there is a net decrease in  $p$  to a value closer to  $1/2$ , which corresponds to a truncated cone geometry (Figure (d)). Such a  $p$  value implies the formation of cylindrical structures such as wormlike micelles.<sup>1,87</sup> In sum, we have used NMR to infer a change in the overall geometry of EHAC-ACA aggregates upon photo-isomerization, which manifests as a transition between two types of self-assembled structures: vesicles and wormlike micelles.

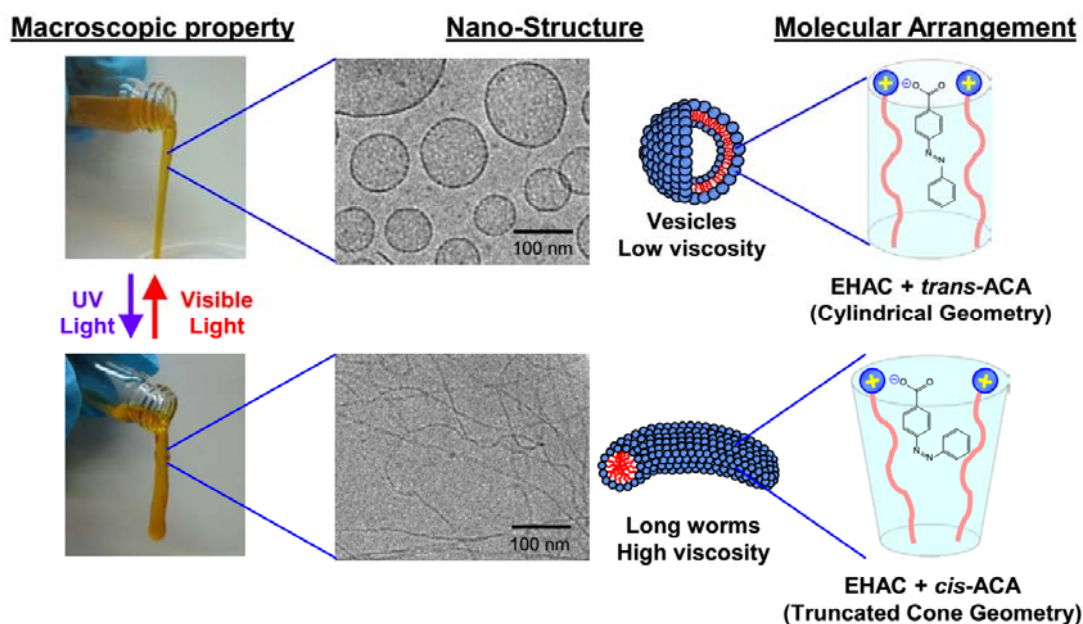


**Figure 3.13.** Photoresponsive character of the EHAC–ACA system at the molecular, nanostructural, and macroscopic scales. At the molecular scale, initially *trans* ACA binds strongly to EHAC and the net molecular arrangement is in a cylindrical geometry, which results in self-assembly into unilamellar vesicles at the nanoscale, and thereby results in a freely flowing low-viscosity fluid at the macroscopic scale. When UV-irradiated, at the molecular scale, *trans* ACA is photoisomerized to *cis* ACA. The arrangement of *cis* ACA with EHAC is altered to a truncated-cone geometry, thus dictating self-assembly into long wormlike micelles at the nanoscale, and thereby producing a highly viscoelastic fluid at the macroscopic scale. Finally, exposure to visible light reverts the ACA back from *cis* to its *trans* isomer, and thereby reverts the nanostructure and rheology to their initial states.

### 3.4. Conclusions

We have demonstrated reversible light-induced rheological and structural transitions in solutions prepared from inexpensive and commercially available chemicals, *viz.* the cationic surfactant EHAC and the azobenzene derivative ACA. Figure 3.13 summarizes our results and illustrates how the molecular structure dictates the nanostructure and in turn, the macroscopic properties. First, in the initial case, *trans* ACA binds strongly with EHAC, leading to a cylinder-like molecular geometry and thereby to unilamellar vesicles. This nanostructure corresponds to a low viscosity. When irradiated with UV light, *trans* ACA is photoisomerized to *cis* ACA, which is displaced towards the headgroup of EHAC, leading to a truncated cone geometry. In turn, the vesicles rearrange into entangled wormlike micelles, which display a dramatically higher viscosity (increase in  $\eta_0$  by up to a factor of  $10^6$ ). Upon subsequent visible light irradiation, *cis* ACA reverts to *trans* ACA, and in turn, the self-assembled structure and viscosity revert to their original states. Among the available photorheological (PR) fluids, the EHAC - ACA system is particularly attractive because it can be easily prepared in any industrial or academic lab and because it exhibits a large PR response and complete photoreversibility. It is hoped that these “smart” fluids will eventually find applications in microscale or mesoscale devices. In addition to the PR response, light-activated vesicle rupture and formation in EHAC–ACA may also be useful for photo-controlled release of vesicle contents.<sup>5,8</sup>

## Chapter 4

### Photoresponsive Vesicles and Vesicle-Gels

---

The results presented in this chapter have been published in the following journal article: H. Oh, V. Javvaji, N. A. Yaraghi, L. Abezgauz, D. Danino and S. R. Raghavan, “Light-induced transformation of vesicles to micelles and vesicle-gels to sols.” *Soft Matter*, 9, 11576-11584 (2013)

#### 4.1. Introduction

Vesicles are nanoscale containers formed by a variety of amphiphilic molecules, including lipids, surfactants, and block copolymers.<sup>1,87,89</sup> They consist of an aqueous core enclosed by a bilayer of the amphiphiles. Vesicles have attracted much interest owing to their potential for the encapsulation and controlled release of substances such as drugs in pharmaceutical applications, flavors and nutrients in foods, fragrances and dyes in cosmetics and textiles, *etc.*<sup>89-95</sup> Payloads encapsulated in the core of vesicles tend to get released slowly through passive diffusion through the bilayer membrane.<sup>5,14</sup> However, passive release usually does not deliver a high payload concentration.<sup>5,14,15</sup> An alternative is to engineer the vesicles for active release; *i.e.*, so that they deliver their entire payload upon activation by an external trigger, such as pH, temperature, ions, enzymes, ultrasound, and light.<sup>5,14,15,96-98</sup>



Light is an attractive stimulus for triggering release from vesicles due to its high spatial resolution, *i.e.*, it can induce release of encapsulated molecules at a precise location with micron-scale resolution.<sup>5,14,15</sup> Accordingly, many researchers have designed light-responsive vesicles, typically using custom-synthesized lipids.<sup>5,14,15</sup> For example, vesicles have been created using lipids that contain photocrosslinkable,<sup>99,100</sup> photoisomerizable,<sup>17,101-103</sup> or photocleavable groups.<sup>104,105</sup> These vesicles exhibit either light-induced disruption of their bilayers or light-activated opening of pores in their bilayers-in both cases, active release of encapsulated payload from the vesicles is triggered by light. However, synthesis of photoresponsive lipids is usually a complex process that requires skills in organic and biochemistry. Thus, the complexity of these previous systems makes them difficult to replicate and scale-up for commercial application. There is a lack of simple and low-cost routes to making photoresponsive vesicles, which is the motivation for the present study.

In our efforts to develop a simple class of photoresponsive vesicles, we focus on vesicles formed by single-tailed amphiphiles (surfactants) due to their simplicity and ease of preparation.<sup>22,23,106,107</sup> It is well-known that a mixture of cationic and anionic surfactants can spontaneously self-assemble into nanoscale unilamellar vesicles in water.<sup>23</sup> These “catanionic” vesicles are indefinitely stable and can be formed by simple mixing (*i.e.*, there is no need for extrusion or sonication).<sup>22,23</sup> The vesicles can encapsulate payloads in their aqueous core much like conventional lipid vesicles.<sup>106,107</sup> How can these vesicles be made photoresponsive? One straightforward possibility is to combine a photoresponsive surfactant with a conventional surfactant of opposite charge.

Indeed, this approach has been tried and does give rise to photoresponsive vesicles, as demonstrated by several authors using azobenzene modified cationic surfactants.<sup>8,19,108,109</sup> However, chemical synthesis is still necessary to incorporate azobenzene or similar groups into the surfactant molecules, and that is something we wish to avoid.

Here, we present a simple design for photoresponsive vesicles that uses only molecules that are commercially available and relatively inexpensive. The impetus for our study was the observation that alkyl-substituted diaryliodonium salts, which are frequently used as cationic photoinitiators,<sup>40,110</sup> have an amphiphilic nature. In particular, we have worked with the molecule, p-octyloxydiphenyliodonium hexafluoroantimonate (ODPI),<sup>111,112</sup> and we confirm that this molecule acts as a cationic surfactant. Accordingly, we combine ODPI with the common anionic surfactant sodium dodecylbenzenesulfonate (SDBS), and as expected, these mixtures form unilamellar catanionic vesicles at certain compositions. The chemical structures of ODPI and SDBS are shown in Figure 4.1 (a) and (b), respectively, and a schematic of the photoresponsive vesicles is shown in Figure 4.1 (c). It is further known that molecules such as ODPI lose their cationic charge by photodissociation when irradiated with ultraviolet (UV) light.<sup>40,110</sup> Thus, when ODPI–SDBS vesicles are exposed to UV light, the loss of charge on ODPI results in a transition from vesicles to spherical micelles (Figure 4.1 (c)). Such a transition will be accompanied by complete release of the internal payload within the vesicles into the surrounding aqueous solution.<sup>106,107</sup>

As an additional potential application, we demonstrate that these photoresponsive vesicles can be used to design a new class of photorheological (PR) fluids whose rheology can be tuned by light irradiation.<sup>67,113</sup> By combining the ODPI–SDBS photoresponsive vesicles with an associating polymer, *viz.* hydrophobically modified alginate (hm-alginate), we demonstrate a photoresponsive vesicle-gel. A vesicle-gel is a volume filling network of vesicles bridged by polymer chains, and it is formed because the hydrophobes on hm-alginate chains insert into the hydrophobic bilayers of vesicles.<sup>24,114-116</sup> Upon UV irradiation, the vesicles in the gel are transformed into micelles, thereby disrupting the original network and causing a gel-to-sol transition.

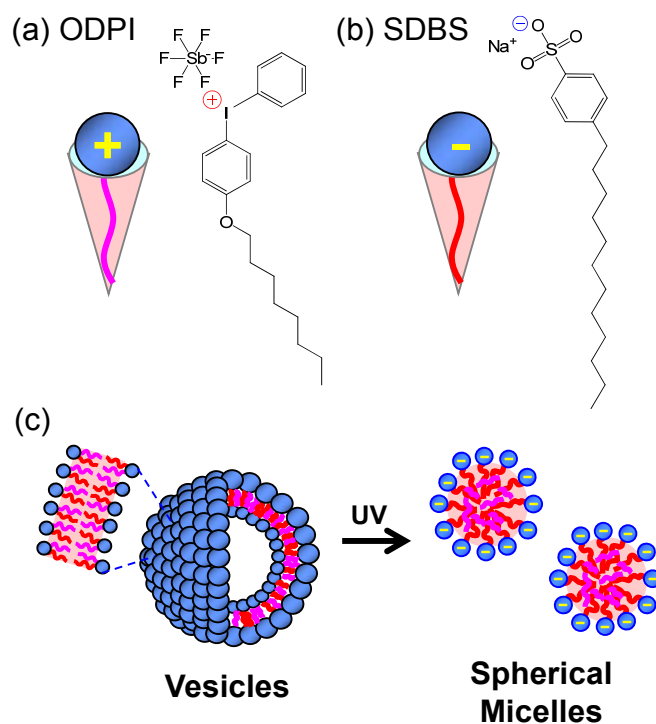


**Figure 4.1.** Components of our photoresponsive vesicles: (a) the cationic amphiphile ODPI and (b) the anionic surfactant SDBS. Vesicles formed by combining ODPI and SDBS are transformed by UV light into spherical micelles. This is shown schematically in (c).

## 4.2. Experimental Section

**Materials.** p-octyloxydiphenyliodonium hexafluoroantimonate (ODPI) was purchased from Gelest and sodium dodecylbenzenesulfonate (SDBS) was purchased from TCI. The nonionic surfactant triton X100, n-octylamine, and the coupling agent N-(3-Dimethylaminopropyl)-N'-ethylcarbodiimide hydrochloride (EDC) were all purchased from Sigma Aldrich. Sodium alginate (product number 4-00005) was purchased from Carbomer, Inc. and the molecular weight was specified by the manufacturer to be around 500 kDa. Disodium phosphate  $\text{Na}_2\text{HPO}_4$  was purchased from J. T. Baker and was used to make a buffer solutions. All chemicals and materials were used as received without further purifications. Ultrapure deionized (DI) water from a Millipore water purification system was used in preparing samples.

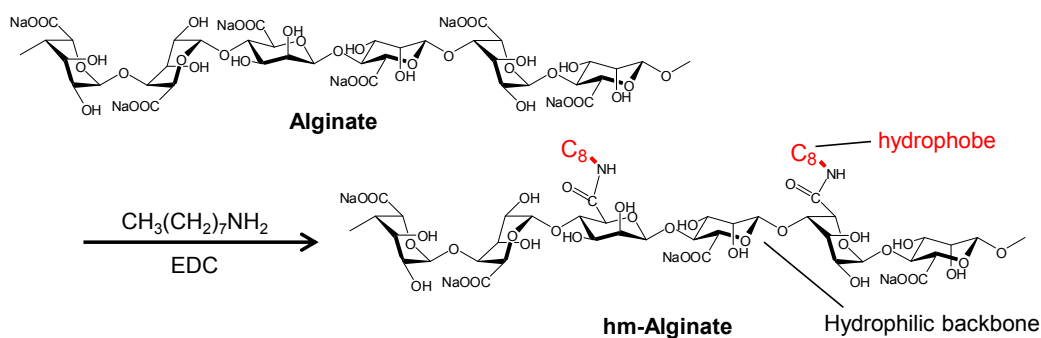
**Surface Tension Measurements.** The surface tension of ODPI solutions in 50 mM  $\text{Na}_2\text{HPO}_4$  at different concentrations was measured by a Surface Tensiomat 21 (Fisher Scientific) using a platinum ring. Each solution was measured three times.

**Sample Preparation.** Stock solutions of ODPI and SDBS were prepared separately by dissolving calculated amounts in 50 mM  $\text{Na}_2\text{HPO}_4$  buffer at room temperature for 24 h. Vesicle solutions were prepared by mixing these stock solutions at the appropriate weight ratio. The mixture was stirred overnight using a magnetic stir bar. Sample vials were wrapped with aluminum foil to prevent exposure to visible light. Vesicle-gel samples

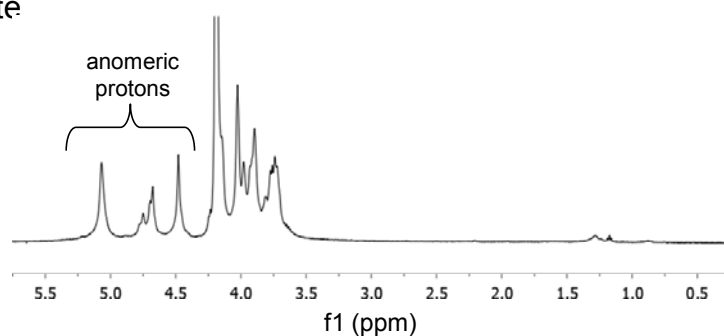
were prepared by mixing appropriate amounts of a vesicle solution and an hm-alginate solution, followed by vortex mixing.

**hm-Alginate Synthesis.** hm-Alginate was synthesized by amidation of sodium alginate as described previously.<sup>117-119</sup> For the synthesis, the coupling agent N-(3-dimethylaminopropyl)-N'-ethylcarbodiimide hydrochloride (EDC) and the hydrophobic compound n-octylamine were purchased from Sigma Aldrich. 1.5 g of sodium alginate was dissolved in 75 mL of DI water and the solution was stirred overnight to obtain a homogeneous solution. To adjust the pH to around 3, 30 mL of 0.1 M HCl was added dropwise and the solution was further stirred for 2 h. 75 mL of methanol was then added dropwise and the solution was again stirred for 2h. Next, a solution of 0.4 g of the coupling agent EDC in 5mL DI water was added dropwise. 1.37 g of n-octylamine (corresponding to 124 mol% of the repeating units of alginate) in 5 mL of methanol was then added slowly and the mixture was stirred for 24 h under ambient conditions. During this stage, hm-alginate is generated by reaction (see Figure 4.2 (a)). The product was precipitated by adding acetone and separated by vacuum filtration. This purification step was repeated 3 times. The final hm-alginate was recovered by vacuum drying at room temperature. The hydrophobic modification degree was determined by <sup>1</sup>H NMR as described previously.<sup>117</sup> <sup>1</sup>H NMR spectra were taken on a Bruker AVANCE 500 MHz spectrometer. Spectra were referenced to the 3-trimethylsilylpropionic acid sodium salt-d4. The calculated degree of hydrophobic modification was 23 mol% (see Figure 4.2 (c)).

(a) hm-alginate synthesis



(b) Alginate



(c) hm-alginate

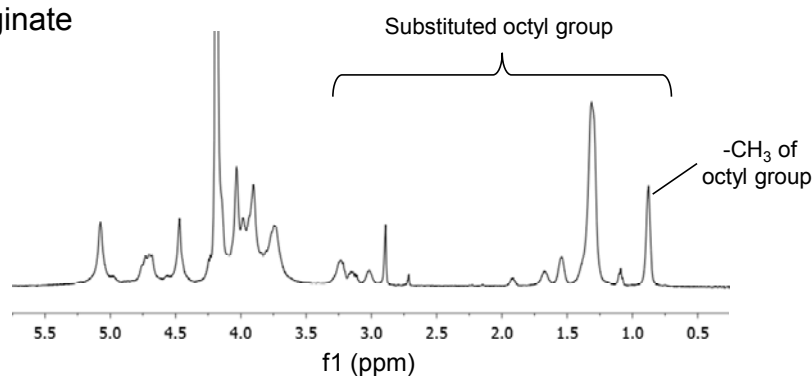


**Figure 4.2.** (a) Reaction scheme for synthesis of hm-alginate. This involves amidation of sodium alginate with n-octylamine using the coupling agent EDC.  $^1\text{H}$  NMR spectra of alginate (b) and hm-alginate (c). From the peaks of anomeric protons, the G content of alginate was calculated to be 51.2%.<sup>120</sup> The  $^1\text{H}$  NMR spectrum of hm-alginate shows additional peaks (0.8 ~ 3.3 ppm, 4.9 ppm) which indicate the successful modification of alginate with octyl groups. From the ratio of methyl protons to anomeric protons, the degree of modification was obtained to be 23%.<sup>118</sup>

**Sample response before and after UV irradiation.** Samples were irradiated with UV light from an Oriel 200 W mercury arc lamp. A dichroic beam turner with a mirror reflectance range of 280 to 400 nm was used to access the UV range of the emitted light. A filter for below 400 nm light was used to eliminate the undesired visible wavelengths. Samples (2.5 mL) were placed in a Petri dish of 60 mm diameter with a quartz cover, and irradiation was done for a specific duration under mild stirring with a magnetic stirring bar.

**Dynamic light scattering (DLS).** Solutions were studied at 25 °C using a Photocor-FC instrument equipped with a 5 mW laser source at 633 nm. The scattering angle was 90°. The autocorrelation function was measured using a logarithmic correlator and this was analyzed by the Dynals software package to yield the average hydrodynamic radius.

**Rheological studies.** Steady and dynamic rheological experiments were performed on an AR2000 stress controlled rheometer (TA Instruments). Samples were run at 25 °C on a cone-and-plate geometry (40 mm diameter, 2° cone angle). Dynamic experiments were performed in the linear viscoelastic range of the respective samples.

**Cryo-TEM.** Specimens were prepared in a controlled environment vitrification system (CEVS) at 25 °C and 100% relative humidity.<sup>75,121</sup> A drop of the sample was placed on a TEM grid covered with a perforated carbon film and blotted with a filter paper to form a thin film on the grid. The blotted sample was allowed to stand in the CEVS for 10–30 s to relax from the shear caused by blotting. The relaxed samples were then plunged into

liquid ethane at its freezing temperature (- 183 °C) to form vitrified specimens, which were then stored at - 196 °C in liquid nitrogen until examination. Specimens were examined in a Tecnai T12 G2 TEM (FEI) at an accelerating voltage of 120 kV. Samples were placed in a Gatan cryo-specimen holder that maintained the samples below – 175 °C. Imaging was done in the low-dose mode to minimize electron-beam radiation damage. Images were recorded digitally at nominal magnifications up to 46 000 x on a cooled UltraScan 1000 Gatan camera, using the DigitalMicrograph.

### **4.3. Results and Discussion**

#### **ODPI-SDBS Vesicles**

The photoresponsive vesicles described here are created by combining aqueous solutions of the cationic photoinitiator ODPI and the anionic surfactant SDBS. ODPI is an alkyl substituted diphenyliodonium salt (Figure 4.1 (a)) that is widely used as a photoinitiator for UV and near-infrared (NIR) polymerization.<sup>111,112</sup> We note that ODPI has an octyl tail and a cationic head group. This suggests that ODPI is amphiphilic and that it could serve as a cationic surfactant. Surface tensiometry confirms this point. As shown in Figure 4.3, the addition of ODPI to water decreases the surface tension up to a plateau value of 32.5 mN m<sup>-1</sup>. From the inflection point of the surface tension plot,<sup>87</sup> we estimate its critical micelle concentration (CMC) to be 1.3 mM. Incidentally, the CMC of the anionic surfactant SDBS is reported to be 1.4 mM.<sup>122</sup> Thus, ODPI and SDBS are surfactants with similar CMC values, but with opposite charges.



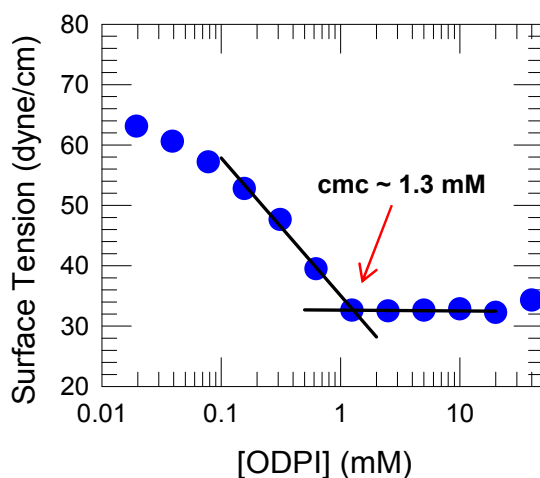


**Figure 4.3.** Surface tension values are plotted over the range of concentrations of ODPI in 50 mM phosphate buffer. The plot shows the typical behavior expected for surfactants, *i.e.*, a drop in surface tension followed by a plateau. The CMC value obtained from the intersection point of the two regressed lines is 1.3mM.

We proceeded to examine the phase behavior of ODPI–SDBS mixtures at a total surfactant concentration of 1 wt%. Samples with various weight ratios of ODPI to SDBS were prepared in 50 mM phosphate buffer solutions. We used a buffer rather than deionized water to ensure that the pH remained stable with time. On their own, both ODPI and SDBS form clear solutions in buffer. When the two solutions are mixed, samples at ODPI : SDBS ratios between 2 : 8 and 4 : 6 are homogeneous and cloudy with a bluish tint, which is indicative of vesicle solutions (Figure 4.4).<sup>77</sup> Samples at ODPI : SDBS ratios of 5 : 5 and 6 : 4 reveal some visible solid precipitation, while samples with higher ODPI content (ODPI : SDBS from 7 : 3 to 9 : 1) separate into co-existing liquid phases. The above phase behavior of ODPI–SDBS mixtures is reminiscent of other cationic/anionic surfactant mixtures. In particular, mixtures of cationic surfactants like cetyl trimethyl-ammonium tosylate (CTAT) with SDBS also give rise to vesicles at ratios similar to those in Figure 4.4.<sup>22,23</sup> For a fixed weight ratio of ODPI : SDBS = 3 : 7

(corresponding to a molar ratio of 1 : 4.3), homogeneous vesicle-bearing samples are found over a window of total surfactant concentration from about 0.1 to 4 wt%. Above 4 wt%, the mixtures become inhomogeneous and show a solid precipitate.

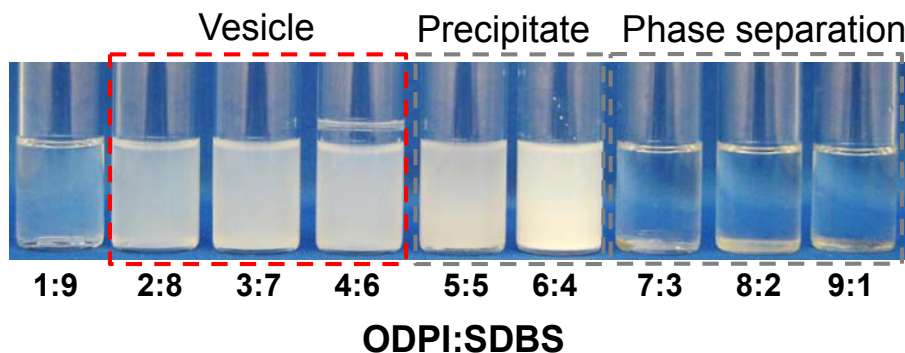


**Figure 4.4.** Phase behavior of ODPI–SDBS mixtures at a fixed total concentration of 1 wt% in aqueous buffer. Samples at ODPI : SDBS weight ratios between 2 : 8 and 4 : 6 show the presence of vesicles. The bluish tinge of these samples reflects light scattering from vesicles. At higher ODPI content (5 : 5 and 6 : 4), samples reveal a whitish precipitate. At even higher ODPI content (7 : 3 to 9 : 1) the samples separate into two liquid phases.

The vesicle-containing ODPI–SDBS mixtures were analyzed further. The samples remained homogeneous and unchanged for several weeks when stored in the dark at room temperature. The size of structures in solution was measured by dynamic light scattering (DLS). For a sample of 1 wt% total surfactant at a ratio of ODPI : SDBS = 3 : 7, the hydrodynamic diameter  $D_h$  measured by DLS was 110 nm. This size was maintained over a period of weeks, *i.e.*, there was no aggregation or coalescence of the vesicles. While DLS and visual observations are strongly suggestive of vesicles, we resorted to the technique of cryotransmission electron microscopy (cryo-TEM) for definitive evidence in this regard.<sup>75,121,123</sup> Figure 4.5 (a) shows a representative cryoTEM

image of the above ODPI–SDBS sample. The image indeed confirms the presence of unilamellar vesicles in the sample, which are each seen to have a distinct dark shell (bilayer) enveloping their aqueous core.<sup>123</sup> The vesicles range from 30 to 120 nm in diameter, which is broadly consistent with the DLS measurement.

### Vesicle to Micelle Transition Induced by Light

We now discuss the effect of UV irradiation on the 1 wt% ODPI : SDBS = 3 : 7 sample. As shown in Photo 1 of Figure 4.5, this vesicular sample is initially turbid with a bluish tint and the  $D_h$  from DLS was 110 nm. Upon UV irradiation, the sample gradually loses its turbidity and becomes transparent and yellowish (Photo 2 in Figure 4.5). The loss of turbidity indicates a structural transformation to much smaller structures.<sup>77</sup> After 1 h of UV irradiation, the  $D_h$  from DLS was found to be 8.2 nm. Such a low value of  $D_h$  suggests that the vesicles must have been converted into micelles.<sup>77</sup> To confirm this

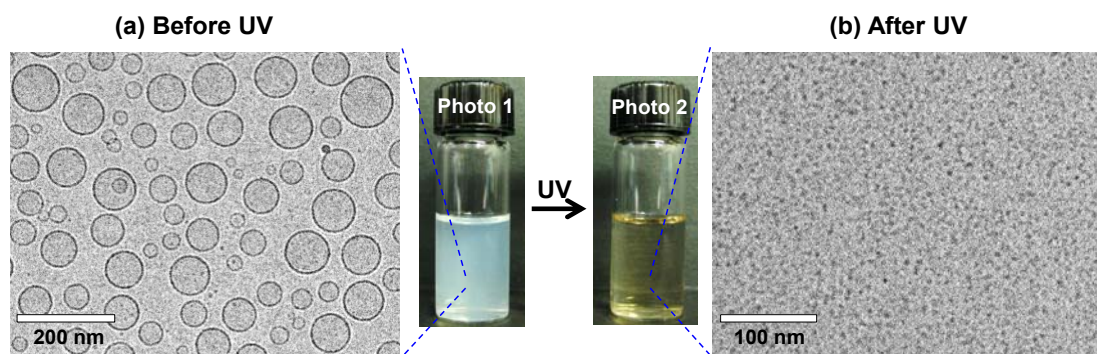


**Figure 4.5.** Vesicle to micelle transition induced by UV light, as shown by visual observations and cryo-TEM images. The sample is a 1 wt% mixture of ODPI : SDBS = 3 : 7. (a) Initially (before UV exposure), the sample shows a bluish tinge and high turbidity (Photo 1). Under cryo-TEM, numerous unilamellar vesicles with diameters between 30 and 120 nm are seen. (b) After 1 h of UV irradiation, the sample is transformed into a transparent, yellowish solution that weakly scatters light (Photo2). Under cryo-TEM, spherical micelles with a size around 3–5 nm are seen.

aspect, we again resorted to cryo-TEM. A representative cryo-TEM image of the irradiated sample is shown in Figure 4.5 (b) and it indeed reveals the presence of spherical micelles, which appear as black spots in the image.<sup>123</sup> The size of these micelles is about 3 to 5 nm, which is much smaller than the vesicles. Note the absence of any larger entities in the photograph as well as the cryo-TEM image, which implies that the irradiated sample is a homogeneous, single-phase micellar solution.

The UV-induced vesicle-to-micelle transition in ODPI–SDBS mixtures is readily explained based on the photochemistry of ODPI. Diphenyliodonium salts like ODPI are known to undergo photodissociation, whereby the molecule loses its positive charge and generates a proton (indeed, ODPI is an example of a “photoacid generator”).<sup>40,110</sup> In the present case, the protons are not responsible for the structural transition. All samples were prepared in buffer solution and the measured pH of the sample before and after UV irradiation was almost the same at around 7.5. Also, ODPI–SDBS vesicles are stable and display identical sizes over a wide range of pH (3–12). Rather than the protons, it is the loss of positive charge on ODPI that explains the UV-induced transition, as depicted in Figure 4.6. Once ODPI dissociates, the molecule becomes nonionic and hydrophobic, which is shown as pink tails (without a head) in Figure 4.6. In contrast, the initial ODPI is a surfactant, shown as a pink tail with a blue cationic head. This difference in molecular geometry impacts the packing of the molecules within self-assembled structures.

It is useful to invoke the concept of the critical packing parameter in this context.<sup>1,87</sup> This parameter  $p = a_{\text{tail}}/a_{\text{head}}$ , *i.e.*, it is a ratio of the average area of the tail

region ( $a_{tail}$ ) to the average area of the head region ( $a_{head}$ ). The head area ( $a_{head}$ ) includes the influence of electrostatic charge, *i.e.*, when the head is charged,  $a_{head}$  will be large. Initially, when ODPI and SDBS are mixed, the cationic heads of ODPI will bind with the anionic heads of SDBS, creating ion-paired complexes.<sup>22,23</sup> These complexes will have

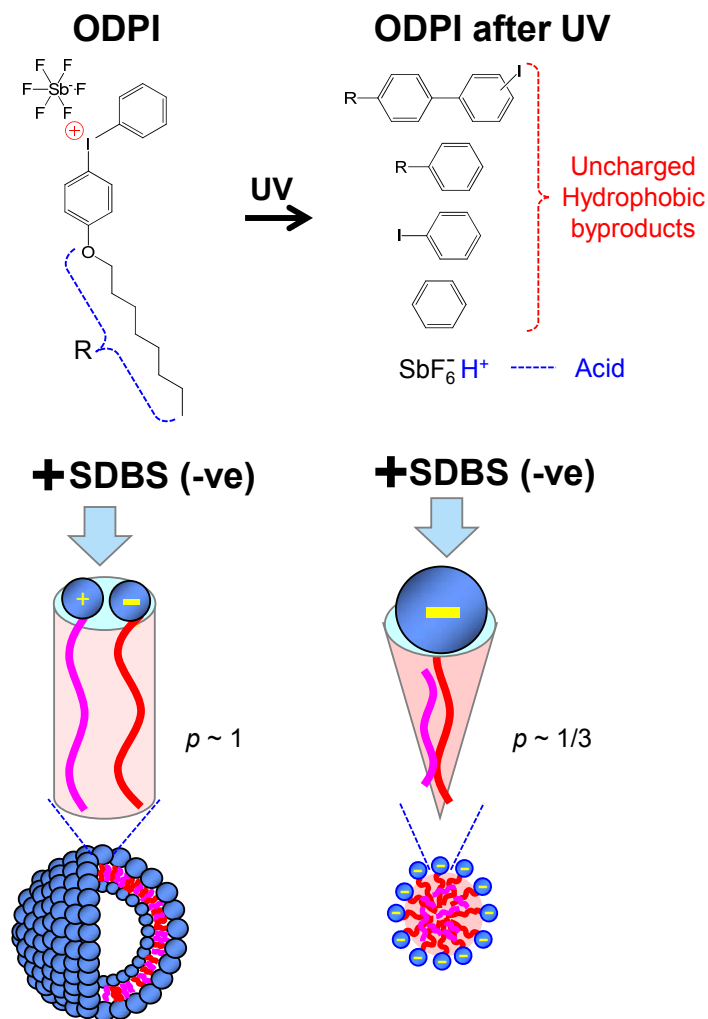


**Figure 4.6.** Mechanism for the UV-induced conversion of ODPI–SDBS vesicles to micelles. Initially, ODPI is cationic and it pairs with the anionic SDBS, giving a cylindrical geometry ( $p \sim 1$ ) that leads to vesicles. UV irradiation transforms ODPI into uncharged byproducts (pink tails). In this case, the lack of cationic species to pair with the anionic heads of SDBS implies a net cone shape ( $p \sim 1/3$ ), in turn leading to spherical micelles. The pink tails are embedded in the hydrophobic cores of these micelles.

comparable  $a_{\text{tail}}$  and  $a_{\text{head}}$  and will assume the overall shape of a cylinder ( $p \sim 1$ ), as shown in Figure 4.6. This geometry favors the formation of bilayers and in turn vesicles.<sup>1,87</sup> (Note that the vesicles still have an excess of one surfactant, which in turn imparts a net charge to the bilayer that may help to stabilize the vesicles.) Upon UV irradiation, the loss of charge on ODPI will leave only the anionic SDBS with a net charge on its head, and this will mean a large  $a_{\text{head}}$ . Such a molecule will take on a cone shape ( $p \sim 1/3$ ), *i.e.*, its head area will far exceed its tail area (Figure 4.6). This geometry favors the formation of spherical micelles.<sup>1,87</sup> Note that the hydrophobic byproducts of ODPI photodissociation are expected to get sequestered in the cores of SDBS micelles. That is why the sample remains homogeneous after UV irradiation.

In closing this section, we reiterate that our photoresponsive vesicles are one of the simplest classes of light-sensitive nanocontainers. The mixture of ODPI and SDBS, two wellknown commercially available compounds, results in spontaneous assembly into unilamellar vesicles, and light causes a phase transition of these vesicles to spherical micelles. A noteworthy aspect here is that both the initial and the irradiated states are stable, homogeneous and well-defined. This is in contrast to many previous light-responsive vesicle systems, where light-induced complete disruption of the bilayer causes the vesicles to aggregate or transform into an undefined precipitate.<sup>8,104,108</sup>

### **Vesicle-Gels using ODPI–SDBS Vesicles and hm-Alginate**

Next, in addition to light-triggered disruption of nanocontainers, we investigated the use of our photoresponsive vesicles to design photorheological (PR) fluids, *i.e.*, fluids

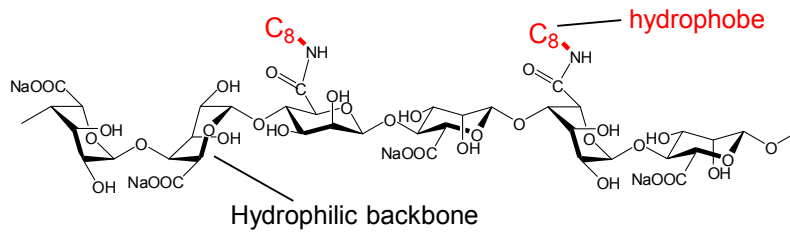
that undergo a significant change in their rheological properties upon exposure to light.<sup>67,113</sup> For this, we created a “vesicle-gel” using ODPI–SDBS vesicles. A vesicle-gel, as demonstrated by us and others, is obtained by adding an associating polymer to a solution of vesicles.<sup>24,114-116</sup> Associating polymers are those with a hydrophilic backbone and hydrophobes that are either attached at the chain ends or along the chain backbone.<sup>36</sup> When added to vesicles, the hydrophobes on the polymer chains get embedded in vesicle bilayers, thus bridging the vesicles into a three-dimensional network (see Figure 4.9 (a)).<sup>24</sup> The sample then becomes either gel-like (highly viscoelastic, with a long, but finite relaxation time) or a true elastic gel with an infinite relaxation time.<sup>24,114-116</sup>

To gel the ODPI–SDBS vesicles, we synthesized a hydrophobic derivative of the biopolymer alginate using established procedures (see Experimental section for details).<sup>117-119</sup> The resulting hydrophobically modified alginate (hm-alginate) bears octyl (C<sub>8</sub>) groups along its backbone, as shown in Figure 4.7 (a). The degree of hydrophobic modification was determined to be 23 % by NMR (see Figure 4.2). Note that hm-alginate has an anionic character due to the residual carboxylate groups on the polymer. The vesicles at a ratio of ODPI : SDBS = 3 : 7 are also anionic (since the anionic surfactant SDBS is in molar excess).

Figure 4.7 (b) describes vesicle-gel formation upon mixing nonviscous solutions of the above ODPI–SDBS vesicles and hmalginate. As seen in Plot 1, a 3 wt% solution of the vesicles is a Newtonian fluid with a low viscosity around 2 mPa s. A 1 wt% solution of hm-alginate also shows a viscous response,<sup>45</sup> as indicated by its dynamic rheological

data in Plot 2. That is, the elastic ( $G'$ ) and viscous ( $G''$ ) moduli are strong functions of frequency  $\omega$ , with  $G'' > G'$  over the frequency range. When 1 wt% hm-alginate is

(a) hm-alginate (associating polymer)



(b) Vesicle-gel formation

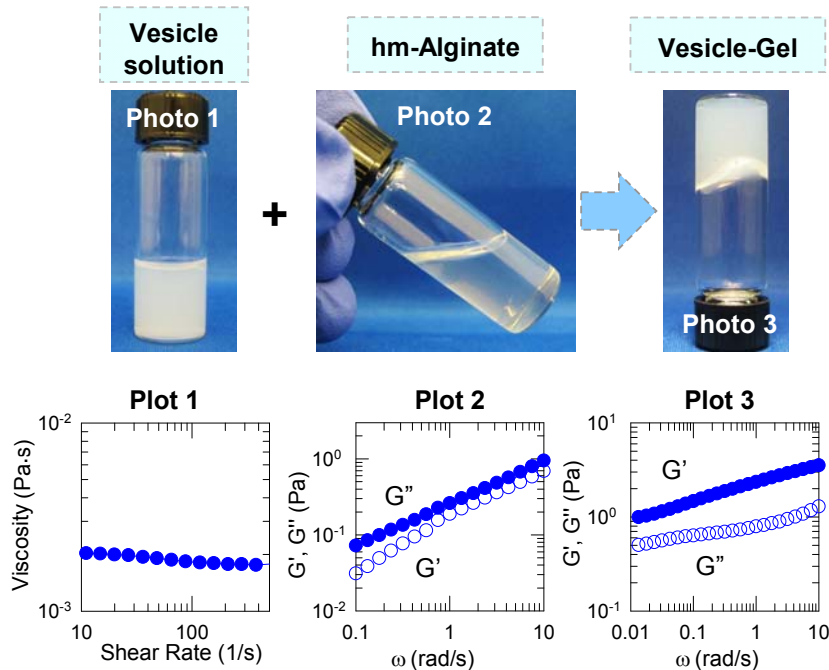


**Figure 4.7.** Vesicle gel formation by combining hm-alginate and ODPI-SDBS vesicles. (a) Molecular structure of hm-alginate. (b) Photographs and rheological data demonstrating the formation of a vesicle gel. A sample of 3 wt% ODPI : SDBS = 3 : 7 vesicles is initially a low-viscosity fluid (Photo 1) and shows Newtonian behavior in steady-shear rheology (Plot 1). This is combined with a 1 wt% solution of hm-alginate (Photo 2), which is moderately viscous, as shown by data from dynamic rheology (Plot 2). The mixture results in a vesicle gel that holds its weight in the inverted vial (Photo 3) and shows an elastic response in dynamic rheology (Plot 3). In plots 2 and 3, the elastic modulus  $G'$  (filled circles) and the viscous modulus  $G''$  (unfilled circles) are depicted as functions of the angular frequency  $\omega$ .



combined with 3 wt% vesicles, the mixture is instantly turned into a gel that holds its weight in the inverted vial (Photo 3). Note that the vesicle-gel is bluish and cloudy, similar to the vesicle sample (Photo 1). The gel shows a predominantly elastic response in dynamic rheology (Plot 3): *i.e.*,  $G' > G''$  over the  $\omega$  range, and with both moduli showing a weak dependence on  $\omega$ . Such a response is indicative of a gellike material comprising a transient physical network.<sup>45</sup> The same sample under steady-shear rheology shows a zero-shear viscosity  $\eta_0$  around 400 Pa s (Figure 4.8 (a)). It also exhibits weak shearthickening beyond the Newtonian regime, which is often observed in solutions of associating polymers.<sup>36</sup> When the shear stress exceeds 5 Pa, a steep drop in viscosity is observed. This is akin to a yield stress, *i.e.*, the sample hardly flows at stresses below this value, as seen in Photo 3.<sup>36,45</sup>

### **Vesicle-Gel to Sol Transition Induced by Light**

Next, we investigated the effect of UV irradiation on the above vesicle-gel. Visual inspection revealed that the gel was turned into a thin, freely flowing liquid (sol) when exposed to UV light. A photograph of the UV-irradiated sample is shown in the inset to Figure 4.8 (a). The sample has the yellowish tinge previously observed in Photo 2 of Figure 4.5; note the contrast in both color and flow properties with the initial vesicle-gel sample. These visual observations are corroborated by data from steady-shear and dynamic rheology. The steady-shear data (Figure 4.8 (a)) indicate that the gel ( $\eta_0 \sim 400$  Pa s) is converted to a Newtonian sol with a viscosity of 10 mPa s (*i.e.*, a reduction by a factor of 40 000). The data from dynamic rheology (Figure 4.8 (b)) confirm the viscous nature of the irradiated sample, *i.e.*,  $G'' > G'$  with the moduli being strong functions of

frequency. This is in contrast to the elastic gel-like response of the sample prior to irradiation.

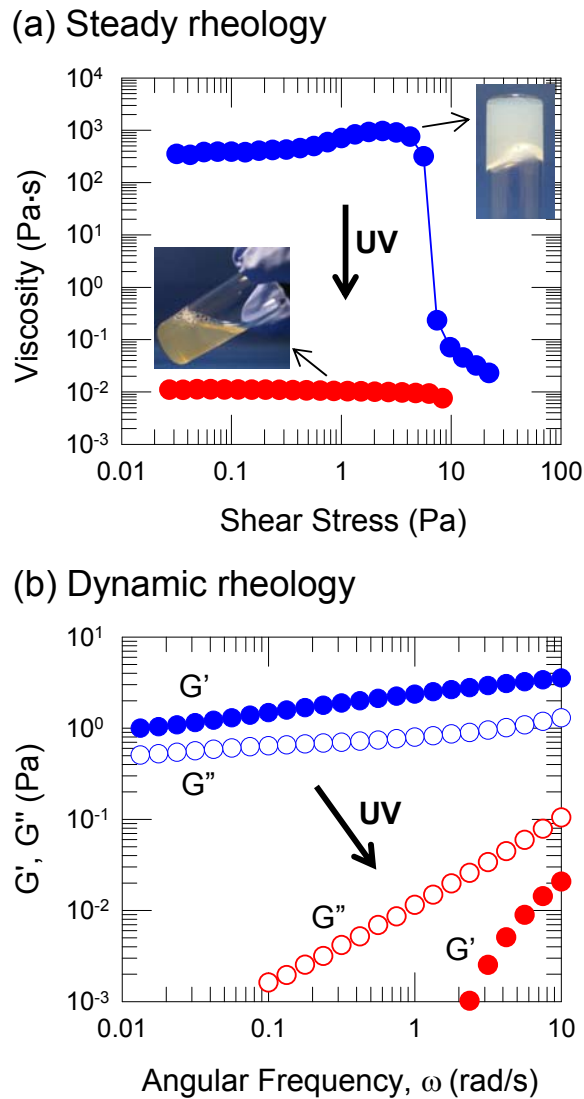


**Figure 4.8.** Gel-to-sol transition of the photoresponsive vesicle gel upon UV irradiation. Data from steady-shear rheology (a) and dynamic rheology (b) are shown for a vesicle-gel obtained by mixing a 3 wt% ODPI : SDBS = 3 : 7 vesicles and a 1 wt% hm-alginate solution. In (a) the apparent viscosity is shown as a function of shear stress. In (b), the elastic modulus  $G'$  (filled circles) and the viscous modulus  $G''$  (unfilled circles) are plotted against the angular frequency  $\omega$ . Before UV irradiation (blue symbols), both sets of data indicate gel-like behavior of the sample. After UV irradiation, the sample is reduced to a thin fluid that exhibits purely viscous, Newtonian behavior. This is corroborated by the photos shown in the inset of (a).

We attribute the light-induced gel-to-sol transition of the above sample to the light-induced transformation of ODPI–SDBS vesicles to micelles. The scenario is depicted in Figure 4.9. Initially, when the vesicles are mixed with hm-alginate, a vesicle-gel is formed as shown in Figure 4.9 (a). Here, the hydrophobes on the polymer chains are inserted into vesicle bilayers and the vesicles thus act as multi-functional crosslinks in a network structure.<sup>24</sup> As demonstrated by dynamic rheology, the bonds in this network relax very slowly, and the sample thus exhibits gel-like behavior with a yield stress.<sup>36</sup> Upon UV irradiation, a transition from vesicles to spherical micelles occurs. The

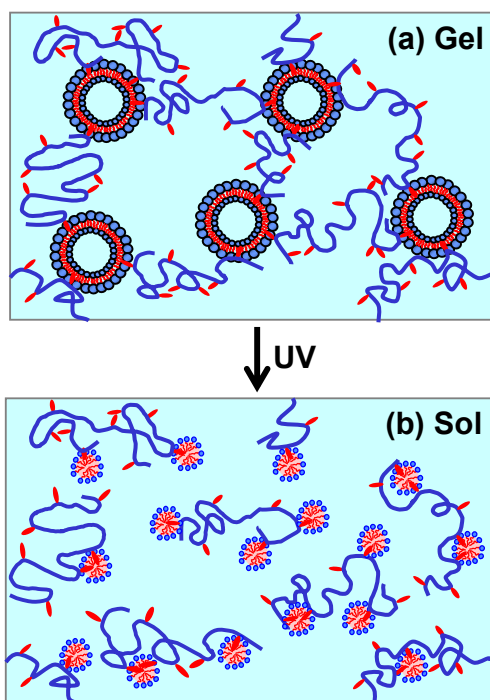


**Figure 4.9.** Mechanism for the UV-induced gel-to-sol transition. Initially, when ODPI–SDBS vesicles and hm-alginate are combined, a vesicle-gel is obtained, as shown in (a). Here, the hm-alginate chains are depicted with a blue backbone and red hydrophobic pendant groups. The hydrophobes embed in the bilayers of vesicles, also shown in red, *via* hydrophobic interactions. The result is that the vesicles become connected by the polymer chains into a network, which explains the gellike behavior. Upon UV irradiation, the vesicles are transformed into spherical micelles (b). These micelles enclose and sequester the hydrophobes on the polymer chains. As a result, the crosslinks in the network are eliminated and the sample is converted to a sol.

hydrophobes are now expected to be embedded (“solubilized”) in the spherical micelles, as shown in Figure 4.9 (b). Because micelles are much smaller than vesicles, they will typically enclose individual hydrophobes, but will be isolated from other polymer chains.<sup>36</sup> Note also that spherical micelles are dynamic structures that break and reform frequently due to rapid surfactant exchange,<sup>124</sup> whereas vesicles are relatively static structures due to a much slower rate of surfactant exchange.<sup>87</sup> In other words, micelles cannot serve as crosslinks in the same way as vesicles.<sup>24</sup> All in all, the transition from vesicles to micelles eliminates the crosslinks that held the network in place. This explains the gel-to-sol transition and thus the PR effect.

We have considered an alternate possibility for the UV-induced PR effect, which is that reflects the scission of hm-alginate chains due to radicals generated by photodissociation of ODPI.<sup>40,110</sup> To test this, we solubilized ODPI in micelles of the nonionic surfactant Triton X100 and added it to solutions of alginate and hm-alginate. No changes in viscosity were observed in these solutions upon UV irradiation. (Note that if ODPI was directly mixed with alginate, it formed a precipitate due to the opposite charges on the two moieties.) Thus, the PR changes cannot be attributed to the effect of radicals. This is probably because the generated radicals are expected to be hydrophobic, and would get buried in the interior of micelles *i.e.*, they would not directly interact with the polymer chains or with the surfactant head groups.

We also studied the PR response for different concentrations of hm-alginate and the vesicles. First, we fixed the vesicles at 2 wt% and varied the hm-alginate

concentration. Data are shown in Figure 4.10 for the low-shear viscosity  $\eta_0$  before and after UV irradiation. At low concentrations of hm-alginate ( $\sim 0.5$  wt%), the sample is not gel-like because there are too few polymer chains to connect the vesicles into a network.<sup>24</sup> On the other hand, at high concentrations of hm-alginate ( $>1.5$  wt%), there is very little difference in  $\eta_0$  before and after irradiation. This is because at high concentrations, hm-alginate can form a gel-like network by itself through associations between its hydrophobes, *i.e.*, even in the absence of vesicles.<sup>117,118</sup> Next, we fixed the hm-alginate at 1 wt% and varied the vesicle content. Below 1 wt% vesicles, the samples are again not gels because there are insufficient vesicles to connect the polymer chains into a network.<sup>24</sup> Gels do form for  $>1$  wt% vesicles, and the viscosity  $\eta_0$  and yield stress of the gels increase with vesicle concentration (Figure 4.11). After UV irradiation, these

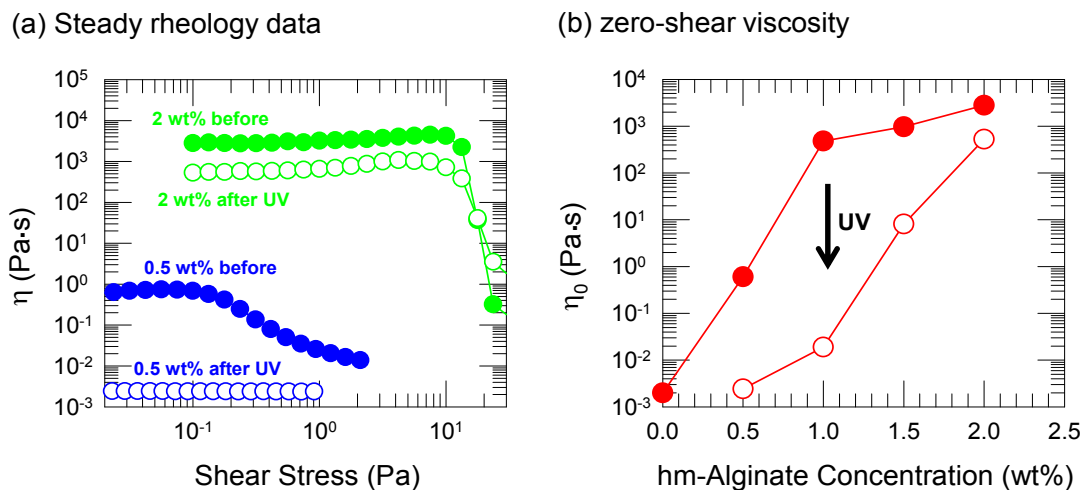


**Figure 4.10.** Rheology of vesicle gels before and after UV irradiation: Effect of altering the hm-alginate concentration at a constant ODPI/SDBS vesicle concentration of 2 wt%. (a) Representative steady-shear rheology data for samples before (closed circles) and after 45 min of UV irradiation (open circles): 2 wt% hm-alginate (green symbols); 0.5 wt% hm-alginate (blue symbols). (b) From the steady rheology data, the zero-shear viscosity  $\eta_0$  is plotted against the hm-alginate concentration: before UV irradiation (closed red circles); after 45 min of UV irradiation (open red circles).

vesicle-gels become non-viscous solutions regardless of the vesicle concentration. Thus, in order to maximize the PR effect, it is better to use a moderate concentration of hm-alginate ( $\sim 1$  wt%) and a high concentration of ODPI–SDBS vesicles.

An attractive feature of these vesicle-gel-based PR fluids is that vesicles, *i.e.*, nanocontainers, are present in the gel state whereas these containers are disrupted and converted to micelles in the sol state. Thus the light-induced gel-to-sol transition can be combined with light-triggered release of payloads encapsulated in the vesicles. Consequently, the current fluids may be envisioned as a type of photoresponsive delivery system (*e.g.*, an injectable gel) for drug delivery or controlled release applications.<sup>116</sup>

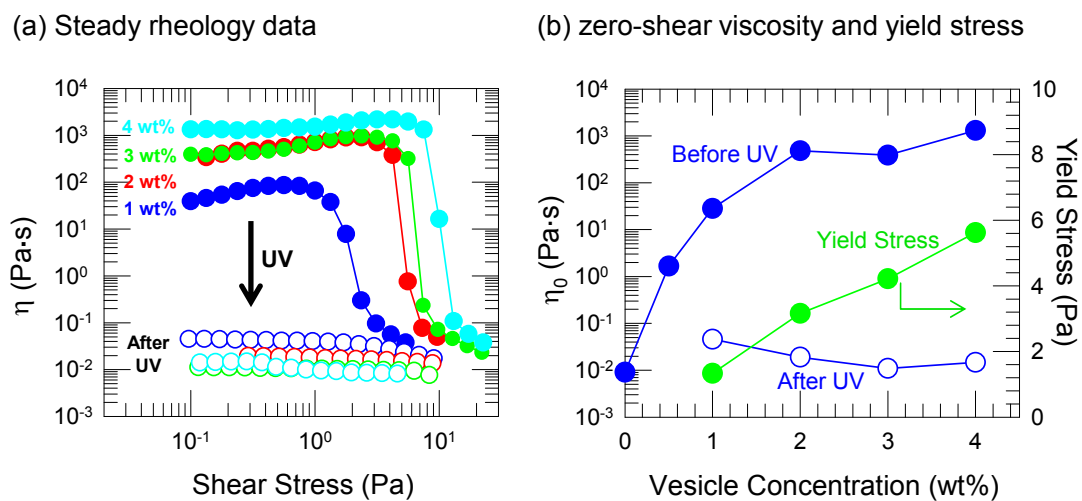


**Figure 4.11.** Rheology of vesicle-gels before and after UV irradiation: Effect of altering the ODPI/SDBS vesicle concentration at a fixed hm-alginate concentration of 1 wt%. (a) Steady-shear rheology data for samples before (closed circles) and after 45 min of UV irradiation (open circles) for vesicle concentrations of 1 wt% (blue symbols), 2 wt% (red), 3 wt% (green) and 4 wt% (cyan). (b) From the steady-shear data, the zero-shear viscosity  $\eta_0$  and the apparent yield stress (point of sharp drop in viscosity) are plotted against the vesicle concentration:  $\eta_0$  before UV irradiation (closed blue circles); yield stress before UV irradiation (closed green circles);  $\eta_0$  after 45 min of UV irradiation (open blue circles).

#### 4.4. Conclusions

We have described a simple class of photoresponsive vesicles that transform into spherical micelles upon UV irradiation. These are prepared by mixing two inexpensive and commercially available surfactants, *viz.* the cationic ODPI and the anionic SDBS. The oppositely charged head groups of ODPI and SDBS bind to each other, resulting in cylinder-shaped pairs of molecules, which spontaneously assemble into vesicles. When these vesicles are irradiated by UV light, ODPI molecules lose their positive charge and become hydrophobic. SDBS head groups then no longer have a binding partner and so the molecular geometry assumes a cone shape, which explains the transition to spherical micelles. Using the above vesicles, we have also demonstrated a photoresponsive vesicle-gel that is converted to a sol by UV irradiation. The gel is created by combining the associating biopolymer hm-alginate with the ODPI–SDBS vesicles. hm-alginate chains bind to the vesicles *via* hydrophobic interactions between the hydrophobes and vesicle bilayers; in turn, the vesicles become connected by polymer chains into a network. Upon UV irradiation, the vesicles are converted into micelles, and the resulting micelles envelop the hydrophobes. In turn, the crosslinks holding the gel network are eliminated and therefore the sample is converted to a sol. Our vesicle-gel thus serves as a photorheological (PR) fluid with a 40 000-fold reduction in sample viscosity due to light. Because the gel-to-sol transition is accompanied by the disruption of vesicles, the above gel could also be envisioned as an injectable material for light-controlled delivery of drugs or other payloads.

## Chapter 5

### Light-Activated Fluidic Valve

---

#### 5.1. Introduction

Fluids whose viscosity can be remotely controlled have been a fascinating research topic among scientists and engineers. Since the first demonstration of the remote control of fluid viscosity via magnetic and electric fields in the late 1940's, a wide range of applications have been envisioned for such fluids in mechanical devices such as dampers, clutches, and valves.<sup>125-128</sup> Recently, light has emerged as a different kind of remote trigger for rheological modulation.<sup>9,49,52</sup> Fluids with light-tunable rheology are termed photorheological (PR) fluids.<sup>16,52</sup> Light as an external stimulus has many advantages over other stimuli: it can be directed from a distance at a precise location with a resolution of few microns, and a wide range of light sources are available with distinct wavelengths and intensities. A potential application of PR fluids that leverages the spatial selectivity of light is a light-activated valve for flow control within fluidic devices. The idea is that, by using light as an external switch, specific flow paths within a network of fluidic channels can be closed and reopened as needed.

Despite many recent advances, PR fluids are not used in applications such as the one described above. One reason is that many PR fluid formulations require complicated synthesis procedures to impart photoresponse to molecules such as surfactants,<sup>9,10,55,56</sup> polymers,<sup>12,44,57-59</sup> organogelators<sup>3,13,60-64</sup> or other species.<sup>65,66</sup> A second reason is that the



magnitude of the PR effect may be insufficient.<sup>10,12,44,55-57,67,113,129-132</sup> The high-viscosity state of most PR fluids relies on physical (non-covalent) bonds, *i.e.*, self-assembly. However, these physical bonds can be disrupted easily when the fluid is subjected to shear stress.<sup>36,45,67,113</sup> A third issue with using PR fluids for practical applications is their response time. Most PR fluids require relatively long irradiation times (more than 10 min) to induce a large change in viscosity, even when a high-power UV lamp (> 100 W) is used.<sup>3,12,13,55-57,67,113,129-132</sup> There do exist a few fast-responsive (response time < 5 min) PR systems, but they show a modest (less than 100-fold)<sup>10,44</sup> or negligible<sup>133,134</sup> change in viscosity upon exposure to light. The above limitations provide the motivation for our current work. Our goal is to develop a PR fluid based on common chemicals that can show a dramatic PR effect and a relatively fast response, and to then apply this fluid to create a light-activated fluidic valve.

It should be noted that in Chapter 3, we demonstrated a PR fluid that shows a million-fold change in its viscosity under light.<sup>113</sup> However, even this system is not suitable for use in a light-activated fluidic valve. The key reason is that this fluid in its high-viscosity state is viscoelastic with a finite relaxation time, *i.e.*, it is not an elastic solid or gel.<sup>32,45</sup> Moreover, when sheared, the fluid exhibits shear-thinning, *i.e.*, the viscosity drops with time. For the valve application, it is desirable to have a PR fluid that transitions between a thin liquid (sol) and a gel (infinite relaxation time) with a sufficient yield stress.<sup>32,45</sup> The yield stress of the gel is the governing factor for the gel to be able to block the flow. In other words, when the shear stress developed by the pressure drop in the channel is smaller than the yield stress of the gel, the flow can be completely blocked.

Accordingly, a light-induced gel with high yield stress is essential for the fluidic valve application.

To obtain a strong gel as a result of the PR effect, we turned to a different PR system that was developed previously in our lab based on light-activated ionic gelation of alginate.<sup>70</sup> This system is composed of alginate, calcium carbonate and photoacid generator (PAG). In this system, the photoactive component PAG is not directly involved in structure formation, but it acts as a photo-trigger to release  $\text{Ca}^{2+}$  ions upon UV irradiation. The released  $\text{Ca}^{2+}$  ions then bind with alginate chains to create physical crosslinks known as “egg-box” junctions.<sup>25,135,136</sup> However, while the irradiated sample does show the rheology of a gel, the yield stress of the gel is too low (less than 10 Pa),<sup>70</sup> making it inapplicable as a fluidic valve.

In this study, we report a new version of alginate-based PR fluids, which show a transition upon UV irradiation from a non-viscous solution (Figure 5.1a) to a gel with a sufficient yield stress that is strong enough to be held by fingers (Figure 5.1b). The fluid is again made using only commercially available components: alginate, PAG as a photo-trigger, and a chelated complex of divalent strontium ( $\text{Sr}^{2+}$ ) ions (Sr-EGTA). In Figure 5.1c, our scheme for the sol-to-gel transition is depicted. Upon exposure to UV, the PAG dissociates to give  $\text{H}^+$  ions,<sup>40,110</sup> which initiate the gelation process in a two-step manner. First,  $\text{H}^+$  ions decrease the pH of the solution, and this leads to a surge of free  $\text{Sr}^{2+}$  ions due to the dissociation of Sr-EGTA.<sup>137</sup> The free  $\text{Sr}^{2+}$  ions then self-assemble with the alginate chains to form physical crosslinks (“egg-box” junctions).<sup>25,135,136</sup> Finally alginate

chains are connected into three-dimensional networks and the solution turns into a solid-like gel as seen in Figure 5.1b. An additional aspect is the rate of PR response. To increase this rate, we ensure that the PR fluid maintains transparency throughout the photogelation process.<sup>40,43</sup> For this purpose, the PAG is inserted into the hydrophobic pockets of a cyclodextrin (CD), forming a PAG-CD complex which makes the system transparent and increases the apparent intensity of UV light.

We then demonstrate a practical application of PR fluids as a light-activated fluidic valve. For this, we flow our PR fluids through a microchannel and expose a specific point in the channel to UV. At that point, in a few minutes, the alginate solution gets converted into a gel strong enough to stop the flow. When UV light is removed, the gel is gradually dissolved, and the flow channel reopens. Moreover, we also demonstrate a different application of this PR fluid, which is for the site-specific deposition and release of material within the microchannel. The successful demonstrations of above applications are possible due to the unique properties of our PR fluids, *i.e.*, they can form a strong gel even though the bonds are physical (non-covalent) bonds. At the same time, the physical nature of the bonds allows reversal of gelation. Because of the simplicity (using only common chemicals), the fast response (within a few minutes), and the dramatic PR effect (transition from solution to a strong gel), we believe that our PR formulation will have wide utility in academic and industrial research.

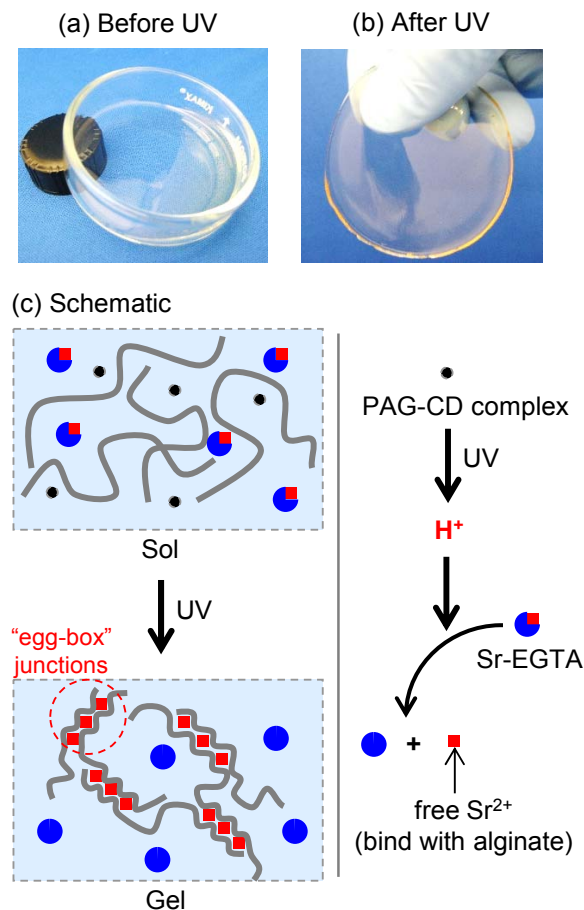


**Figure 5.1.** Visual description and schematic of UV-induced photogelation of alginate. Sodium alginate (2.5 wt%) is combined with Sr-EGTA ( $\text{Sr}^{2+}$  source) and PAG-CD complex ( $\text{H}^+$  source). The resulting sample is a clear solution that flows freely in the petri dish, photo (a). (c) Upon exposure to UV light, the PAG is photolyzed and thereby releases  $\text{H}^+$  ions, which decrease the chelating efficiency of EGTA. Consequently,  $\text{Sr}^{2+}$  ions are released from the Sr-EGTA chelates and gel the alginate. As shown in the schematic,  $\text{Sr}^{2+}$  ions bind with adjacent alginate chains and form “egg-box” junctions, which act as physical crosslinks. As shown in photo (b), the final gel is transparent and strong enough to hold by one’s fingers.

## 5.2. Experimental Section

**Materials.** Sodium alginate (product number 4-00005) was purchased from Carbomer, Inc. and the molecular weight was specified by the manufacturer to be around 500 kDa.<sup>138</sup> Alginate extracted from a brown algae usually contains impurities,<sup>139</sup> thus its solution is slightly turbid. To purify alginate, first it was dissolved in water at 1 wt% and the solution pH was adjusted to around 10 with NaOH. Suspended impurities in the solution were removed by filtration with Fisherbrand™ Glass Fiber Circles, grade G6. After filtration, clear alginate solution was precipitated in acetone and dried in vacuum oven at room temperature. A type of photoacid generator (PAG), diphenyliodonium Nitrate, and methyl- $\beta$ -cyclodextrin (m- $\beta$ -CD) were purchased from TCI. A chelating agent, ethylene glycol tetraacetic acid (EGTA), strontium chloride (SrCl<sub>2</sub>), D-(+)-gluconic acid  $\delta$ -lactone (GDL), and phenol red were obtained from Sigma-Aldrich. Aqueous solutions of green fluorescent beads (Fluoresbrite® YG, 0.10  $\mu$ m) and red fluorescent beads (Fluoresbrite® Polychromatic Red, 0.5  $\mu$ m) were purchased from Polysciences. For all sample preparation, deionized (DI) water was used.

**Sample Preparation.** All samples were prepared by mixing stock solutions of alginate, Sr-EGTA, PAG-CD complex. The purified alginate was dissolved in DI water by 5 wt%. Sr-EGTA solution was prepared by dissolving desired amount of SrCl<sub>2</sub> in EGTA tetrasodium salt solution. The molar ratio of EGTA to SrCl<sub>2</sub> was fixed with 1.25. To prepare PAG-CD complex, weight amount of PAG and m- $\beta$ -CD was dissolved in DI water, then the solution was sonicated for 5 minutes. The molar ratio of m- $\beta$ -CD to PAG was fixed at 3. To formulate PR fluids, first, equal volumes of Sr-EGTA and PAG-CD

complex stock solutions were mixed, and then, to this solution, equal volume of alginate 5wt% solution was added and vortex mixed. The final concentration of alginate in our PR fluids is 2.5 wt%. The pH of our PR fluids before light irradiation was around 9.0.

**Sample Response Before and After UV Irradiation.** Samples were irradiated with UV light from an Oriel 200 W mercury arc lamp. A dichroic beam turner with a mirror reflectance range of 280 to 400 nm was used to access the UV range of the emitted light. A filter for below 400 nm light was used to eliminate the undesired visible wavelengths. Samples (2.5 mL) were placed in a Petri dish of 60 mm diameter with a quartz cover, and irradiation was done for a specific duration without stirring.

**Rheological Studies.** A TA Instruments AR2000 stress-controlled rheometer was used to perform steady and dynamic rheological experiments. Samples were run at 25°C on a cone-and-plate geometry (40 mm diameter and 2° cone angle) for solutions or a parallel plate geometry (20 mm diameter). A solvent trap was used to minimize drying of the sample during measurements. Dynamic frequency spectra were conducted in the linear viscoelastic regime of the samples, as determined by prior dynamic strain sweeps.

**Microfluidic Chip Fabrication and Operations.** The microfluidic chip comprised a PMMA substrate (4" × 2" × 1/16") containing microchannels bonded to a PMMA lid having access ports.<sup>140</sup> PMMA sheets (FF grade; 4" × 4" × 1/16") were purchased from Piedmont Plastics and cut into two pieces to form the milled channel substrate and the cover piece. The microchannels were fabricated by mechanical milling using an end mill

on a CNC milling machine. Holes for the needle interface was drilled into the substrate plate using a 650-  $\mu\text{m}$ -diameter drill bit. The machined PMMA plate was sequentially cleaned by DI water and isopropyl alcohol to remove the milling debris, followed by a 24 h degassing step in a 40 °C vacuum oven to remove the residual solvents. After vacuum drying, both the processed PMMA and a raw PMMA chip were oxidized by 8 min of exposure to ultraviolet light in the presence of ozone.<sup>141</sup> The oxidized PMMA wafers were immediately mated together and thermally bonded at 85 °C in a hot press under a pressure of 3.45 MPa for 15 min. The world-to-chip interfaces were established by inserting hypodermic stainless steel needles into the 650-  $\mu\text{m}$ -diameter mating holes, with an additional 30 min of annealing at 85 °C to release the residual stresses from the fitting process.<sup>142</sup> The needle ports on the PMMA chip was connected to syringes with PTFE tubing (I.D. 650  $\mu\text{m}$ ). Two different PMMA chips were prepared to show applications of PR fluids, a light-activated fluidic valve and site-selective deposition and release. The channels with a rectangular cross section (200  $\mu\text{m}$  height and 300  $\mu\text{m}$  width) were used to demonstrate a valving action. For the site-selective deposition and release, channels with a rectangular cross section (200  $\mu\text{m}$  height and 350  $\mu\text{m}$  width) were used. In the channel, three wells (600  $\mu\text{m}$  depth and 500  $\mu\text{m}$  length) separated by 500  $\mu\text{m}$  were added. Precision syringe pumps (PHD 2000, Harvard Apparatus) were used to control the infusion of fluids into the chip. Optical detection was performed using a fluorescence microscope (Olympus MVX10 Macroview) with 2X magnification.

### 5.3. Results and Discussion

The PR fluids described here are composed of three major components: linear alginate chains as a matrix for a 3-D network, Sr-EGTA as a source of ions ( $\text{Sr}^{2+}$ ) that cause gelation, and the PAG-CD complex as a phototrigger. Each component was chosen to maximize the PR effect in a short time. As shown in Figure 5.1, a strong alginate gel is formed by UV light-triggered ionic gelation. Alginate is a linear copolymer of two different uronic acid sodium salts, which are  $\alpha$ -L-guluronate (G) and  $\beta$ -D-mannuronate (M).<sup>25</sup> The binding affinity of alginate toward divalent cations like  $\text{Sr}^{2+}$  depends on the ratio of G to M units. In particular, the “near mirror images” of G-blocks of alginate chains provide strong chelating sites to divalent cations, which can form so-called “egg-box” junctions for interchain ionic binding as shown in Figure 5.1c.<sup>25,135,136</sup> Accordingly, alginates with higher G content generally form stronger gels. In this study, we selected an alginate with a relatively high G content (51.2%)<sup>138</sup> to obtain a strong gel as a result of photogelation.

As a source of divalent cations, we incorporated Sr-EGTA chelates. Sr-EGTA is highly soluble in water thus the mixture of Sr-EGTA and alginate gives a clear homogeneous aqueous solution. Previously, nanoparticles of  $\text{CaCO}_3$  have been used as a source of divalent cations for gelation of alginate;<sup>143,144</sup> however, the particles make the sample turbid and inhomogeneous. Therefore, when using  $\text{CaCO}_3$ , there is poor penetration depth of light into the sample due to light scattering from the particles. Also, compared to  $\text{Ca}^{2+}$  ions,  $\text{Sr}^{2+}$  ions bind stronger to alginate chains, resulting in a stronger gel.<sup>25</sup> Thus using soluble Sr-EGTA instead of suspended  $\text{CaCO}_3$  is advantageous with



regard to both a faster response as well as stronger PR effects. EGTA is a widely used chelating agent. The chelating capacity of EGTA for divalent cations is highly pH-sensitive because of the protonation capability of the moieties (four acetate groups and two nitrogen atoms) at the chelating site.<sup>137</sup> As shown in Figure 5.2, the chelating efficiency of EGTA toward  $\text{Sr}^{2+}$  ions shows a dramatic decrease around a pH of 7.5, which implies a surge of free  $\text{Sr}^{2+}$  below this pH. Note that this plot of % released  $\text{Sr}^{2+}$  ions vs. pH has a reverse sigmoidal shape rather than a linear shape, which is indicative of a co-operative process and it therefore implies a switch-like response.<sup>145</sup> In other words, a small difference in pH around the threshold value (pH  $\sim$  7.5) results in an amplified release of free  $\text{Sr}^{2+}$  into the solution.

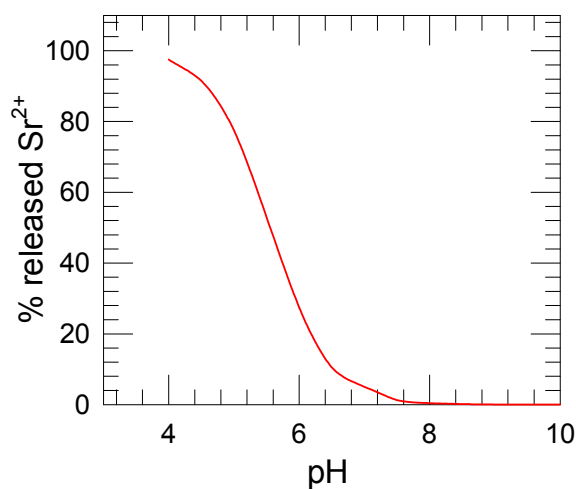


**Figure 5.2.** pH-dependent release of free  $\text{Sr}^{2+}$  ions is presented as a plot of mol% of released  $\text{Sr}^{2+}$  ions vs. pH. As pH decreases, mol% of released  $\text{Sr}^{2+}$  ions is increasing in a reverse sigmoidal pattern which has an onset pH of around 7.5. (data points obtained from MaxChelator)<sup>146</sup>

We then combined Sr-EGTA and alginate, and studied gelation in response to pH without using light (Figure 5.3). As an acid source, D-(+)-gluconic acid  $\delta$ -lactone (GDL) was added. When GDL is dissolved in water, it is gradually hydrolyzed and decreases the pH of the solution.<sup>143,144</sup> To visualize the pH change, a small amount (0.05 mM) of phenol red was added to the mixture of 2.5 wt% alginate, 40 mM Sr-EGTA, and GDL at various concentrations. (As described in the experimental section, 40 mM of Sr-EGTA represents 40 mM of SrCl<sub>2</sub> and 50 mM of EGTA). Initially all solutions were non-viscous and had a purple color. Thereafter, the color and viscosity changed depending on the concentration of GDL. The sample photos in Figure 5.3 were acquired 5 h after GDL

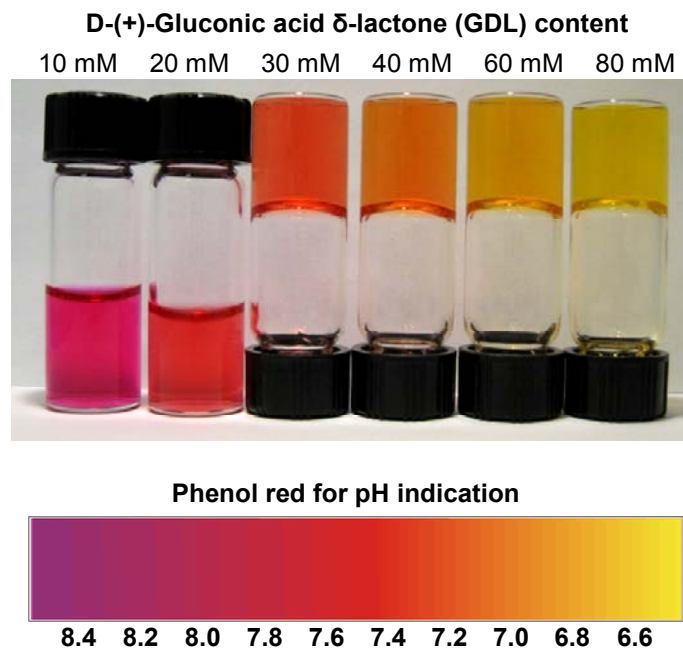


**Figure 5.3.** pH sensitive gelation of alginate (2.5 wt%) and Sr-EGTA (40 mM) solution. 0.05 mM of phenol red was added to indicate the pH with different concentration of GDL (D-(+)-gluconic acid  $\delta$ -lactone). When GDL is added to aqueous alginate solution, GDL gradually undergoes hydrolysis and decreases pH. The final pH values of the solutions depend on the amount of GDL added. As a reference, the color of phenol red with different pH is presented on the bottom.

addition, which is enough for the complete hydrolysis of GDL.<sup>147</sup> Here, the sol-to-gel transition is indicated by vial inversion.<sup>148</sup> The color of phenol red is purple at pH 8.0 corresponding to 10 mM GDL, and at this stage the sample is a sol. On the other hand, phenol red turns yellow at pH below 7.0 corresponding to 60 and 80 mM GDL, and these samples are gels (hold their weight in the inverted vial). Thus the sol-gel transition occurs around a pH 7.5 (phenol red shows an orange color), which is as expected. As noted earlier, the chelating efficiency of EGTA decreases below a pH of 7.5 and in turn free  $\text{Sr}^{2+}$  ions are released.<sup>137,146</sup> These free  $\text{Sr}^{2+}$  ions bind with alginate to form egg-box junctions, which connect alginate chains into a 3-D network, resulting in a strong Sr-alginate gel.<sup>25,135,136</sup> Figure 5.3 shows that the color change of phenol red can be used to visualize the sol-gel transition.

The final piece of the puzzle for our PR formulation is a PAG that can be phototriggered. As illustrated in Figure 5.1c, the PAG absorbs light (external signal) and releases  $\text{H}^+$  ions due to a photodissociation reaction.<sup>40,110</sup> In addition to protons, the dissociation of PAG also generates hydrophobic byproducts,<sup>40,110</sup> which are insoluble and turn the system opaque upon UV irradiation. As shown in the left panel of Figure 5.4, when a transparent PAG solution (photo 1) is exposed to UV, the solution turns opaque (photo 3). The opacity hinders the penetration of light into the sample, resulting in a slow response even though our PAG has a high quantum yield and a large molar absorption coefficient<sup>149</sup> (which are both generally required for fast response). To solve this problem, we incorporated a cyclodextrin (CD) into our sample. The hydrophobic cavity of the CD is expected to envelop any hydrophobic groups, including the hydrophobic

byproducts of PAG dissociation.<sup>150</sup> In terms of the CD, we chose a m- $\beta$ -CD due to its high water solubility ( $> 300$  mM at  $25^\circ\text{C}$ ).<sup>151</sup> Various molar ratios of m- $\beta$ -CD to PAG were examined, and the samples with this ratio  $\geq 3$  remained transparent during the entire duration of UV irradiation, as shown by photo 2 and 4 of Figure 5.4.

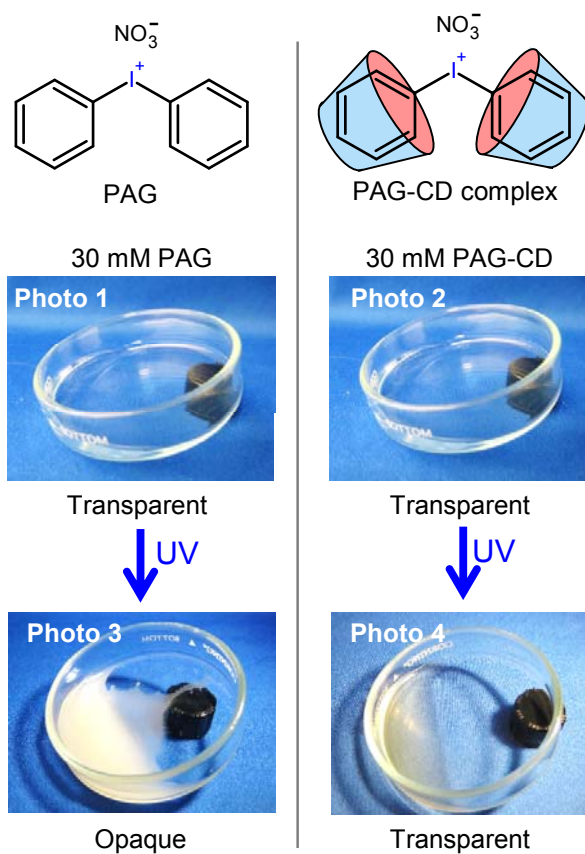


**Figure 5.4.** Transparent photoacid generating system. Upon exposure to UV, transparent 30 mM PAG solution (photo 1) become opaque (photo 3) due to the hydrophobic byproducts of photodissociation. Meanwhile, the sample containing 30 mM PAG and 90 mM m- $\beta$ -CD remains transparent before (photo 2) and after (photo 4) UV irradiation.

Next, we examined the response to light of our PR fluid containing 2.5 wt% alginate, 40 mM Sr-EGTA, and 30 mM PAG-CD complex. As shown by photo 1 of Figure 5.5a, this mixture is initially a low-viscosity solution that flows freely in the tilted Petri dish. Upon exposure to UV light for 20 min, the entire solution becomes a solid-like gel that can be hold by one's fingers. (UV irradiation was done without stirring.) Note that the gel is transparent and homogeneous. The above visual observations were quantified using dynamic rheology. Figure 5.5 present plots of the elastic modulus  $G'$  and the viscous modulus  $G''$  as function of the frequency  $\omega$  for the sample before (Plot a) and after 20 min UV irradiation (Plot b). The dynamic rheology data before UV represents a purely viscous response, *i.e.*,  $G''$  is a strong function of  $\omega$  ( $G' \sim \omega^1$ ) but  $G'$  is negligible and hence not seen on the plot.<sup>45</sup> In contrast, after 20 min UV irradiation, the sample shows the response of an elastic gel with an infinite relaxation time, *i.e.*,  $G' > G''$  and the moduli are independent of  $\omega$ .<sup>45</sup> The gel modulus (value of  $G'$ ) is about 2000 Pa, which is comparable to that of chemically photocrosslinked alginate (in the latter case, the alginate was functionalized with methacrylate groups and the polymer was crosslinked by standard free-radical polymerization).<sup>152</sup>

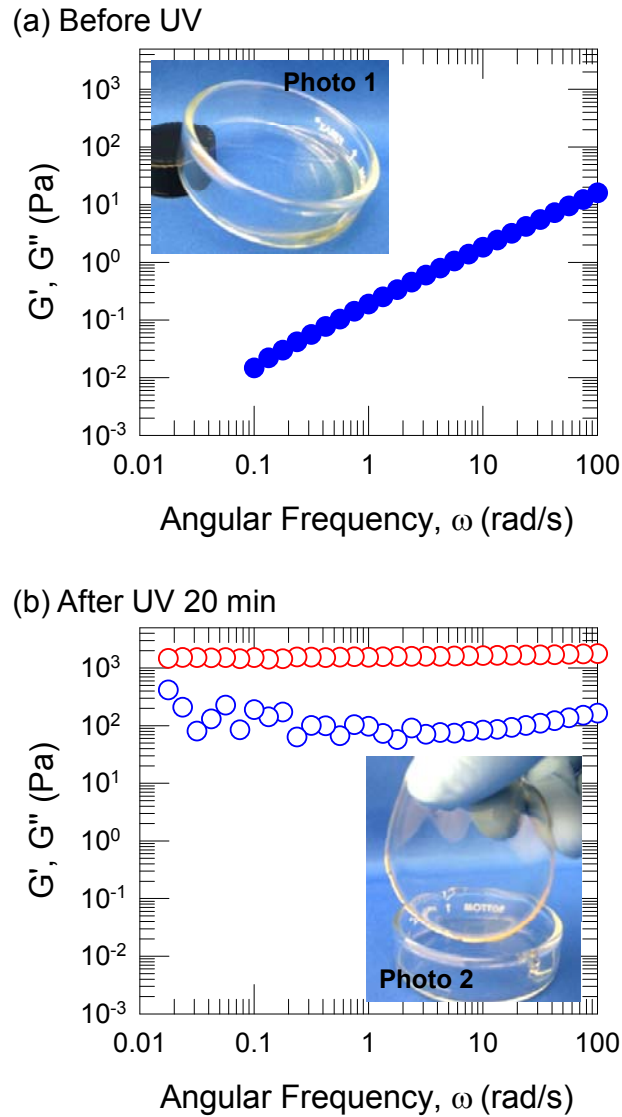


**Figure 5.5.** Dynamic rheology of the sample containing alginate 2.5 wt%, Sr-EGTA 40mM, and PAG-CD complex 30mM before (a) and after 20 min UV irradiation (b). (a) Before UV irradiation, the sample is freely flowing transparent solution as seen on photo 1. Dynamic rheology data confirms this visual observation and shows a viscous response with strong dependency of viscous modulus  $G''$  on frequency while elastic modulus  $G'$  is almost negligible. (b) After 20 min UV irradiation, the sample becomes a transparent gel which can be hold with fingers as seen on the photo 2. The dynamic rheology data also shows an elastic response (*i.e.*,  $G' > G''$ ) with both moduli being nearly independent on frequencies.

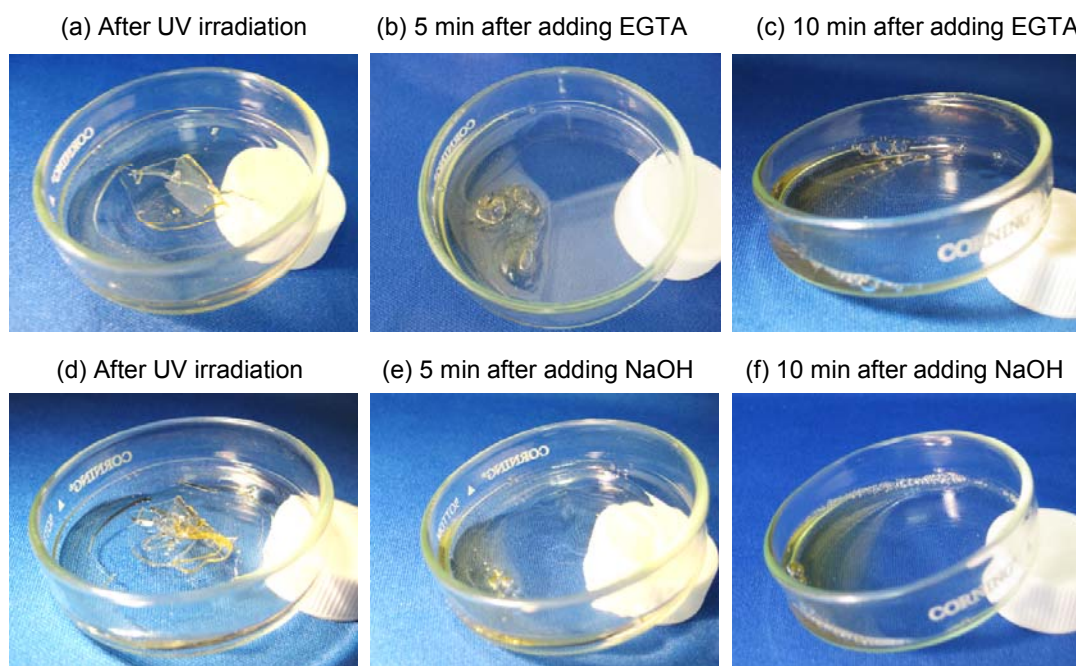


**Figure 5.6.** Ungelling of an alginate photogel upon addition of chelating agent EGTA or base solution. Due to the physical nature of crosslinks rather than a covalent bond, the gel formed through photogelation can be ungelled by adding 100 ml of EGTA 0.3M ((a)-(c)) or NaOH 0.3M solution ((d)-(f)). When EGTA or NaOH solution was added, a gel turn into a non-viscous solution in 10 min with gentle shaking by chelating  $\text{Sr}^{2+}$  ions involving formation of egg-box junctions with alginate.

In contrast to chemically crosslinked alginate,<sup>152-154</sup> our alginate photogel based on physical crosslinks can be easily converted back to the solution state by the addition of a chelating agent such as EGTA or even by adding base (NaOH). Figure 5.6 shows ungelling of an alginate photogel; when 100  $\mu\text{L}$  of 0.3 M EGTA (photo a – c) or 100  $\mu\text{L}$  of NaOH (photo d – f) is added to an alginate photogel, the gel gradually dissolves and the sample becomes a freely flowing solution within 10 min with gentle shaking. Here, upon addition of chelating agents or the base, the  $\text{Sr}^{2+}$  ions involved in forming egg-box junctions detach from the alginate chains and are chelated again to form Sr-EGTA complexes. Such reversibility of gelling is critical for valving action in flow channels.

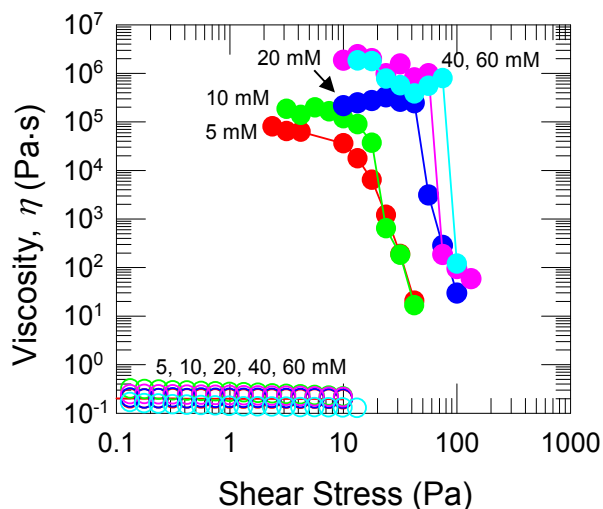


**Figure 5.7.** The effect of Sr-EGTA concentration on the steady shear rheology of samples before UV irradiation (open circle) and after 20 min UV irradiation (closed circle). The concentration of alginate and PAG-CD complex was fixed at 2.5 wt% and 30 mM each. All samples showed clear transitions from a low-viscous solutions to gels with different yield stresses upon UV irradiation. As Sr-EGTA concentration increases from 5 mM to 60 mM, the yield stress of the gel increased from around 10 Pa to 60 Pa.

We also investigated the photogelation phenomenon at various Sr-EGTA concentrations. For this, we fixed the alginate at 2.5 wt% and the PAG-CD complex at 30 mM. Steady-shear rheology data on samples before and after 20 min of UV irradiation are shown in Figure 5.7 for the viscosity  $\eta$  as a function of shear stress. All initial samples before UV irradiation have a low viscosity around 0.2 Pa.s. However, when exposed to UV, the samples undergo photogelation indicated by the increase in the low-shear viscosity (up to 2 MPa.s) and the emergence of a yield stress. The yield stress of the photogel increases with Sr-EGTA content and reaches 60 Pa at 40 mM. Further increase of Sr-EGTA does not give a significant increase in the yield stress.



Next, we varied the concentration of the PAG-CD complex. All samples had 2.5 wt% alginate and 40 mM Sr-EGTA and steady-shear rheology was used to study samples before and after UV irradiation (Figure 5.8). We again see similar behavior: the samples are initially thin liquids, whereas after 20 min of UV exposure, they turn into gels with appreciable yield stresses. The yield stress of the photogel is much more sensitive to the concentration of the PAG-CD complex and increases as the PAG-CD concentration is increased. At 60 mM of PAG-CD, the yield stress is 400 Pa. Above 60 mM, the sample became translucent due to the solubility limit of the PAG-CD complex being reached, and significant retardation of photogelation was observed. Also, the photogel had a lower yield stress even after 40 min UV irradiation (data not shown).

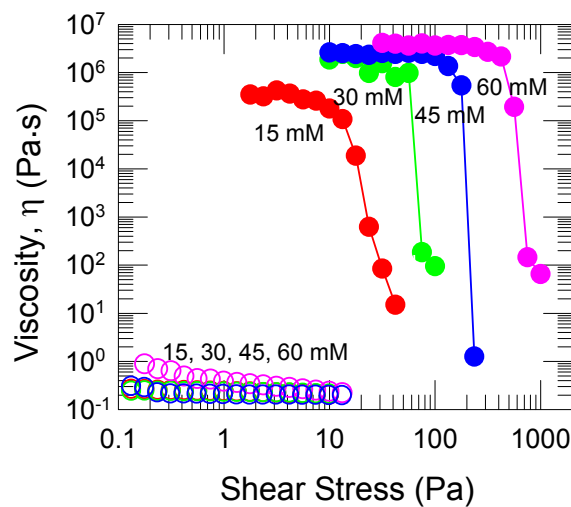


**Figure 5.8.** The effect of PAG-CD complex concentration on the steady shear rheology of samples before UV irradiation (open circle) and after 20 min UV irradiation (closed circle). The concentration of Sr-EGTA, and alginate was fixed at 40 mM and 2.5 wt% each. Upon UV irradiation, samples with PAG-CD complex with concentrations of 15 – 60 mM shows clear transitions from a low-viscous Newtonian fluids to gels. However, the yield stress depends on the PAG-CD complex concentration, and increases from 10 Pa to 300 Pa as increasing its concentration.

The high sensitivity of gel strength to PAG-CD complex is related to the  $\text{Sr}^{2+}$  release pattern upon pH decrease. As described in Figure 5.2, there is a sharp increase of free  $\text{Sr}^{2+}$  ions between pH 7 and 6. Initially all samples before UV irradiation had a pH value of 8.0. After 20 min of UV irradiation, the extent of pH decrease varied with the amount of PAG. With increase of PAG-CD from 15 mM to 60 mM, the pH of the photogel changed from 7.0 to 6.5 (measured by a pH test strip). Therefore, with higher amount of PAG, more  $\text{Sr}^{2+}$  ions are involved in forming a sample-spanning network of alginate chains, thus making the photogel stronger.

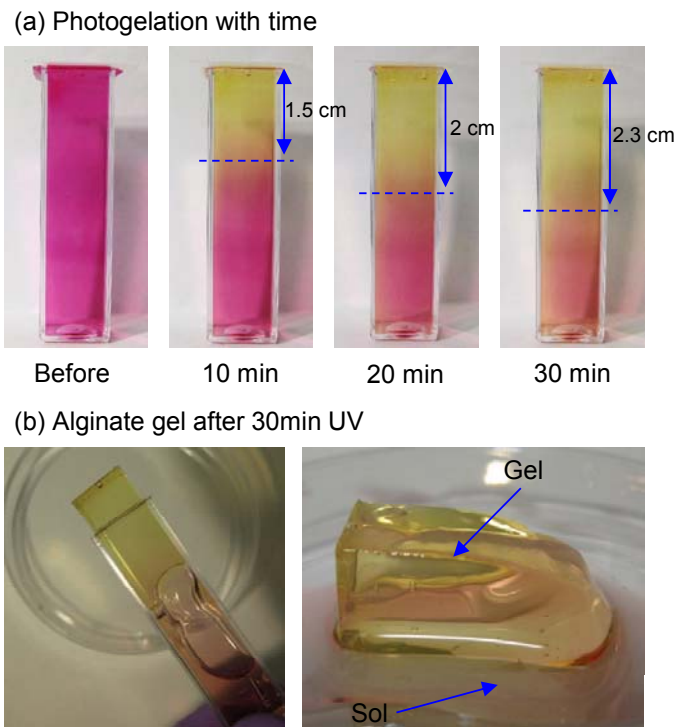


**Figure 5.9.** Fast growth of gel with UV exposure. (a) A sample with alginate 2.5 wt%, Sr-EGTA 40 mM, phenol red 0.05 mM, and PAG-CD complex 60 mM was placed in rectangular cuvette and exposed to UV. Upon UV exposure, the gel grew rapidly from the top, and the thickness became around 1.5 cm after 10 min UV irradiation. After 30 min the thickness reaches 2.3 cm and the gel was extruded from the container (b). The color boundary clearly represents the interphase of gel and solution layers.

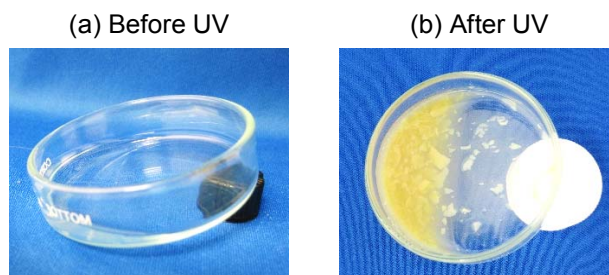


**Figure 5.10.** Slow photogelation of the alginate 2.5 wt% solution containing Sr-EGTA 40 mM and PAG 30 mM. With opaque photoacid generation system, *i.e.*, a sample without cyclodextrin, upon UV exposure, opaque gel layer was formed on the surface and prevent UV light penetrating deep into the solution. Before UV irradiation, the sample was non-viscous and transparent (a), while the sample after 20 min UV became a non-viscous opaque solution with fragments of an opaque gel layer (after UV, the sample was scraped with a spatula).

Next, we studied time-dependent gelation of our PR fluids upon exposure to UV. For this, we placed our sample containing 2.5 wt% alginate, 40 mM Sr-EGTA, and 60 mM PAG-CD in a rectangular cuvette (1 cm × 1cm × 4.5 cm) covered with a glass coverslip. To visualize the pH change and sol-to-gel transition, we also added 0.05 mM phenol red to the sample. As shown in Figure 5.9a, when the sample is placed under UV light, the alginate solution transforms into a gel rapidly from the top. In 10 min, the photogel layer grows 1.5 cm and it becomes 2.3 cm after 30 min. After 30 min UV irradiation, we extruded the sample from the cuvette and placed it on a Petri dish. As seen in Figure 5.9b, there is an apparent boundary between the gel layer and solution, which is clearly indicated by the color of phenol red. Note that the sharp transition of sol-to-gel arises due to the sigmoidal release pattern of Sr<sup>2+</sup> upon decreasing pH. There is a reduction in the growth rate of the gel with time (1.5 cm in the first 10 min, 0.5 cm between 10 and 20 min, and 0.3 cm between 20 and 30 min). When UV light travels through the sample, its intensity is attenuated by absorption, resulting in a decrease of the

intensity with depth. However, this response is much faster than observed if the sample was opaque, *i.e.*, in the case where alginate, Sr-EGTA, and PAG were studied without the addition of the CD. In that case, only the top portion of the sample turned into a thin opaque gel, and this layer prevented UV light from penetrating deeper into the sample (see Figure 5.10). In fact, the sample below the thin gel layer remains a solution, as shown in Figure 5.10b.

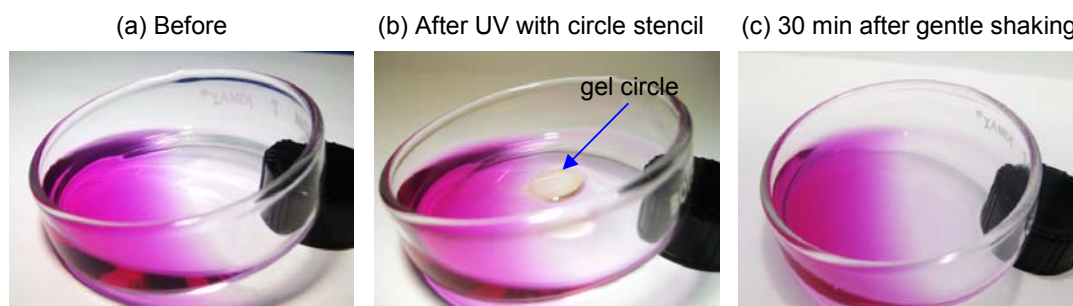


**Figure 5.11.** Self-dissolution of a gel with time. In order to demonstrate photogelation and subsequent self-ungelling of our PR fluid, part of solution (circular with 1cm diameter) was gelled with UV irradiation (b). After 30 min of gentle shaking in dark, the circular gel was dissolved completely (c).

Another important feature of our alginate photogel is that it undergoes ungeling when placed in its initial solution. This self-dissolution property is demonstrated in Figure 5.11. Using a circle stencil, a part of the 2.5 wt% alginate solution containing 40 mM Sr-EGTA, 30 mM PAG-CD, and 0.05 mM phenol red was gelled as shown in Figure 5.11b. After 30 min gentle shaking, the gel was completely dissolved by the surrounding solution (Figure 5.11c). The recovery of chelating ability of EGTA is responsible for this ungeling. Through diffusion from the surrounding solution to the Sr-alginate gel, the pH of the gel increases and the  $\text{Sr}^{2+}$  ions are again chelated by EGTA. Due to this self-

dissolution phenomenon, valving action is expected to be possible without infusion of additional chemicals such as EGTA or NaOH solution; flow in the channel can be blocked with photogelation, and the photogel can be self-ungelled with time (once the UV light source is removed) to open the flow.

Our results so far show that our biopolymer-based PR formulation satisfies the essential requirements for use as a light-activated fluidic valve. These include a high contrast in rheological properties between the initial and final states (low-viscosity solution before UV and a high-yield-stress-gel after UV), and a relatively rapid gelation

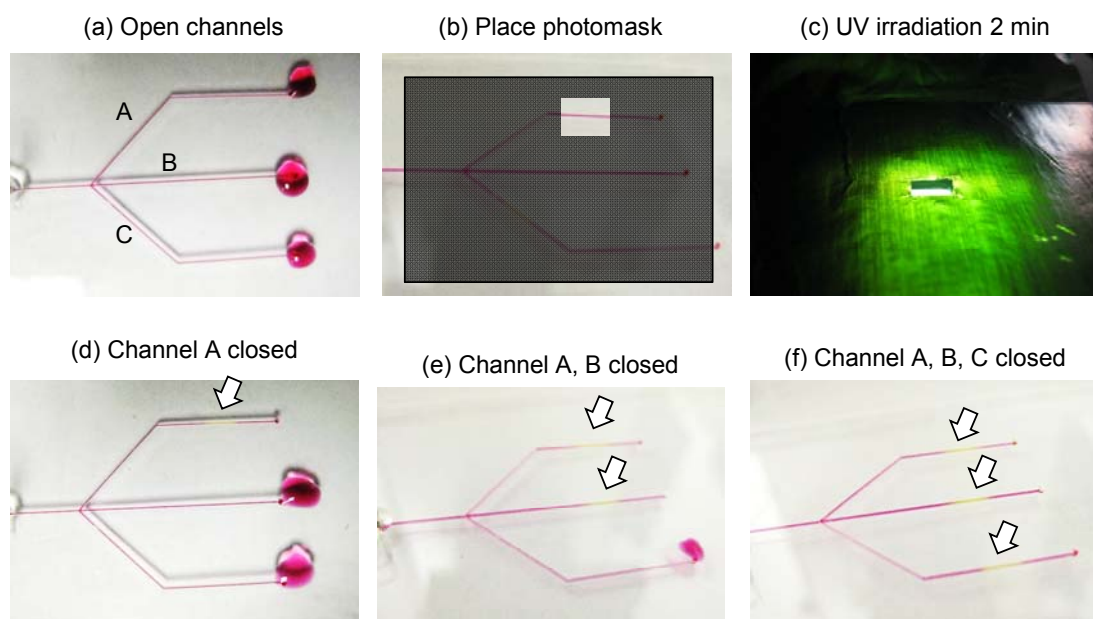


**Figure 5.12.** Demonstration of flow control with photogelation of alginate. Initially, all three microchannels are open and solution is flowing freely (a). The flow is stopped and the photomask is placed (b), and then, a specific part (~ 3 mm length) of microchannel is exposed to UV (c) for 2 min. The irradiated part turns to a gel (yellow gel indicated by arrow) and block the channel A (d). Once the channel is blocked, it takes around 2 hours to reopen the channel through self-ungelling. This valving action can be done selectively; channel A and B are blocked (e), all channels are blocked (f).

under UV (1 cm-thick gel formed in 10 min). More importantly, only commercially available inexpensive chemicals are used to formulate this PR fluid. Now, we demonstrate application of this PR fluids for valving action in microchannels. First, we flowed our PR fluid composed of alginate 2.5 wt%, Sr-EGTA 40 mM, phenol red 0.5 mM, and PAG-CD complex 60 mM through a microchannel that branches into three side channels. Each microchannel has a rectangular cross-section of 200  $\mu\text{m}$  height and 300  $\mu\text{m}$  width. As seen in Figure 5.12a, initially all channels are open, and the fluid flows out of the three outlets at the end of each branch. Next, we stopped the flow and placed a photomask to expose a specific point in channel A to UV light (Figure 5.12b, c). After 2 min UV irradiation, we started the flow again. As indicated by the arrow in Figure 5.12d, at the exposed point, the alginate solution is converted into a strong gel. As explained previously, the color change of phenol red from purple to yellow in the fluid correlates with the sol-to-gel transition. We find that the resulting gel has enough strength to block the flow. As shown in Figure 5.12d, channel A is blocked while channel B and C are still open. This procedure is then repeated with the other branches and we can selectively block the different flow channels (Figure 5.12e, f). When the UV light is removed, the gel gradually dissolved by the flow and the channels reopen in 2 h.

In addition, we demonstrate a new application of our PR fluid, which is site-selective deposition and release of materials.<sup>155</sup> For this application, we used a fluid containing alginate 2.5 wt%, Sr-EGTA 40 mM, PAG-CD complex 60 mM, and red and green fluorescent microbeads as model materials to be deposited. The procedure for this demonstration is illustrated in Figure 5.13. We used a flow channel with a rectangular

cross section (200  $\mu\text{m}$  height and 350  $\mu\text{m}$  width) and three separate wells (600  $\mu\text{m}$  depth and 500  $\mu\text{m}$  length). First, we flowed the solution carrying red fluorescent beads through the microchannel. Then, we stopped the flow and placed a photomask to shine UV at specific points (Well A and C). After 2 min UV irradiation, the solution in the channel was flushed with water, while the alginate photogel entrapping red fluorescent beads was deposited in Well A and C. Next, the PR fluid carrying green fluorescent beads was flowed in the channel. Using a photomask, specific areas corresponding to Well A, B and C were exposed to UV for 2 min. (By irradiating UV on Well A and C, the self-dissolution of photogel at those points are prevented.) The channel was again flushed with water. Finally, the deposited alginate photogel was reinforced by flowing 30 mM

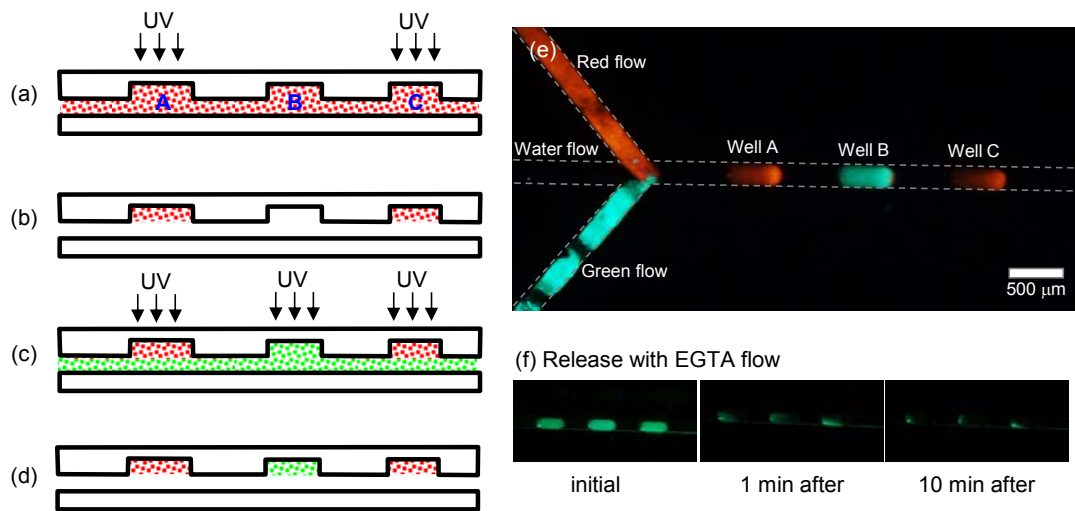


**Figure 5.13.** Spatial selective deposition of model material (red and green fluorescent beads) in the microchannel. (a) First, flow our PR fluid containing red fluorescent beads through the microchannel with three wells. Then, stop the flow and shine UV on specific area (corresponding to well A and C of (e)). The channel is flushed with water. Red fluorescent beads in alginate photogel are deposited in Well A and C selectively (b). (c - d) These steps are repeated with another PR fluid containing green fluorescent beads. Finally, the deposited gels are reinforced by flowing 30 mM  $\text{SrCl}_2$  solution. (e) Fluorescent microscope image clearly shows site-selective deposition of red and green fluorescent beads in the microchannel. (f) Deposited beads are released by flowing EGTA solution by ungelting Sr-alginate gel.

SrCl<sub>2</sub> solution. As shown by the fluorescent image in Figure 5.13e, the model materials (red and green fluorescent beads) are selectively deposited at the specific points of the microchannel. In addition, as seen in Figure 5.13f the deposited beads can be released easily by flowing EGTA solution through the channel. (The images were acquired under dimmed white light to visualize both microbeads.)

The above experiment shows how an Sr-alginate gel can act as a matrix for entrapping model materials. Alginate has been widely used for encapsulating biological substances such as enzymes, and cells.<sup>25</sup> Therefore, by incorporating these substances into our PR system instead of fluorescent beads, our PR fluid can provide a platform for fabricating micro-bioreactors or sensors in microfluidic chips.

#### **4.4. Conclusions**

We have described biopolymer based PR fluids that show transition from a low-viscosity solution ( $\eta \sim 0.2$  Pa.s) to a solid-like gel that can maintain its integrity when held with fingers. Our PR fluids are composed of commercially available inexpensive chemicals. PAG enveloped with cyclodextrin acts as a phototrigger and decreases the pH of the solution upon UV irradiation. Because cyclodextrin solubilizes the hydrophobic byproducts formed by PAG photolysis, the sample remains transparent before and after UV exposure. As a divalent cation source, we use Sr-EGTA, which is sensitive to pH change and gives a surge of free Sr<sup>2+</sup> ions upon pH decrease. The biopolymer alginate serves as the matrix, and alginate chains get connected at egg-box junctions via Sr<sup>2+</sup> ions.



The overall result is that the alginate solution is converted to a strong transparent gel with a modulus of  $\sim 2000$  Pa. In addition, the fluid shows a fast response enabled by the transparent nature of the system. We also show that this PR fluid can be used to make a light-activated fluidic valve. When a specific point of the flow channel is exposed to UV, the alginate at that point turns into a strong gel in a few minutes, and the resulting gel blocks the flow. When the UV is switched off, the gel undergoes self-dissolution and the flow reopens. In addition to successful demonstration of a valving action, we also demonstrate a new method for the site-selective deposition and release of model materials within the microchannels. These applications are enabled by the physical nature of crosslinks that allows reversal of the gelation. In conclusion, we address major limitations of currently available PR formulations and demonstrate practical applications that leverage the spatial selectivity of light.

## Chapter 6

### Conclusions and Recommendations

---

#### 6.1. Project Summary and Principal Contributions

In this dissertation, we have shown three different kinds of photoresponsive systems. These systems were developed based on self-assembly of common amphiphilic molecules that are already commercialized and used widely. The photoresponsive properties were imparted to various self-assembled structures, *i.e.*, wormlike micelles in Chapter 3, vesicles in Chapter 4, and nanostructured gels in Chapter 5. A small amount of photoresponsive molecules added to these systems acted as a light-activated trigger. Upon light irradiation, these photoresponsive molecules initiate a transition of nanoscale self-assembled structures, which is followed by macroscopic property changes.

In Chapter 3, we described simple photoreversible photorheological (PR) fluids that can undergo nearly a million-fold changes in viscosity reversibly with different wavelengths of light. These fluids were created by combining an azobenzene derivative, 4-azobenzene carboxylic acid (ACA), into micelles of the cationic surfactant erucyl bis(2-hydroxyethyl)methyl ammonium chloride (EHAC). The reversible transition of self-assembled structures between vesicles and wormlike micelles were responsible for the dramatic viscosity changes.

In Chapter 4, we reported a simple class of photoresponsive vesicles composed of inexpensive and commercially available cationic photoinitiator and anionic surfactants.

The mixture of these amphiphiles self-assembled into vesicles due to ionic interactions between the cationic and anionic headgroups. Upon UV exposure, these vesicles that can serve as nano-containers ruptured completely and turned into spherical micelles. In addition, when the solution of photoresponsive vesicles were mixed with hydrophobically modified biopolymers, the mixture resulted in a photoresponsive vesicle-gel that can undergo a gel-to-sol transition with UV light.

In Chapter 5, we demonstrate practical applications of PR Fluids as a light-activated fluidic valve and a platform for the site-specific deposition and release in microchannels. For these applications, we overcame the limitations of currently available PR formulations, which were slow response to light and a weak strength of the resulting gel. To achieve this goal, we presented a new class of biopolymer based PR fluids composed of alginate, a complex of a photoacid generator (PAG) and cyclodextrin as a photo-trigger, and a chelated complex of divalent strontium ( $\text{Sr}^{2+}$ ) ions (Sr-EGTA). Upon exposure to UV, free  $\text{Sr}^{2+}$  ions are released, and then they self-assemble with the alginate chains to give a nanostructured gel with a high gel modulus ( $\sim 2000$  Pa). With these PR fluids, we demonstrated valving actions and the site-specific deposition and release of model materials in microchannels.

We believe that the introduction of above simple photoresponsive systems will find a wide range of applications because of their simplicity and significant changes in macroscopic properties.

## 6.2. Recommendations for Future Work

The concepts that we have reported in this dissertation can be extended to explore and envision new applications and utilities. Here, we briefly describe the outline for the future work.

### 6.2.1. Photoresponsive Capsules

In chapter 4, we described nano containers, *i.e.*, vesicles, which can carry many kinds of payloads.<sup>89-95</sup> The payloads also can be remotely released on demand by light.<sup>5,14,15</sup> However, the bilayer membrane of vesicles have weak mechanical strength which makes them vulnerable to the unwanted rupture and release of payloads.<sup>156</sup> In addition, it is difficult to control the permeability of the membrane and, generally, it requires extensive efforts to obtain a sustained release pattern of payloads.<sup>157</sup> For these reasons, many researchers pay attention to polymeric system that can compose a strong wall for the containers. The most common approaches for this goal have been LBL (layer-by-layer deposition).<sup>158</sup> However, LBL requires laborious works and sacrificial templates that limit the species of payloads.<sup>158</sup> Recently, polymersomes, artificial vesicles made by amphiphilic synthetic block copolymers, have been introduced.<sup>159</sup> However, they are not easy to prepare due to the requirement of complicated chemical synthesis. In addition, it is difficult to impart photoresponsive properties to them.

As an alternative route to polymeric containers with a strong membrane, a complex coacervation is promising because of its simplicity and no limitation of payloads.<sup>160</sup> By introducing drops of anionically charged polymer solution into a

reservoir solution containing positively charged polymers or amphiphilic molecules, liquid droplets turn into capsules with a thin membrane of coacervates comprised from oppositely charged polymers or amphiphiles. In this case, the photoresponsive properties can be easily imparted by using photoresponsive amphiphiles, such as photoresponsive surfactants that already introduced in chapter 4. The photoinitiator ODPI carries positive charge in its head group and it loses its charge upon exposure to UV.

The capsule formation was tested using alginate (anionically charged polymer) and ODPI (positively charged surfactant) solution. When alginate solutions (2 wt%) were dropped into the 1 wt% ODPI solution, spherical capsules were created spontaneously through complex coacervation (Figure 6.1 (a)). With this method, the payloads can be easily incorporated into the capsules by dispersing or dissolving substances in the alginate solution. As shown in Figure 6.1, these capsules show substantial mechanical

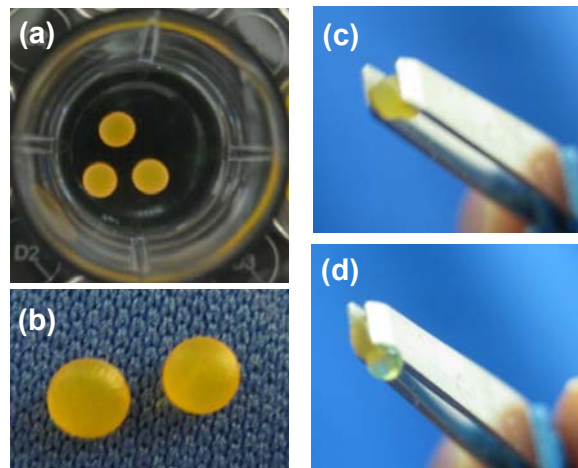


**Figure 6.1.** Photoresponsive capsules made by alginate and ODPI solution. (a) Three drops of 2 wt% alginate solution turned into capsules in 1 wt% ODPI solution. (b) Alginate-ODPI capsules on the benchtop. (c) An alginate-ODPI capsule held by tweezers. (d) The liquid core squeezed out when ruptured by tweezers.

strength. They can be picked with tweezers (c), they can also maintain their integrity of the spherical shape when placed on the benchtop (b). We also confirmed the liquid core when the capsule was ruptured by squeezing strongly (d). Note that the color of the capsules is attributed to the dye (fluorescein) encapsulated.

Next, we examined light-triggered rupture of this capsule. Figure 6.2 describes time-dependent rupture of the capsule under UV light. For this, we placed the capsules in a Petri dish filled with water, and then, irradiated with UV light. Initially the capsule was an intact sphere (UV 0 min). After 60 min of UV irradiation, the top portion of the shell (exposed area to UV) disappeared and finally turned into a half sphere after 90 min UV irradiation. Upon UV exposure, the capsule wall made of alginate and ODPI is thought to be dissolved due to the charge loss of ODPI. The electrostatic interactions between negatively charged alginate and positively charged ODPI are no longer valid upon UV irradiation,<sup>40,110</sup> and the alginate chains on the shell are dissolved.

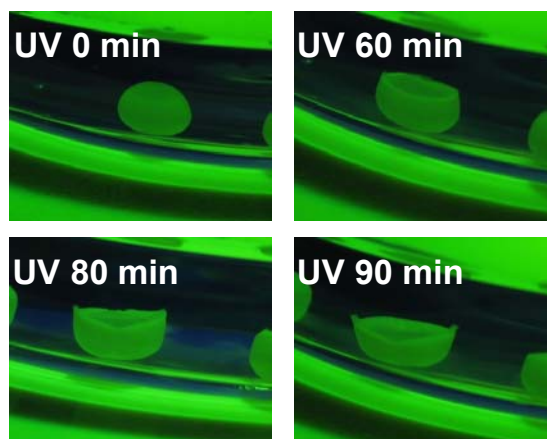


**Figure 6.2.** Time-dependent rupture of the alginate ODPI capsules under UV light.

Although, complex coacervation can provide a simple method to photoresponsive capsules, it is not easy to make them on smaller scales, *i.e.*, micron sizes. In order to prepare micron-scale capsules, we have devised a simple micro-dropper from micro-capillaries and a micropipette tip. The flowing solution (alginate) is surrounded by a coaxial airflow. Liquid microdroplets are created with this homemade device and introduced into a reservoir (ODPI solution) whereupon they are converted into microcapsules via coacervation. Figure 6.3 presents alginate ODPI microcapsules ( $\sim 280 \mu\text{m}$ ). To test the photoresponsive property, the Petri dish containing microcapsules were placed under the microscope, and UV was irradiated through the liquid light guide. After 3 hr of UV irradiation, the capsule was ruptured and its inner solution started to leak out. After 4 hr, the capsule was completely dismantled as seen in Figure 6.3 (e) and (f).

We have shown preliminary experimental data that demonstrate the concept of light-activated rupture of microcapsules made by the simple coacervation method. These

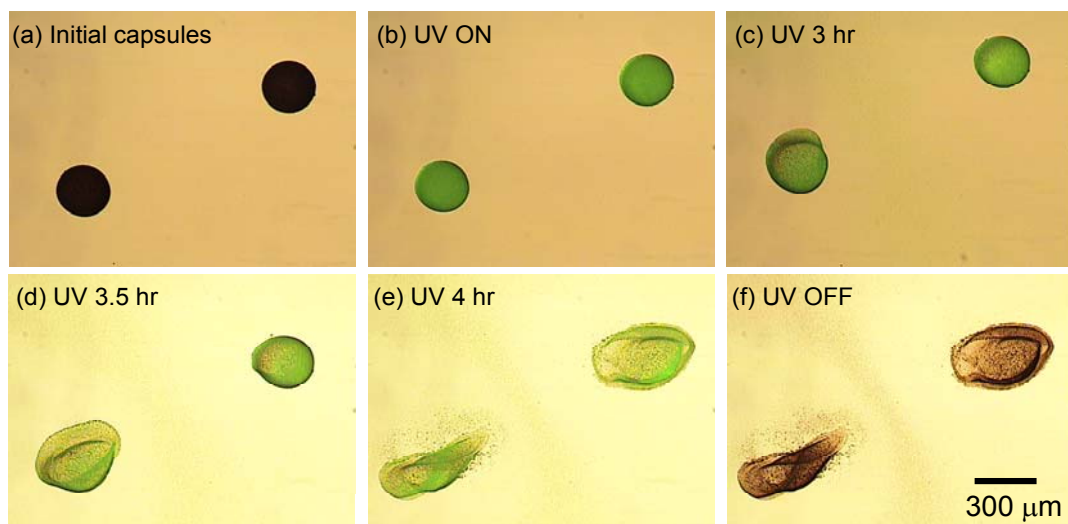


**Figure 6.3.** Photoresponsive micro capsules were ruptured by UV.

preliminary results are encouraging, but further experiments are needed to improve the impermeability of the capsules. In addition, by incorporating these photoresponsive capsules into the a larger capsule, we can design multi-compartmentalized capsules that mimicking the biological cell architecture. Light-triggered rupture of inner capsules can initiate further reactions in the capsule, *e.g.*, the enzymes in the inner capsules can be exposed to the reactants in the bigger capsule and the enzymatic reaction can be initiated upon light irradiation.

### **6.2.2. Reversible gel-to-sol transition**

In Chapter 5, we have demonstrated PR fluids which can show a dramatic transition in viscosity, *i.e.*, from a non-viscous liquid to a solid-like gel. We also proved that this system can be applied to a light-activated fluidic valve. However, this system is not able to show a photoreversible transition. Thus, the ungelling process depends on a slow diffusion of NaOH or EGTA from surrounding solution to the gel that blocking the flow. Because of this reason, the reverse transition was slow and took around 2 hours to reopen the flow channel. Therefore, for the fluidic valve applications, it would be much more beneficial to use a photoreversible PR formulation that can undergo a reversible transition between solution and a strong gel.

The one way transition of the PR system in Chapter 5 is attributed to the photochemistry of PAG. Upon UV exposure, PAG undergoes an irreversible dissociation. Therefore, to make this system reversible, it requires photoresponsive molecules which can tune the pH of the system reversibly. In this context, malachite green carbinol base



(MGCB) is an attractive molecule. MGCB is a very common chemical, which has been used as an effective fungicide in the fish industry.<sup>161</sup> As shown in Figure 6.4, in aqueous solution, MGCB can be ionized and turned into malachite green (MG) cation with light to give OH<sup>-</sup> ions.<sup>161,162</sup> When light is removed, ionized MGCB is brought back to its initial form quickly. In the most pronounced case, the pH jump from 5.4 to 10 upon 3 min UV irradiation was reported.<sup>162</sup> The pH of the solution was also reverted to the initial pH when UV was removed.<sup>161,162</sup>

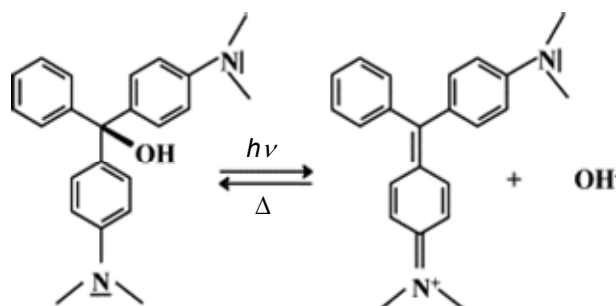


**Figure 6.4.** Reversible transition of MGCB between non-ionized (left) and ionized (right) form.<sup>161</sup> When MGCB is ionized, it gives OH<sup>-</sup> ions and increases the pH of the solution.

Due to the low solubility of MGCB in water, in previous studies, MGCB was usually solubilized in the cationic surfactant CTAB solution.<sup>162,163</sup> However, CTAB is not compatible with our alginate-based PR fluid. The mixture of CTAB and alginate solution precipitates upon mixing. Thus, finding a method to solubilize MGCB in alginate solution is the challenging part of this study. This issue has been tackled by adopting a similar strategy as seen in Chapter 5, *i.e.*, enveloping with cyclodextrin. We were able to solubilize MGCB 100 mM in 300 mM  $\gamma$ -cyclodextrin ( $\gamma$ -CD). Upon UV irradiation for 10 min, this solution showed a pH jump from 7.3 to 8.6. Thereafter, the pH of the

solution reverted to the original value in 10 min when kept in dark. Even, under sunlight, this solution showed slight pH jump (from 7.3 to 7.8).

The final shape of the reversible alginate-based PR fluids will be composed of MGCB-CD complex, Sr-EGTA, and alginate. Initially, this solution is expected to form a gel at around pH 6. Upon exposure to light, the pH of the sample will be increased and  $\text{Sr}^{2+}$  ions will be chelated by EGTA, resulting in ungelting. When light is removed, the solution will be reverted to a gel again. Due to the fast response of MGCB to light, above modulation of viscosity will be fast.

## 7. References

---

- [1] Israelachvili, J. N. *Intermolecular and surface forces*, 2nd ed.; Academic, 1991.
- [2] Grzelczak, M.; Vermant, J.; Furst, E. M.; Liz-Marzan, L. M. "Directed self-assembly of nanoparticles." *Acs Nano* **2010**, *4*, 3591-3605.
- [3] Matsumoto, S.; Yamaguchi, S.; Ueno, S.; Komatsu, H.; Ikeda, M.; Ishizuka, K.; Iko, Y.; Tabata, K. V.; Aoki, H.; Ito, S.; Noji, H.; Hamachi, I. "Photo gel-sol/sol-gel transition and its patterning of a supramolecular hydrogel as stimuli-responsive biomaterials." *Chemistry-a European Journal* **2008**, *14*, 3977-3986.
- [4] Khetan, S.; Burdick, J. A. "Patterning hydrogels in three dimensions towards controlling cellular interactions." *Soft Matter* **2011**, *7*, 830-838.
- [5] Shum, P.; Kim, J. M.; Thompson, D. H. "Phototriggering of liposomal drug delivery systems." *Advanced Drug Delivery Reviews* **2001**, *53*, 273-284.
- [6] Sugiura, S.; Sumaru, K.; Ohi, K.; Hiroki, K.; Takagi, T.; Kanamori, T. "Photoresponsive polymer gel microvalves controlled by local light irradiation." *Sensors and Actuators a-Physical* **2007**, *140*, 176-184.
- [7] Sershen, S. R.; Mensing, G. A.; Ng, M.; Halas, N. J.; Beebe, D. J.; West, J. L. "Independent optical control of microfluidic valves formed from optomechanically responsive nanocomposite hydrogels." *Advanced Materials* **2005**, *17*, 1366-1370.
- [8] Sakai, H.; Matsumura, A.; Yokoyama, S.; Saji, T.; Abe, M. "Photochemical switching of vesicle formation using an azobenzene-modified surfactant." *Journal of Physical Chemistry B* **1999**, *103*, 10737-10740.
- [9] Eastoe, J.; Vesperinas, A. "Self-assembly of light-sensitive surfactants." *Soft Matter* **2005**, *1*, 338-347.
- [10] Lee, C. T.; Smith, K. A.; Hatton, T. A. "Photoreversible viscosity changes and gelation in mixtures of hydrophobically modified polyelectrolytes and photosensitive surfactants." *Macromolecules* **2004**, *37*, 5397-5405.
- [11] Baglioni, P.; Braccalenti, E.; Carretti, E.; Germani, R.; Goracci, L.; Tiecco, M.; Savelli, G. "Surfactant-Based photorheological fluids: Effect of the surfactant structure." *Langmuir* **2009**, *25*, 5467-5475.

- [12] Pouliquen, G.; Tribet, C. "Light-triggered association of bovine serum albumin and azobenzene-modified poly(acrylic acid) in dilute and semidilute solutions." *Macromolecules* **2006**, *39*, 373-383.
- [13] Yagai, S.; Nakajima, T.; Kishikawa, K.; Kohmoto, S.; Karatsu, T.; Kitamura, A. "Hierarchical organization of photoresponsive hydrogen-bonded rosettes." *Journal of the American Chemical Society* **2005**, *127*, 11134-11139.
- [14] Alvarez-Lorenzo, C.; Bromberg, L.; Concheiro, A. "Light-sensitive intelligent drug delivery systems." *Photochemistry and Photobiology* **2009**, *85*, 848-860.
- [15] Gerasimov, O. V.; Boomer, J. A.; Qualls, M. M.; Thompson, D. H. "Cytosolic drug delivery using pH- and light-sensitive liposomes." *Advanced Drug Delivery Reviews* **1999**, *38*, 317-338.
- [16] Wolff, T.; Emming, C. S.; Suck, T. A.; Vonbunau, G. "Photorheological effects in micellar solutions containing anthracene-derivatives - a rheological and static low-angle light-scattering study." *Journal of Physical Chemistry* **1989**, *93*, 4894-4898.
- [17] Kuiper, J. M.; Engberts, J. B. F. N. "H-aggregation of azobenzene-substituted amphiphiles in vesicular membranes." *Langmuir* **2004**, *20*, 1152-1160.
- [18] Tong, X.; Wang, G.; Soldera, A.; Zhao, Y. L. "How can azobenzene block copolymer vesicles be dissociated and reformed by light?" *Journal of Physical Chemistry B* **2005**, *109*, 20281-20287.
- [19] Hubbard, F. P.; Santonicola, G.; Kaler, E. W.; Abbott, N. L. "Small-angle neutron scattering from mixtures of sodium dodecyl sulfate and a cationic, bolaform surfactant containing azobenzene." *Langmuir* **2005**, *21*, 6131-6136.
- [20] Wang, Y. P.; Ma, N.; Wang, Z. Q.; Zhang, X. "Photocontrolled reversible supramolecular assemblies of an azobenzene-containing surfactant with alpha-cyclodextrin." *Angewandte Chemie-International Edition* **2007**, *46*, 2823-2826.
- [21] Wang, Y. P.; Han, P.; Xu, H. P.; Wang, Z. Q.; Kabanov, A. V.; Zhang, X. "Photocontrolled self-assembly and disassembly of block ionomer complex vesicles: A facile approach toward supramolecular polymer nanocontainers." *Langmuir* **2010**, *26*, 709-715.
- [22] Kaler, E. W.; Herrington, K. L.; Murthy, A. K.; Zasadzinski, J. A. N. "Phase-behavior and structures of mixtures of anionic and cationic surfactant." *Journal of Physical Chemistry* **1992**, *96*, 6698-6701.

- [23] Kaler, E. W.; Murthy, A. K.; Rodriguez, B. E.; Zasadzinski, J. A. N. "Spontaneous vesicle formation in aqueous mixtures of single-tailed surfactants." *Science* **1989**, *245*, 1371-1374.
- [24] Lee, J. H.; Gustin, J. P.; Chen, T. H.; Payne, G. F.; Raghavan, S. R. "Vesicle-biopolymer gels: Networks of surfactant vesicles connected by associating biopolymers." *Langmuir* **2005**, *21*, 26-33.
- [25] Rehm, B. Alginates biology and applications. *Microbiology monographs v. 13* **2009**, 1 online resource.
- [26] Shi, H.; Ge, W.; Oh, H.; Pattison, S. M.; Huggins, J. T.; Talmon, Y.; Hart, D. J.; Raghavan, S. R.; Zakin, J. L. "Photoreversible micellar solution as a smart drag-reducing fluid for use in district heating/cooling systems." *Langmuir* **2013**, *29*, 102-109.
- [27] Hoffmann, H. "Fascinating phenomena in surfactant chemistry." *Advances in Colloid and Interface Science* **1990**, *32*, 123-150.
- [28] Israelachvili, J. N.; Mitchell, D. J.; Ninham, B. W. "Theory of self-assembly of hydrocarbon amphiphiles into micelles and bilayers." *Journal of the Chemical Society-Faraday Transactions Ii* **1976**, *72*, 1525-1568.
- [29] Mitchell, D. J.; Ninham, B. W. "Micelles, vesicles and micro-emulsions." *Journal of the Chemical Society-Faraday Transactions Ii* **1981**, *77*, 601-629.
- [30] Dreiss, C. A. "Wormlike micelles: where do we stand? Recent developments, linear rheology and scattering techniques." *Soft Matter* **2007**, *3*, 956-970.
- [31] Hoffmann, H. "Viscoelastic surfactant solutions." *Structure and Flow in Surfactant Solutions* **1994**, *578*, 2-31.
- [32] Weiss, R. G.; Terech, P. *Molecular gels : materials with self-assembled fibrillar networks*; Springer: Dordrecht, 2006.
- [33] Cates, M. E.; Candau, S. J. "Statics and dynamics of worm-like surfactant micelles." *Journal of Physics-Condensed Matter* **1990**, *2*, 6869-6892.
- [34] Ezrahi, S.; Tuval, E.; Aserin, A. "Properties, main applications and perspectives of worm micelles." *Advances in Colloid and Interface Science* **2006**, *128*, 77-102.
- [35] Yang, J. "Viscoelastic wormlike micelles and their applications." *Current Opinion in Colloid & Interface Science* **2002**, *7*, 276-281.
- [36] Larson, R. G. *The structure and rheology of complex fluids*; Oxford University Press: New York ; Oxford, 1999.

- [37] Raghavan, S. R.; Kaler, E. W. "Highly viscoelastic wormlike micellar solutions formed by cationic surfactants with long unsaturated tails." *Langmuir* **2001**, *17*, 300-306.
- [38] Raghavan, S. R.; Edlund, H.; Kaler, E. W. "Cloud-point phenomena in wormlike micellar systems containing cationic surfactant and salt." *Langmuir* **2002**, *18*, 1056-1064.
- [39] Davies, T. Thermoreversible transitions between self-assembled nanostructures in aqueous solution., University of Maryland, 2005.
- [40] Horspool, W. M.; Lenci, F. *CRC handbook of organic photochemistry and photobiology*, 2nd ed.; CRC Press: Boca Raton, 2004.
- [41] Sekkat, Z.; Knoll, W. *Photoreactive organic thin films*; Academic Press: Amsterdam ; Boston, 2002.
- [42] Zhao, Y.; Ikeda, T. *Smart light-responsive materials : azobenzene-containing polymers and liquid crystals*; Wiley: Hoboken, N.J., 2009.
- [43] Klán, P.; Wirz, J. *Photochemistry of organic compounds : from concepts to practice*; Wiley: Hoboken, NJ, 2009.
- [44] Deshmukh, S.; Bromberg, L.; Smith, K. A.; Hatton, T. A. "Photoresponsive behavior of amphiphilic copolymers of azobenzene and N,N-dimethylacrylamide in aqueous solutions." *Langmuir* **2009**, *25*, 3459-3466.
- [45] Macosko, C. W. *Rheology : principles, measurements, and applications*; Wiley-VCH: New York, 1994.
- [46] Morrison, F. A. *Understanding rheology*; Oxford University Press: New York, 2001.
- [47] Hammouda, B. Probing nanscale structures - the SANS toolbox..
- [48] Jag, M. *Organic spectroscopy : principles and applications*, 2nd ed.; Alpha Science International Ltd.: Harrow, U.K., 2004.
- [49] Paulusse, J. M. J.; Sijbesma, R. P. "Molecule-based rheology switching." *Angewandte Chemie-International Edition* **2006**, *45*, 2334-2337.
- [50] Stuart, M. A. C.; Huck, W. T. S.; Genzer, J.; Muller, M.; Ober, C.; Stamm, M.; Sukhorukov, G. B.; Szleifer, I.; Tsukruk, V. V.; Urban, M.; Winnik, F.; Zauscher, S.; Luzinov, I.; Minko, S. "Emerging applications of stimuli-responsive polymer materials." *Nature Materials* **2010**, *9*, 101-113.

- [51] Yager, K. G.; Barrett, C. J. "Novel photo-switching using azobenzene functional materials." *Journal of Photochemistry and Photobiology a-Chemistry* **2006**, *182*, 250-261.
- [52] Wolff, T.; Klaussner, B. "Overlap of colloid chemistry and photochemistry in surfactant systems." *Advances in Colloid and Interface Science* **1995**, *59*, 31-94.
- [53] Bates, S. W. Quantifying the stimuli of photorheological fluids. Thesis S.M., Massachusetts Institute of Technology, 2010.
- [54] Shi, H. F.; Wang, Y.; Fang, B.; Talmon, Y.; Ge, W.; Raghavan, S. R.; Zakin, J. L. "Light-responsive threadlike micelles as drag reducing fluids with enhanced heat-transfer capabilities." *Langmuir* **2011**, *27*, 5806-5813.
- [55] Sakai, H.; Orihara, Y.; Kodashima, H.; Matsumura, A.; Ohkubo, T.; Tsuchiya, K.; Abe, M. "Photoinduced reversible change of fluid viscosity." *Journal of the American Chemical Society* **2005**, *127*, 13454-13455.
- [56] Song, B. L.; Hu, Y. F.; Zhao, J. X. "A single-component photo-responsive fluid based on a gemini surfactant with an azobenzene spacer." *Journal of Colloid and Interface Science* **2009**, *333*, 820-822.
- [57] Tomatsu, I.; Hashidzume, A.; Harada, A. "Contrast viscosity changes upon photoirradiation for mixtures of poly(acrylic acid)-based alpha-cyclodextrin and azobenzene polymers." *Journal of the American Chemical Society* **2006**, *128*, 2226-2227.
- [58] Zhao, Y. L.; Stoddart, J. F. "Azobenzene-based light-responsive hydrogel system." *Langmuir* **2009**, *25*, 8442-8446.
- [59] Chen, D.; Liu, H.; Kobayashi, T.; Yu, H. F. "Multiresponsive reversible gels based on a carboxylic azo polymer." *Journal of Materials Chemistry* **2010**, *20*, 3610-3614.
- [60] Murata, K.; Aoki, M.; Suzuki, T.; Harada, T.; Kawabata, H.; Komori, T.; Ohseto, F.; Ueda, K.; Shinkai, S. "Thermal and light control of the sol-gel phase-transition in cholesterol-based organic gels - novel helical aggregation modes as detected by circular-dichroism and electron-microscopic observation." *Journal of the American Chemical Society* **1994**, *116*, 6664-6676.
- [61] Kumar, N. S. S.; Varghese, S.; Narayan, G.; Das, S. "Hierarchical self-assembly of donor-acceptor-substituted butadiene amphiphiles into photoresponsive vesicles and gels." *Angewandte Chemie-International Edition* **2006**, *45*, 6317-6321.

- [62] Kuang, G. C.; Ji, Y.; Jia, X. R.; Li, Y.; Chen, E. Q.; Zhang, Z. X.; Wei, Y. "Photoresponsive organogels: an amino acid-based dendron functionalized with p-nitrocinnamate." *Tetrahedron* **2009**, *65*, 3496-3501.
- [63] Wu, Y. P.; Wu, S.; Tian, X. J.; Wang, X.; Wu, W. X.; Zou, G.; Zhang, Q. J. "Photoinduced reversible gel-sol transitions of dicholesterol-linked azobenzene derivatives through breaking and reforming of van der Waals interactions." *Soft Matter* **2011**, *7*, 716-721.
- [64] Rajaganesh, R.; Gopal, A.; Das, T. M.; Ajayaghosh, A. "Synthesis and properties of amphiphilic photoresponsive gelators for aromatic solvents." *Organic Letters* **2012**, *14*, 748-751.
- [65] Lin, Y. Y.; Cheng, X. H.; Qiao, Y.; Yu, C. L.; Li, Z. B.; Yan, Y.; Huang, J. B. "Creation of photo-modulated multi-state and multi-scale molecular assemblies via binary-state molecular switch." *Soft Matter* **2010**, *6*, 902-908.
- [66] Pereira, M.; Leal, C. R.; Parola, A. J.; Scheven, U. M. "Reversible photorheology in solutions of cetyltrimethylammonium bromide, salicylic acid, and trans-2,4,4'-trihydroxychalcone." *Langmuir* **2010**, *26*, 16715-16721.
- [67] Ketner, A. M.; Kumar, R.; Davies, T. S.; Elder, P. W.; Raghavan, S. R. "A simple class of photorheological fluids: Surfactant solutions with viscosity tunable by light." *Journal of the American Chemical Society* **2007**, *129*, 1553-1559.
- [68] Kumar, R.; Raghavan, S. R. "Photogelling fluids based on light-activated growth of zwitterionic wormlike micelles." *Soft Matter* **2009**, *5*, 797-803.
- [69] Sun, K. S.; Kumar, R.; Falvey, D. E.; Raghavan, S. R. "Photogelling colloidal dispersions based on light-activated assembly of nanoparticles." *Journal of the American Chemical Society* **2009**, *131*, 7135-7141.
- [70] Javvaji, V.; Baradwaj, A. G.; Payne, G. F.; Raghavan, S. R. "Light-activated ionic gelation of common biopolymers." *Langmuir* **2011**, *27*, 12591-12596.
- [71] Kumar, R.; Ketner, A. M.; Raghavan, S. R. "Nonaqueous photorheological fluids based on light-responsive reverse wormlike micelles." *Langmuir* **2010**, *26*, 5405-5411.
- [72] Lee, H. Y.; Diehn, K. K.; Sun, K. S.; Chen, T. H.; Raghavan, S. R. "Reversible photorheological fluids based on spiropyran-doped reverse micelles." *Journal of the American Chemical Society* **2011**, *133*, 8461-8463.
- [73] Yu, X. L.; Wolff, T. "Rheological and photorheological effects of 6-alkyl coumarins in aqueous micellar solutions." *Langmuir* **2003**, *19*, 9672-9679.



- [74] Matsumura, A.; Sakai, K.; Sakai, H.; Abe, M. "Photoinduced Increase in Surfactant Solution Viscosity Using Azobenzene Dicarboxylate for Molecular Switching." *Journal of Oleo Science* **2011**, *60*, 203-207.
- [75] Danino, D.; Bernheim-Groswasser, A.; Talmon, Y. "Digital cryogenic transmission electron microscopy: an advanced tool for direct imaging of complex fluids." *Colloids and Surfaces a-Physicochemical and Engineering Aspects* **2001**, *183*, 113-122.
- [76] Ziserman, L.; Abezgauz, L.; Ramon, O.; Raghavan, S. R.; Danino, D. "Origins of the viscosity peak in wormlike micellar solutions. 1. Mixed cationic surfactants. A cryo-transmission electron microscopy study." *Langmuir* **2009**, *25*, 10483-10489.
- [77] Davies, T. S.; Ketner, A. M.; Raghavan, S. R. "Self-assembly of surfactant vesicles that transform into viscoelastic wormlike micelles upon heating." *Journal of the American Chemical Society* **2006**, *128*, 6669-6675.
- [78] Li, L.; Yang, Y.; Dong, J. F.; Li, X. F. "Azobenzene dye induced micelle to vesicle transition in cationic surfactant aqueous solutions." *Journal of Colloid and Interface Science* **2010**, *343*, 504-509.
- [79] Pedersen, J. S. "Analysis of small-angle scattering data from colloids and polymer solutions: modeling and least-squares fitting." *Advances in Colloid and Interface Science* **1997**, *70*, 171-210.
- [80] Kakehashi, R.; Karlsson, G.; Almgren, M. "Stomatosomes, blastula vesicles and bilayer disks: Morphological richness of structures formed in dilute aqueous mixtures of a cationic and an anionic surfactant." *Journal of Colloid and Interface Science* **2009**, *331*, 484-493.
- [81] Almgren, M. "Stomatosomes: perforated bilayer structures." *Soft Matter* **2010**, *6*, 1383-1390.
- [82] Bachofer, S. J.; Simonis, U. "Determination of the ion exchange constants of four aromatic organic anions competing for a cationic micellar interface." *Langmuir* **1996**, *12*, 1744-1754.
- [83] Bachofer, S. J.; Simonis, U.; Nowicki, T. A. "Orientational binding of substituted naphthoate counterions to the tetradecyl trimethyl-ammonium bromide micellar interface." *Journal of Physical Chemistry* **1991**, *95*, 480-488.
- [84] Kreke, P. J.; Magid, L. J.; Gee, J. C. "<sup>1</sup>H and <sup>13</sup>C NMR studies of mixed counterion, cetyltrimethylammonium bromide cetyltrimethylammonium dichlorobenzoate, surfactant solutions: The intercalation of aromatic counterions." *Langmuir* **1996**, *12*, 699-705.

- [85] Vermathen, M.; Stiles, P.; Bachofer, S. J.; Simonis, U. "Investigations of monofluoro-substituted benzoates at the tetradecyl trimethyl-ammonium micellar interface." *Langmuir* **2002**, *18*, 1030-1042.
- [86] Rakitin, A. R.; Pack, G. R. "Necessity of aromatic carboxylate anions to be planar to induce growth of cationic micelles." *Langmuir* **2005**, *21*, 837-840.
- [87] Evans, D. F.; Wennerstrom, H. *The Colloidal Domain: Where physics, chemistry, biology, and technology meet*; Wiley-VCH: New York, 2001.
- [88] Wang, D.; Dong, R. H.; Long, P. F.; Hao, J. C. "Photo-induced phase transition from multilamellar vesicles to wormlike micelles." *Soft Matter* **2011**, *7*, 10713-10719.
- [89] Lasic, D. D. "Novel applications of liposomes." *Trends in Biotechnology* **1998**, *16*, 307-321.
- [90] Wang, A. Z.; Langer, R.; Farokhzad, O. C. "Nanoparticle delivery of cancer drugs." *Annual Review of Medicine, Vol 63* **2012**, *63*, 185-198.
- [91] Torchilin, V. P. "Recent advances with liposomes as pharmaceutical carriers." *Nature Reviews Drug Discovery* **2005**, *4*, 145-160.
- [92] Fathi, M.; Mozafari, M. R.; Mohebbi, M. "Nanoencapsulation of food ingredients using lipid based delivery systems." *Trends in Food Science & Technology* **2012**, *23*, 13-27.
- [93] Mozafari, M. R.; Johnson, C.; Hatziantoniou, S.; Demetzos, C. "Nanoliposomes and their applications in food nanotechnology." *Journal of Liposome Research* **2008**, *18*, 309-327.
- [94] Betz, G.; Aeppli, A.; Menshutina, N.; Leuenberger, H. "In vivo comparison of various liposome formulations for cosmetic application." *International Journal of Pharmaceutics* **2005**, *296*, 44-54.
- [95] Barani, H.; Montazer, M. "A review on applications of liposomes in textile processing." *Journal of Liposome Research* **2008**, *18*, 249-262.
- [96] Needham, D.; Dewhirst, M. W. "The development and testing of a new temperature-sensitive drug delivery system for the treatment of solid tumors." *Advanced Drug Delivery Reviews* **2001**, *53*, 285-305.
- [97] Karanth, H.; Murthy, R. S. R. "pH-sensitive liposomes - principle and application in cancer therapy." *Journal of Pharmacy and Pharmacology* **2007**, *59*, 469-483.

- [98] Schroeder, A.; Kost, J.; Barenholz, Y. "Ultrasound, liposomes, and drug delivery: principles for using ultrasound to control the release of drugs from liposomes." *Chemistry and Physics of Lipids* **2009**, *162*, 1-16.
- [99] Mueller, A.; Bondurant, B.; O'Brien, D. F. "Visible-light-stimulated destabilization of PEG-liposomes." *Macromolecules* **2000**, *33*, 4799-4804.
- [100] Spratt, T.; Bondurant, B.; O'Brien, D. F. "Rapid release of liposomal contents upon photoinitiated destabilization with UV exposure." *Biochimica Et Biophysica Acta-Biomembranes* **2003**, *1611*, 35-43.
- [101] Bisby, R. H.; Mead, C.; Morgan, C. C. "Wavelength-programmed solute release from photosensitive liposomes." *Biochemical and Biophysical Research Communications* **2000**, *276*, 169-173.
- [102] Zou, J.; Tao, F.; Jiang, M. "Optical switching of self-assembly and disassembly of noncovalently connected amphiphiles." *Langmuir* **2007**, *23*, 12791-12794.
- [103] Liang, X. L.; Yue, X. L.; Dai, Z. F.; Kikuchi, J. "Photoresponsive liposomal nanohybrid cerasomes." *Chemical Communications* **2011**, *47*, 4751-4753.
- [104] Thompson, D. H.; Gerasimov, O. V.; Wheeler, J. J.; Rui, Y. J.; Anderson, V. C. "Triggerable plasmalogen liposomes: Improvement of system efficiency." *Biochimica Et Biophysica Acta-Biomembranes* **1996**, *1279*, 25-34.
- [105] Chandra, B.; Subramaniam, R.; Mallik, S.; Srivastava, D. K. "Formulation of photocleavable liposomes and the mechanism of their content release." *Organic & Biomolecular Chemistry* **2006**, *4*, 1730-1740.
- [106] Wang, X.; Danoff, E. J.; Sinkov, N. A.; Lee, J. H.; Raghavan, S. R.; English, D. S. "Highly efficient capture and long-term encapsulation of dye by cationic surfactant vesicles." *Langmuir* **2006**, *22*, 6461-6464.
- [107] Danoff, E. J.; Wang, X.; Tung, S. H.; Sinkov, N. A.; Kemme, A. M.; Raghavan, S. R.; English, D. S. "Surfactant vesicles for high-efficiency capture and separation of charged organic solutes." *Langmuir* **2007**, *23*, 8965-8971.
- [108] Liu, Y. C.; Le Ny, A. L. M.; Schmidt, J.; Talmon, Y.; Chmelka, B. F.; Lee, C. T. "Photo-assisted gene delivery using light-responsive cationic vesicles." *Langmuir* **2009**, *25*, 5713-5724.
- [109] Diguët, A.; Yanagisawa, M.; Liu, Y. J.; Brun, E.; Abadie, S.; Rudiuk, S.; Baigl, D. "UV-Induced bursting of cell-sized multicomponent lipid vesicles in a photosensitive surfactant solution." *Journal of the American Chemical Society* **2012**, *134*, 4898-4904.

- [110] Ren, K. T.; Malpert, J. H.; Gu, H. Y.; Li, H. Y.; Neckers, D. C. "Synthesis, properties and photolysis of new iodonium tetrakis(pentafluorophenyl)gallate photoinitiators and comparison with their indate and aluminate analogs." *Tetrahedron* **2002**, *58*, 5267-5273.
- [111] Crivello, J. V.; Sangermano, M. "Visible and long-wavelength photoinitiated cationic polymerization." *Journal of Polymer Science Part a-Polymer Chemistry* **2001**, *39*, 343-356.
- [112] Green, W. A. *Industrial photoinitiators: a technical guide*; CRC Press: Boca Raton, 2010.
- [113] Oh, H.; Ketner, A. M.; Heymann, R.; Kesselman, E.; Danino, D.; Falvey, D. E.; Raghavan, S. R. "A simple route to fluids with photo-switchable viscosities based on a reversible transition between vesicles and wormlike micelles." *Soft Matter* **2013**, *9*, 5025-5033.
- [114] Meier, W.; Hotz, J.; GuntherAusborn, S. "Vesicle and cell networks: Interconnecting cells by synthetic polymers." *Langmuir* **1996**, *12*, 5028-5032.
- [115] Antunes, F. E.; Marques, E. F.; Gomes, R.; Thuresson, K.; B., L.; Miguel, M. G. "Network formation of cationic vesicles and oppositely charged polyelectrolytes. Effect of polymer charge density and hydrophobic modification." *Langmuir* **2004**, *20*, 4647-4656.
- [116] Lee, J. H.; Oh, H.; Baxa, U.; Raghavan, S. R.; Blumenthal, R. "Biopolymer-connected liposome networks as injectable biomaterials capable of sustained local drug delivery." *Biomacromolecules* **2012**, *13*, 3388-3394.
- [117] Bu, H. T.; Kjoniksen, A. L.; Knudsen, K. D.; Nystrom, B. "Effects of surfactant and temperature on rheological and structural properties of semidilute aqueous solutions of unmodified and hydrophobically modified alginate." *Langmuir* **2005**, *21*, 10923-10930.
- [118] Galant, C.; Kjoniksen, A. L.; Nguyen, G. T. M.; Knudsen, K. D.; Nystrom, B. "Altering associations in aqueous solutions of a hydrophobically modified alginate in the presence of beta-cyclodextrin monomers." *Journal of Physical Chemistry B* **2006**, *110*, 190-195.
- [119] Choudhary, S.; Bhatia, S. R. "Rheology and nanostructure of hydrophobically modified alginate (HMA) gels and solutions." *Carbohydrate Polymers* **2012**, *87*, 524-530.
- [120] Pawar, S. N.; Edgar, K. J. "Alginate derivatization: A review of chemistry, properties and applications." *Biomaterials* **2012**, *33*, 3279-3305.

- [121] Danino, D. "Cryo-TEM of soft molecular assemblies." *Current Opinion in Colloid & Interface Science* **2012**, *17*, 316-329.
- [122] Yu, D. Y.; Huang, F.; Xu, H. "Determination of critical concentrations by synchronous fluorescence spectrometry." *Analytical Methods* **2012**, *4*, 47-49.
- [123] Danino, D.; Talmon, Y.; Zana, R. "Vesicle-to-micelle transformation in systems containing dimeric surfactants." *Journal of Colloid and Interface Science* **1997**, *185*, 84-93.
- [124] Oh, S. G.; Shah, D. O. "Micellar lifetime - Its relevance to various technological processes." *Journal of Dispersion Science and Technology* **1994**, *15*, 297-316.
- [125] Sheng, P.; Wen, W. J. "Electrorheological fluids: Mechanisms, dynamics, and microfluidics applications." *Annual Review of Fluid Mechanics, Vol 44* **2012**, *44*, 143-174.
- [126] Liu, Y. D.; Choi, H. J. "Electrorheological fluids: smart soft matter and characteristics." *Soft Matter* **2012**, *8*, 11961-11978.
- [127] Wang, D. H.; Liao, W. H. "Magnetorheological fluid dampers: a review of parametric modelling." *Smart Materials and Structures* **2011**, *20*.
- [128] de Vicente, J.; Klingenberg, D. J.; Hidalgo-Alvarez, R. "Magnetorheological fluids: a review." *Soft Matter* **2011**, *7*, 3701-3710.
- [129] Vesperinas, A.; Eastoe, J.; Wyatt, P.; Grillo, I.; Heenan, R. K. "Photosensitive gelatin." *Chemical Communications* **2006**, 4407-4409.
- [130] Tamesue, S.; Takashima, Y.; Yamaguchi, H.; Shinkai, S.; Harada, A. "Photoswitchable supramolecular hydrogels Formed by cyclodextrins and azobenzene polymers." *Angewandte Chemie-International Edition* **2010**, *49*, 7461-7464.
- [131] Lin, Y. Y.; Qiao, Y.; Tang, P. F.; Li, Z. B.; Huang, J. B. "Controllable self-assembled laminated nanoribbons from dipeptide-amphiphile bearing azobenzene moiety." *Soft Matter* **2011**, *7*, 2762-2769.
- [132] Verploegen, E.; Soulages, J.; Kozberg, M.; Zhang, T.; McKinley, G.; Hammond, P. "Reversible switching of the shear modulus of photoresponsive liquid-crystalline polymers." *Angewandte Chemie-International Edition* **2009**, *48*, 3494-3498.
- [133] Moniruzzaman, M.; Sabey, C. J.; Fernando, G. F. "Photoresponsive polymers: An investigation of their photoinduced temperature changes during photoviscosity measurements." *Polymer* **2007**, *48*, 255-263.

- [134] Kim, S. H.; Park, S. Y.; Shin, C. J.; Yoon, N. S. "Photochromic behaviour of poly N,N (3-dimethylamino)propyl methacrylamide having spiroxazine pendant group." *Dyes and Pigments* **2007**, *72*, 299-302.
- [135] Sikorski, P.; Mo, F.; Skjak-Braek, G.; Stokke, B. T. "Evidence for egg-box-compatible interactions in calcium-alginate gels from fiber X-ray diffraction." *Biomacromolecules* **2007**, *8*, 2098-2103.
- [136] Fang, Y. P.; Al-Assaf, S.; Phillips, G. O.; Nishinari, K.; Funami, T.; Williams, P. A.; Li, L. B. "Multiple steps and critical behaviors of the binding of calcium to alginate." *Journal of Physical Chemistry B* **2007**, *111*, 2456-2462.
- [137] Chang, D.; Hsieh, P. S.; Dawson, D. C. "Calcium - a program in basic for calculating the composition of solutions with specified free concentrations of calcium, magnesium and other divalent-cations." *Computers in Biology and Medicine* **1988**, *18*, 351-366.
- [138] Oh, H.; Javvaji, V.; Yaraghi, N. A.; Abezgauz, L.; Danino, D.; Raghavan, S. R. "Light-induced transformation of vesicles to micelles and vesicle-gels to sols." *Soft Matter* **2013**, *9*, 11576-11584.
- [139] Tam, S. K.; Dusseault, J.; Polizu, S.; Menard, M.; Halle, J. P.; Yahia, L. "Impact of residual contamination on the biofunctional properties of purified alginates used for cell encapsulation." *Biomaterials* **2006**, *27*, 1296-1305.
- [140] Yang, S.; Liu, J. K.; Lee, C. S.; Devoe, D. L. "Microfluidic 2-D PAGE using multifunctional in situ polyacrylamide gels and discontinuous buffers." *Lab on a Chip* **2009**, *9*, 592-599.
- [141] Tsao, C. W.; Hromada, L.; Liu, J.; Kumar, P.; DeVoe, D. L. "Low temperature bonding of PMMA and COC microfluidic substrates using UV/ozone surface treatment." *Lab on a Chip* **2007**, *7*, 499-505.
- [142] Zheng, B.; Tice, J. D.; Ismagilov, R. F. "Formation of droplets of in microfluidic channels alternating composition and applications to indexing of concentrations in droplet-based assays." *Analytical Chemistry* **2004**, *76*, 4977-4982.
- [143] Kuo, C. K.; Ma, P. X. "Ionically crosslinked alginate hydrogels as scaffolds for tissue engineering: Part 1. Structure, gelation rate and mechanical properties." *Biomaterials* **2001**, *22*, 511-521.
- [144] Shchipunov, Y. A.; Koneva, E. L.; Postnova, I. V. "Homogeneous alginate gels: Phase behavior and rheological properties." *Polymer Science Series A* **2002**, *44*, 758-766.

- [145] Tyson, J. J.; Chen, K. C.; Novak, B. "Sniffers, buzzers, toggles and blinkers: dynamics of regulatory and signaling pathways in the cell." *Current Opinion in Cell Biology* **2003**, *15*, 221-231.
- [146] Patton, C. <http://maxchelator.stanford.edu/maxc.html>.
- [147] Pocker, Y.; Green, E. "Hydrolysis of D-glucono-delta-lactone .1. General acid-base catalysis, solvent deuterium-Isotope effects, and transition-state characterization." *Journal of the American Chemical Society* **1973**, *95*, 113-119.
- [148] Raghavan, S. R.; Cipriano, B. H. Gel formation: Phase diagrams using tabletop rheology and calorimetry. In *Molecular Gels*; Weiss, R. G., Terech, P., Eds.; Springer: Dordrecht, 2005; pp 233-244.
- [149] Yagci, Y.; Reetz, I. "Externally stimulated initiator systems for cationic polymerization." *Progress in Polymer Science* **1998**, *23*, 1485-1538.
- [150] Szejtli, J. "Introduction and general overview of cyclodextrin chemistry." *Chemical Reviews* **1998**, *98*, 1743-1753.
- [151] Wray-Cahen, D.; Caperna, T. J.; Steele, N. C. "Methyl-beta-cyclodextrin: an alternative carrier for intravenous infusion of palmitate during tracer studies in swine (*Sus scrofa domestica*)." *Comparative Biochemistry and Physiology a-Molecular and Integrative Physiology* **2001**, *130*, 55-65.
- [152] Bonino, C. A.; Samorezov, J. E.; Jeon, O.; Alsberg, E.; Khan, S. A. "Real-time in situ rheology of alginate hydrogel photocrosslinking." *Soft Matter* **2011**, *7*, 11510-11517.
- [153] Jeon, O.; Bouhadir, K. H.; Mansour, J. M.; Alsberg, E. "Photocrosslinked alginate hydrogels with tunable biodegradation rates and mechanical properties." *Biomaterials* **2009**, *30*, 2724-2734.
- [154] Rouillard, A. D.; Berglund, C. M.; Lee, J. Y.; Polacheck, W. J.; Tsui, Y.; Bonassar, L. J.; Kirby, B. J. "Methods for photocrosslinking alginate hydrogel scaffolds with high cell viability." *Tissue Engineering Part C-Methods* **2011**, *17*, 173-179.
- [155] Chueh, B. H.; Zheng, Y.; Torisawa, Y. S.; Hsiao, A. Y.; Ge, C. X.; Hsiong, S.; Huebsch, N.; Franceschi, R.; Mooney, D. J.; Takayama, S. "Patterning alginate hydrogels using light-directed release of caged calcium in a microfluidic device." *Biomedical Microdevices* **2010**, *12*, 145-151.
- [156] De Gier, J.; Mandersloot, J. G.; Van Deene. L. L. "Lipid composition and permeability of liposomes." *Biochimica Et Biophysica Acta* **1968**, *150*, 666-675.

- [157] Qiu, J.; Wei, X. H.; Geng, F.; Liu, R.; Zhang, J. W.; Xu, Y. H. "Multivesicular liposome formulations for the sustained delivery of interferon alpha-2b." *Acta Pharmacologica Sinica* **2005**, *26*, 1395-1401.
- [158] Esser-Kahn, A. P.; Odom, S. A.; Sottos, N. R.; White, S. R.; Moore, J. S. "Triggered release from polymer capsules." *Macromolecules* **2011**, *44*, 5539-5553.
- [159] Du, J. Z.; O'Reilly, R. K. "Advances and challenges in smart and functional polymer vesicles." *Soft Matter* **2009**, *5*, 3544-3561.
- [160] Dowling, M. B.; Bagal, A. S.; Raghavan, S. R. "Self-Destructing "mothership" capsules for timed release of encapsulated contents." *Langmuir* **2013**, *29*, 7993-7998.
- [161] Fischer, A. R.; Werner, P.; Goss, K. U. "Photodegradation of malachite green and malachite green carbinol under irradiation with different wavelength ranges." *Chemosphere* **2011**, *82*, 210-214.
- [162] Irie, M. "Light-induced reversible pH change." *Journal of the American Chemical Society* **1983**, *105*, 2078-2079.
- [163] Eom, K.; Jung, H.; Lee, G.; Park, J.; Nam, K.; Lee, S. W.; Yoon, D. S.; Yang, J.; Kwon, T. "Nanomechanical actuation driven by light-induced DNA fuel." *Chemical Communications* **2012**, *48*, 955-957.



## List of Publications

---

1. H-Y. Lee, **H. Oh**, J. H. Lee and S. R. Raghavan, Shedding light on helical tubules: Real-time observations of tubule self-assembly by light microscopy. **(Co-first author)** *Journal of the American Chemical Society*, **134**, 14375 (2012)
2. K. Sun, **H. Oh**, J. F. Emerson and S. R. Raghavan, A new method for centrifugal separation of blood components using a UV-curable gel. **(Cover)** *Journal of Materials Chemistry*, **22**, 2378 (2012)
3. J. H. Lee, **H. Oh**, U. Baxa, S. R. Raghavan and R. Blumenthal, Biopolymer-connected liposome networks as injectable materials capable of sustained drug delivery. *Biomacromolecules*, **13**, 3388 (2012)
4. **H. Oh**, V. Javvaji, N. A. Yaraghi, L. Abezgauz, D. Danino and S. R. Raghavan, Light-induced transformation of vesicles to micelles and vesicle-gels to sols. *Soft Matter*, **9**, 11576 (2013)
5. **H. Oh**, A. M. Ketner, R. Heymann, E. Kesselman, D. Danino, D. Falvey and S. R. Raghavan, A simple route to fluids with photo-switchable viscosities based on vesicle-micelle transitions. *Soft Matter*, **9**, 5025 (2013)
6. H. Shi, W. Ge, **H. Oh**, S. Pattison, J. Huggins, Y. Talmon, D. Hart, S. R. Raghavan and J. L. Zakin, Photoreversible micellar solutions as smart drag-reducing fluids for district heating/cooling systems. *Langmuir*, **29**, 102 (2013)
7. Z. Wei, J. He, T. Liang, **H. Oh**, J. Athas, Z. Tong, C. Wang and Z. Nie, Autonomous self-healing of poly(acrylic acid) hydrogels induced by the migration of ferric ions. *Polymer Chemistry*, **4**, 4601, (2013)
8. V. Javvaji, M. B. Dowling, **H. Oh**, I. M. White and S. R. Raghavan, Reversible gelation of cells using self-assembling hydrophobically-modified biopolymers: towards self-assembly of tissue. *Biomaterials Science*, (2014)
9. K. K. Diehn, **H. Oh**, R. Hashemipour, R. G. Weiss and S. R. Raghavan, Insights into organogelation and its kinetics from Hansen solubility parameters. Toward a priori predictions of molecular gelation. *Soft Matter*, **15**, 2632 (2014)
10. **H. Oh**, N. A. Yaraghi and S. R. Raghavan, Gelation of oil upon contact with water: A bioinspired scheme for sealing oil leaks. Submitted to *Journal of the American Chemical Society*
11. **H. Oh**, V. Javvaji, A. Lu, R. Hashemipour, and S. R. Raghavan, Light-activated fluidic valve by triggering the nanoscale assembly of a biopolymer. *Manuscript in progress*

**12. H. Oh, V. Javvaji, A. Lu, R. Hashemipour, and S. R. Raghavan, Multicompartment capsules that mimic the architecture of biological cells. *Manuscript in progress***

## List of conference presentations (underline refers to speaker)

---

1. H. Oh, A. Ketner, R. Heymann, E. Kesselman, D. Danino, D. Falvey and S. R. Raghavan, “Reversible photorheological fluids induced by transition between vesicles and wormlike micelles.” , The Society of Rheology 83<sup>rd</sup> Annual Meeting, Cleveland, Ohio, October **2011**
2. H. Lee, H. Oh, J. Lee, S. R. Raghavan, “Self-Assembly of Helical Microtubules Directly Visualized by Optical Microscopy in Real-Time” , 2011 MRS Fall Meeting & Exhibit, Boston, Massachusetts, December **2011**
3. H. Shi, H. Oh, Y. Talmon, D. J. Hart, S. M. Pattison, T. A. Russell, J. T. Huggins, S. R. Raghavan and J. Zakin, “Switching between drag reduction and enhanced heat transfer of a reversible photo-responsive micellar solution.” , The Society of Rheology 83<sup>rd</sup> Annual Meeting, Cleveland, Ohio, October **2011**
4. H. Oh, A. Ketner, R. Heymann, E. Kesselman, D. Danino, D. Falvey and S. R. Raghavan, “Reversible Photorheological Fluids Induced by Transition between Vesicles and Wormlike Micelles in Aqueous System.” , American Conference on Neutron Scattering (ACNS), Washington D.C., June **2012**
5. H. Oh, A. Ketner, R. Heymann, E. Kesselman, D. Danino, D. Falvey and S. R. Raghavan, “Reversible photorheological fluids induced by transition between vesicles and wormlike micelles in aqueous system.” , The 243<sup>rd</sup> ACS National Meeting & Exposition, San Diego, California, March **2012**
6. H. Lee, H. Oh, J. Lee, S. R. Raghavan, “Self-assembly of helical microtubules directly visualized by optical microscopy in real-time.” , The 243<sup>rd</sup> ACS National Meeting & Exposition, San Diego, California, March **2012**
7. K. Diehn, H. Oh, R. Hashemipour and S. Raghavan, “Insight into Slow vs. Instant Gelation of Organic Solvents by Self-Assembly of an Organogelator.” , The 86<sup>th</sup> ACS Colloids and Surface Science Symposium, Baltimore, Maryland, June **2012**
8. H. Oh, V. Javvji, N. Yaraghi, R. Hashemipour and S. R. Raghavan, “Photoresponsive vesicles and vesicle gels.” , The XVI<sup>th</sup> International Congress on Rheology, Joao Maia, Portugal, August **2012**
9. H. Lee, H. Oh, J. Lee, S. R. Raghavan, “Shedding Light on Helical Microtubules: Real-Time Observations of Microtubule Self-Assembly by Optical Microscopy.” , The 86<sup>th</sup> ACS Colloids and Surface Science Symposium, Baltimore, Maryland, June **2012**

10. **H. Oh**, V. Javvaji, N. A. Yaraghi, R. Hashemipour, D. Danino and S. R. Raghavan, “Photoresponsive vesicles and vesicle gels.” , The 245th ACS National Meeting & Exposition, New Orleans, Louisiana, April **2013**
11. **K. Diehn**, **H. Oh**, R. Hashemipour and S. R. Raghavan, “Distinct outcomes for molecular self-assembly: A simple framework for discriminating between instant gel, slow gel, sol, and precipitate based on Hansen solubility parameters” , The 245th ACS National Meeting & Exposition, New Orleans, Louisiana, April **2013**
12. **H. Oh**, A. Ketner, R. Heymann, E. Kesselman, D. Danino, D. Falvey and **S. R. Raghavan**, “Reversible Photorheological Fluids Made Easy: A Simple, Low-cost Route to Fluids with Photo-switchable Viscosities Based on a Reversible Transition between Vesicles and Wormlike Micelles.” , 2013 MRS Spring Meeting & Exhibit, San Francisco, California, April **2013**
13. **H. Oh**, A. X. Lu, V. Javvaji, R. Hashemipour and Srinivasa R. Raghavan, “Light-activated fluidic valve by triggering the nanoscale assembly of a biopolymer.” , The 247rd ACS National Meeting & Exposition, Dallas, Texas, March **2014**
14. **H. Oh**, N. Yaraghi and Srinivasa R. Raghavan, “Gelation of oil upon contact with water: A bioinspired scheme for sealing oil leaks.” , The 247rd ACS National Meeting & Exposition, Dallas, Texas, March **2014**
15. **H. Oh**, N. Yaraghi and S. Raghavan, “Water sensitive molecular self-assembly of organogelators in oil: A bioinspired strategy for sealing oil leaks.” , The 88<sup>th</sup> ACS Colloids and Surface Science Symposium, Philadelphia, Pennsylvania, June **2014** (abstract accepted)
16. **H. Oh**, A. Lu, V. Javvaji, R. Hashemipour and S. R. Raghavan, “Light-activated fluidic valve by triggering the ionic gelation of a biopolymer.” , The 88<sup>th</sup> ACS Colloids and Surface Science Symposium, Philadelphia, Pennsylvania, June **2014** (abstract accepted)
17. **H. Oh**, A. Goyal and S. R. Raghavan, “Multicompartment capsules that mimic the architecture of biological cells” , The 88<sup>th</sup> ACS Colloids and Surface Science Symposium, Philadelphia, Pennsylvania, June **2014** (abstract accepted)
18. **H. Oh**, N. Yaraghi and S. Raghavan, “Water sensitive molecular self-assembly of organogelators in oil: A bioinspired strategy for sealing oil leaks.” , 86th Annual Meeting of The Society of Rheology, Philadelphia, Pennsylvania, **2014** (submitted)
19. **H. Oh**, A. Lu, V. Javvaji, R. Hashemipour and S. R. Raghavan, “Light-activated fluidic valve by triggering the ionic gelation of a biopolymer.” , 86th Annual Meeting of The Society of Rheology, Philadelphia, Pennsylvania, **2014** (submitted)